UNIVERSITÀ DEGLI STUDI DI ROMA "LA SAPIENZA"

Facoltà di Scienze Matematiche, Fisiche e Naturali

Institute of Physics "G. Marconi"

"**STUDY AND REALIZATION OF HYDROGENATED AMORPHOUS SILICON SCHOTTKY BARRIER PHOTODIODES**"

Thesis for the Laurea Degree

Thesis advisor: Dr. Piero Migliorato

Candidate: Alessandro Lucchesini

Opposer: Prof. Umberto Maria Grassano

A. A. 1982-83

INDEX

INTRODUCTION

The recent developments of the research on amorphous semiconductors as silicon and germanium have induced quite a lot of research groups to increase their efforts in the realization and the analysis of devices obtainable with such materials. Moreover the low cost of production as well as the simplicity of realization the amorphous silicon has in comparison to the crystalline one increases the industry interest.
Such a stimulus to the research has already given its fruits with the realization of p-n, p-i-n, metal-semiconductor and MIS junctions as well as silicon and germanium amorphous or silicon-carbide amorphous alloys etherojunctions with the purpose of increasing the efficiency of the devices in the photovoltaic conversion of the solar energy.

The present work concerns the realization and the study of hydrogenated amorphous-silicon (a-Si:H) metal-semiconductor (M-S) photodiodes.

A first phase of the experimental work has been devoted to the preparation and to the analysis of conventional metal-semiconductor structures with the purpose of comparing the properties of our material with the results gotten in other laboratories.

Then new devices that use a thin layer of a-SiC:H (100 ÷ 200 Å) between the metal and the a-Si:H have been realized. These devices show very low inverse current and elevated collection efficiencies. Besides, such diodes introduce a very much dependence of their spectral response by the applied inverse voltage, in a way that it increases their response from the yellow to the green spectral region. These preliminary results suggest the potential employment of the devices in the color detection.

The present Thesis is articulated as it follows.

In Chapter I the amorphous silicon properties are mentioned, and particularly the structure, the electronic levels, the electrical conduction.

The technique for the production of the material is described in Chapter II.

In Chapter III the properties and the production of the silicon-carbide are discussed, by comparing two methods of preparation.

The theory of the metal-semiconductor Schottky barriers is introduced in Chapter IV by comparing the potential profile of the crystalline, with that of the amorphous material.

The mechanisms of transport under these type of potentials are analyzed in Chapter V.

The analysis is then completed by the elementary theory of the phototransport of the metal-semiconductor devices in the in the a-Si:H (Chapter VI).

Elements of the theory of the etherojunctions are introduced in Chapter VII.

Chapter VIII is devoted to the experimental results.

The discussion and the conclusions are written in Chapter IX.

CHAPTER I

AMORPHOUS SILICON PROPERTIES

1.1 GENERALITIES ON THE AMORPHOUS SILICON MATERIAL

The essential characteristic that distinguishes an amorphous material from a crystalline one is the lack of a long range order. This substantially means that the reticular structure of such a type of solid cannot be simply schematized by a periodic repetition of a single elementary cell.

For example, for the amorphous silicon a deviation from the structure of the diamond, proper of the crystalline silicon, is observed due to a distortion of the bond angles. This is seen in Figure 1.1), where the radial density of the amorphous silicon is showed in a comparison with that of the crystalline silicon.

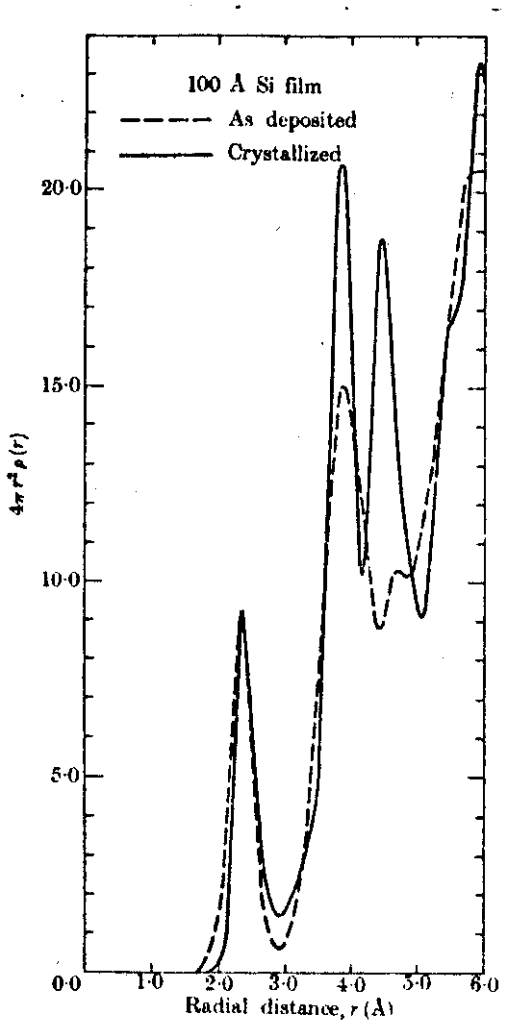

Fig. 1.1 Radial distribution function of the amorphous silicon (evaporated) and crystalline determined by the analysis of the electronic diffraction data.

The number of first neighbors can be obtained from the area under the first peak, which results to be four in this case, as well from the area under the second, twelve second neighbors can be recognized, as it should be in a tetrahedral structure; this points out that the order is maintained up to this level, but the influence of a variation of the bond angles is already noticed.

But the most evident effect of the disorder manifests itself in the drastic decrease of the peak relates to the third neighbors.

As a consequence, in such a structure the electronic wave-function cannot be anymore a simple Bloch function.

We can look for the correct eigenfunction by starting from the Schrödinger equation of the crystal and by considering the effect of the short-range periodicity of the potential through an additive perturbative term[1].

The result will be the existence of "localized states" of intrinsic nature (not due to defects) in the ideal amorphous material. Moreover, the overlap of the atomic neighbors wave-functions allows the formation of channels along which the electron can travel, giving origin to the so-called "extended states."

The energy separation between the localized and the extended states, the so-called "mobility threshold" (where E_c stands the electrons and E_v for the holes) is clear, because the two types of states cannot coexist at the same energy in the same configuration, as explained by Cohen[2]. We will then define "mobility gap" the energy interval between E_c and E_v.

1.2 GAP STATES AND BANDS MODELS

We have just defined an “ideal amorphous” the one that has only intrinsic states in the gap, that is the one in which all the bonds are saturated; experimentally it has been seen that such states are placed immediately below the conduction band and above the valence band to form the so-called “gap tails.”

However, besides them an amorphous semiconductor possesses a continuous density of states in the gap due the contribution of the extrinsic states associated to defects or impurities, that have the tendency to localize themselves in the center of the gap of the forbidden energy.

Actually various pictures of the amorphous semiconductors bands exist, two of the most interesting of them are the Cohen-Fritzsce-Ovshinsky (C.F.O.)[3] and the Mott-Davis[4] ones.

In the C.F.O. model it is assumed that the disorder creates intrinsic localized states with a continuous decreasing density when approaching the center of the forbidden energy gap. In substance the model hypothesizes that the tails of the valence and conduction bands come to overlap, as it can be seen in Fig. 1.2), precluding a clean distinction of the valence and the conduction thresholds.

This kind of scheme is appropriate for the calcogens, where a high degree of disorder exists.

For someone the Mott-Davis model is more appropriated for silicon and germanium, as it considers band tails less broad within the gap, but situated few tenth of electron-volt under the respective bands. Moreover it hypothesizes the existence of a certain density of extrinsic states near the center of the gap, ought to defects like vacancies or unsaturated bonds.

From Fig. 1.3) this can be better understood, as well as that the zone between the two mobility thresholds E_c and E_v is well separated.

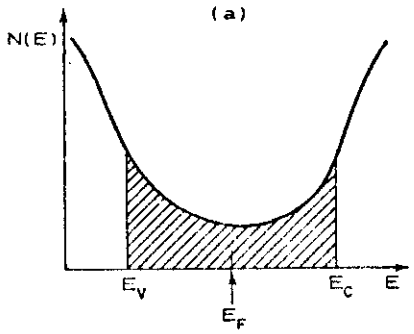

Fig. l.2) Density of states for the C.F.O. model.

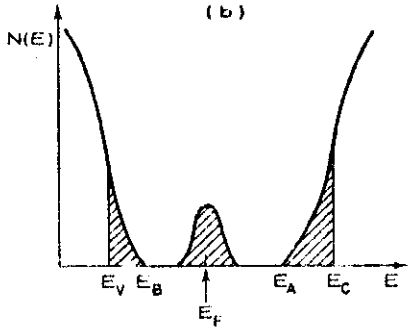

Fig. l.3) Density of states for the Davis-Mott model.

There are various methods to realize the amorphous material such as the “evaporation”, the “sputtering” and the “glow-discharge” (G.D.). The last is based on the decomposition of molecular gases by a radio-frequency discharge. Sometimes the discharge gas (SiH_4 is used for the amorphous silicon) is mixed with other gases as Ar, He or H_2 to increase the homogeneity of the material. Comparisons among samples of the amorphous silicon obtained by the G.D. with and without hydrogen induced Brodsky, Spear and other researchers to assign an essential role to this element in the reduction of the density of the extrinsic states in the gap; this is due to the fact that the hydrogen saturates the vacancy bonds, always present in the amorphous material, creating silicon hydrides.

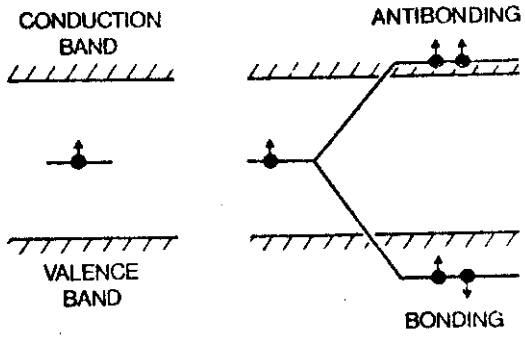

Fig. 1.4) Localized state that gives a single level in the gap (“deep”).

The addition of another electron, coming from the atomic hydrogen, creates states of bond or antibond that are placed in the valence and conduction bands respectively.

In Fig. 1.4) such a hydrogen saturation is schematized for a much localized state, the so-called “deep.”

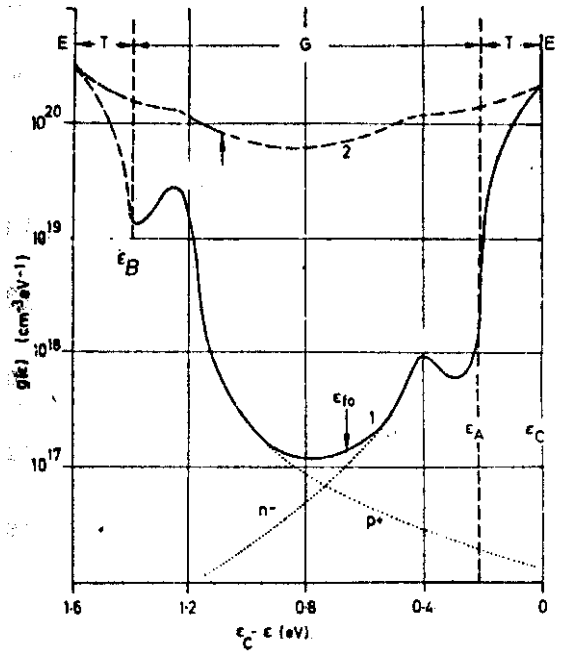

Fig. 1.5) Amorphous silicon density of states determined by field-effect experiments. The arrows in each curve point the position of the Fermi level. Curve 1 refers to the silicon obtained by the G.D.. Curve 2 refers to what obtained by evaporation.

E = extended states;
T = band tails;
G = gap states;
ε_{fo} = Fermi level in the intrinsic case[5].

In order to dope the material p or n extrinsic states can be created in the gap by using the elements of the III or the V group of the periodic table as contaminants, such as for instance boron or phosphorus, respectively. But the level of doping of an amorphous semiconductor does not depend only on the concentration of impurities in the solid, as it happens in the crystalline phase, but also on the value of the density of states in the forbidden band.

This can be understood remembering that the doping element is it because of the more or less electron it has in comparison to the element it replaces in the crystalline lattice, but in the amorphous such an electron could go to form a covalent bond for the many not saturated bonds that characterize the material.

The influence of the doping on the room temperature conductivity and therefore its effect can be seen in the following Fig. 1.6). Such a figure is based on Spear's data[5] gotten by samples realized through the G.D. in SiH_4 atmosphere, with a percentage of B_2H_6 for the p doping or PH_3 for the n doping. It is noted that the minimum of the conductivity is in the material slightly doped p.

This means that the not intentionally doped material has indeed the characteristics of a lightly doped n.

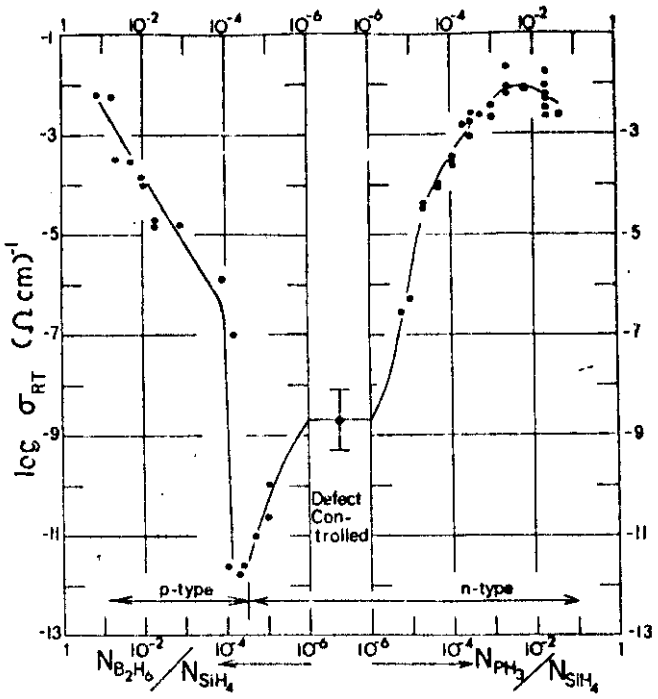

Fig. 1.6) n and p amorphous silicon conductivity at room temperature as a function of the gas composition in the G.D.. The central part corresponds to the undoped silicon.

1.3 ELECTRICAL CONDUCTIVITY

The electrical conductivity in the amorphous semiconductors is essentially driven by three fundamental mechanisms [$\sigma = e\Sigma_i n_i \mu_i$ with i = 1, 2, 3]:

a) extended states conduction;

b) hopping by localized states in the band tails;

c) hopping by localized states at the Fermi energy.

For what the extended states conductivity concerns, that is above E_c, the same road of the crystalline semiconductors can be followed by introducing the general expression of the conductivity for an isotropic solid:

1.1) $$\sigma = -\frac{1}{3}\int e^2\tau(E) < v^2 > \frac{\partial f_{F.D.}}{\partial E} G(E)dE \ ,$$

$\tau(E)$ is the time between two collisions and generally it depends on the electron energy.

By using the Maxwell-Boltzmann statistic, the general expression of the mobility, that is valid for any charged particle, can be obtained:

1.2) $$\mu = \frac{e < v^2 > \tau}{3KT} \ ,$$ that can be easily included in Eq. 1.1).

Finally the conductivity of our semiconductor can be expressed by the integral over the energy:

1.3) $$\sigma = -e\int G(E)\mu(E)KT\frac{\partial f_{F.D.}}{\partial E}dE \ .$$

If the Mott-Davis' model on the density of states behavior is adopted, it follows that the Fermi energy is located around the center of the forbidden gap and quite far from the mobility threshold (E_c-E_f » KT). Therefore this permits to shift from the Fermi-Dirac's to the Boltzmann's statistic:

1.4) $$f_{F.D.}(E) = \frac{1}{\exp\left(\frac{E - E_f}{KT}\right) + 1} \Rightarrow f_{B.}\exp\left(-\frac{E - E_f}{KT}\right) \ .$$

The first derivative of $f_{B.}$ is:

1.5) $$\frac{\partial f_{B.}(E)}{\partial E} = -\frac{1}{KT}\exp\left(-\frac{E - E_f}{KT}\right) \ ,$$ therefore the integral 1.3) becomes:

1.6) $\sigma = e\int_{E_c}^{+\infty} G(E)\mu(E)\exp\left(-\frac{E-E_f}{KT}\right)dE$.

By considering constant either the density of states and the mobility, the result valid off the degenerative case, that it is not reachable by the amorphous anyway, can be attained:

1.7) $\sigma = eG(E_c)\mu_c KT\exp\left(-\frac{E_c-E_f}{KT}\right)$, being "μ_c" now a mobility mean value over the E_c threshold.

Let us put:

1.8) $\sigma_0 = eG(E_c)\mu_c KT$; now such a term would result independent on the temperature if the μ_c depends on T in the way described in 1.2). From Mott's calculations the mean free path of the electron right at the energy E_c results of the order of the interatomic distances, therefore under these conditions Cohen[6] has proposed right the diffusive or Brownian conduction model, in which the mobility got through the theory of Einstein is just like the 1.2). We expect then an expression of the conductivity of the type:

1.9) $\sigma = \sigma_0\exp\left(-\frac{E_c-E_f}{KT}\right)$.

Since optical absorption measurements have shown a behavior of the forbidden gap energy opposite to the temperature, it can be assumed that the same thing happens to the interval E_c-E_f. Therefore, if E_c-$E_f = E_0 - CT$ is assumed, the 1.9) becomes:

1.10) $\sigma=\sigma_0\exp\left(\frac{-E_0}{KT}\right)\exp\left(\frac{C}{K}\right)=\text{cost.}\cdot\exp\left(\frac{-E_0}{KT}\right)$.

The conduction in the localized states of the band tails can only happen through a thermally activated hopping, that is through jumps of an electron from a localized state to another with the exchange of the energy with a phonon.

Here, as in the previous model, we can start from the mobility by asserting that in this case we expect this is strongly activated by the temperature with a dependence of the type:

1.11) $\mu_{hop} = \mu_0\exp\left(\frac{-W(E)}{KT}\right)$,

where *W(E)* is the activation energy of the process $(\cong KT)$, that in general will depend on the electron energy.

For the conductivity we can start again from the general expression 1.1), for which *G(E)* has to be known.

A general behavior of the density of states as a function of the energy can be thought of the type:

1.12) $G(E) = \frac{G(E_c)}{\Delta E^s}(E - E_A)^s$, that is dependent on a power of the energy. ΔE is the band tail energy extension and E_A is the beginning of it.

Therefore by solving the integral we get the hopping conductivity:

1.13) $\sigma_{hop} = \sigma_{0hop} C_s \left(\frac{KT}{\Delta E}\right)^s \exp\left(-\frac{E_A - E_f + W}{KT}\right)$, where

1.14) $\sigma_{0hop} = e\mu_0 G(E_c)$ and $C_s = s! - \left(\frac{\Delta E}{KT}\right)^s \exp\left(-\frac{\Delta E}{KT}\right)\cdot\left(a\ power\ series\ of\ \frac{KT}{\Delta E}\right)$;

a quite complicated expression, that comes easier when a linear dependence of the density of states on the energy is assumed ($s=1$):

1.15) $\sigma_{hop} = \sigma_{0hop} C_1 \left(\frac{KT}{\Delta E}\right)^s \exp\left(-\frac{E_A - E_f + W}{KT}\right)$ with

1.16) $C_1 = 1 - \exp\left(-\frac{\Delta E}{KT}\right)\cdot\left(\frac{\Delta E}{KT} + 1\right)$.

Anyway, for $E_a - E_f + W > KT$ the exponential term that decreases with T is predominant.

For what the conduction in the localized states at the Fermi energy concerns we refer to the Mott's work[7].

Substantially he takes into account a conduction mechanism similar to the one of the heavy doped and compensated semiconductors (see Fig. 1.7)).

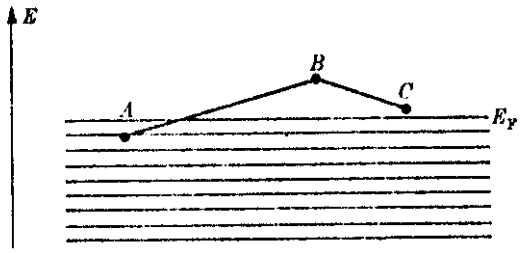

Fig. 1.7) Hopping conduction mechanism. Two hops are shown, from A (an occupied state) to B and from B to C.

If the Fermi energy lies in a band of localized states, as it happens for instance in the Davis and Mott's model, the carriers can move between such states through a process of phonon-assisted tunnel. Consequently, the probability with which an electron can effect a jump will depend on the overlap of the eigenfunctions of the departure and arrival state through a factor of the type: exp(-2αR), where R is the distance between the departure and the arrival states and α is a measure of the

extinction of the localized state wave-function. The probability to find a phonon with a proper energy will also influence it, and it will be given by the expression of Boltzmann $\exp\left(-\frac{W}{KT}\right)$, and so will do the frequency at which this process can happen, that will not be able to get over the maximum phononic one (~ $10^{13}s^{-1}$).

In conclusion the probability for unit of time of the process can be expressed as:

1.17) $p = \nu_{ph} \exp\left(-2\alpha R - \frac{W}{KT}\right)$.

Contemporary it must be taken into account the "variable range hopping" that comes from the fact that, as the temperature decreases, the electrons find phonons of smaller and smaller energy, for which are forced to lengthen the jump toward states more and more distant from the first neighbors, but energetically closer to theirs; in fact the 1.17) exponential term does not have its maximum value in correspondence of the next neighbors.

To calculate the optimal distance of jump, Mott thought about the fact that the electron will abandon its state only if there will be at least another available; besides, the number of states at energy W or within a distance R from the particular atom is:

1.18) $\frac{4}{3}\pi R^3 G(W) W$.

Substituting now Eq. 1.19) in the 1.17) and minimizing the exponential of the obtained expression, the most probable jumping distance is obtained:

1.20) $R = \left[\frac{9}{8\pi\alpha G(E_f) KT}\right]^{1/4}$.

The 1.17) with the 1.19) and the 1.20) gives:

1.21) $p = \nu_{ph} \exp\left(-\frac{A}{T^{1/4}}\right)$, where in A are all the constants of calculus.

The 1.21) can be bound to the conductivity by the mobility expression: $\mu = \frac{eD}{KT}$, where the diffusion constant in the case of a casual motion, i.e. Brownian, is expressed by: $D = \frac{1}{6} pR^2$.[8]

By making use of the conductivity expression 1.6), it is obtained:

1.22) $\sigma = \frac{1}{6} e^2 R^2 \nu_{ph} G(E_f) \exp\left(-\frac{A}{T^{1/4}}\right) = \sigma_0(T) \exp\left(-\frac{A}{T^{1/4}}\right)$

where now σ_0 depends on T, remembering the previous sentence about the jump distance R.

There are experimental evidences of the $ln\sigma$ dependence by $T^{-1/4}$, but the values gotten on the A constant do not coincide with those of Mott, perhaps for the approximation [ref. 1.19)] by considering the density of states at the Fermi level as independent from the energy[9].

BIBLIOGRAPHY

General: P. Nagels “Electronic Transport in Amorphous Semiconductors”, Cap. V of the Volume edited by M. Brodsky (1979)

1 W. Anderson, Phys. Rev. **109**(5), 1492 (1958)

2 M.H. Cohen, Can. J. Chem. **55**, 1906 (1977)

3 M.H. Cohen - H. Fritzsce - S. Ovshinsky, Phys. Rev. Lett. **22**, 1065 (1969)

4 N.F. Mott - E. Davis, Phil. Mag. **22**, 903 (1970)

5 W. Spear - F.G. Le Comber, Phil. Mag. **33**(5), 935 (1976)

6 M.H. Cohen, J. Non Cryst. Sol. **4**, 391 (1970)

7 N.F. Mott, Phil. Mag. **19**, 835 (1969)

8 P.C. Shewmon “Diffusion in Solids” (1963)

9 H. Overhof, Adv. Sol. State Phys. **16**, 239 (1976)

CHAPTER II

RADIOFREQUENCY “GLOW DISCHARGE” TECHNIQUE

The amorphous silicon used in the present work has been deposited by using the “Glow-Discharge” (G.D.) technique in a silane atmosphere (SiH_4)

The equipment is composed by two flat electrodes (ELETTRODI) connected to a Plasma-Therm 13.56 MHz radio frequency generator [see Fig.2.1)]. The electrodes are contained in closed quartz bell (CAMPANA DI QUARZO) where a pre-vacuum around 10^{-3} torr is made through an Alcatel rotary pump (POMPA ROTATIVA). The substrate is put on one of the electrodes, the lower.

Different ionic species are produced in the discharge such as $(SiH_3)^+$, $(SiH_2)^{++}$, $(SiH)^{+++}$, that through processes not yet well understood, create the hydrogenated amorphous material.

The parameters that influence the growth of the material are the pressure, the gas flow and the temperature of the substrate, but the more critic, especially for the speed of growth, is the discharge power.

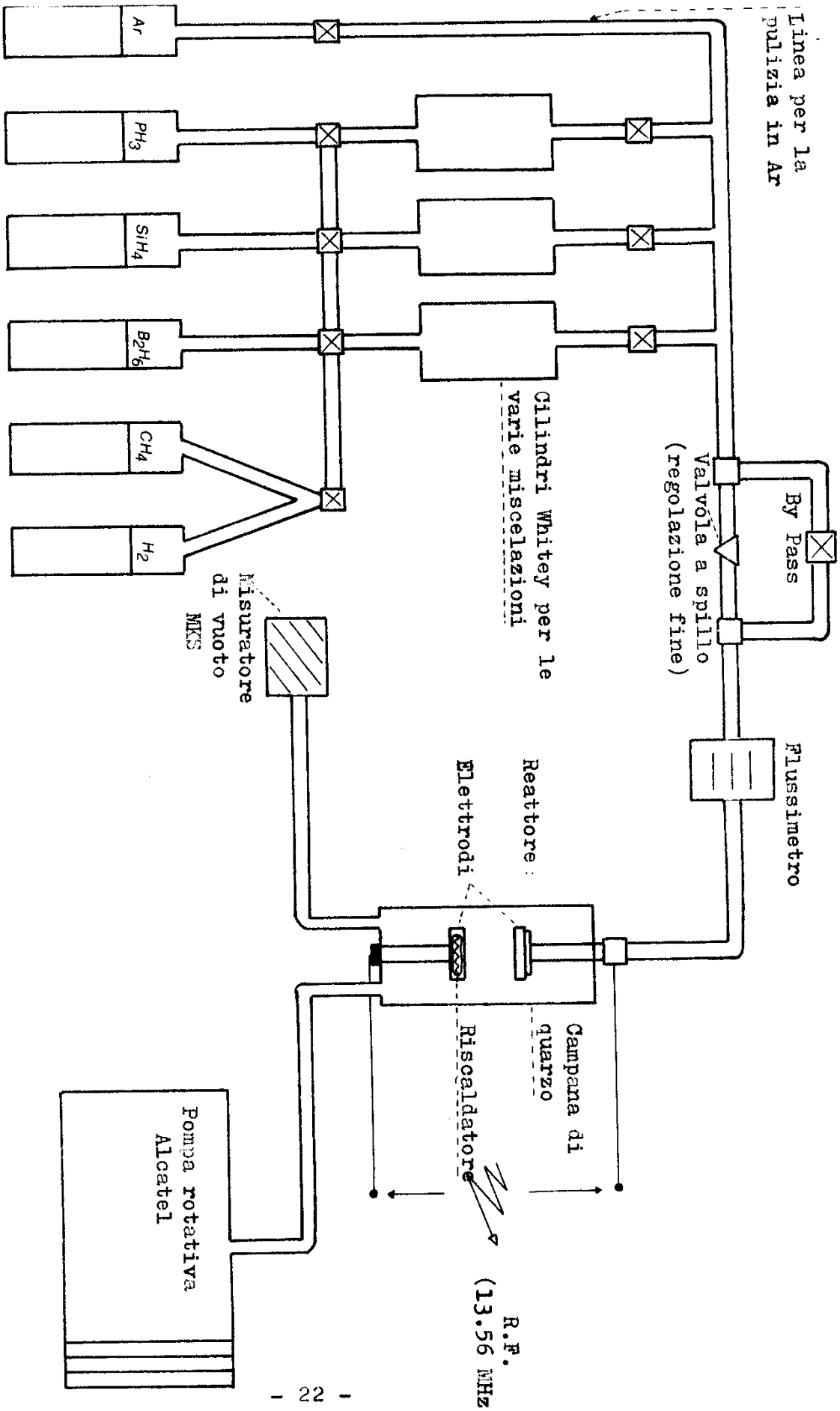
Linea per la pulizia in Ar
Ar
PH3
SiH4
B2H6
CH4
H2
Cilindri Whitey per le varie miscelazioni
Valvola a spillo (regolazione fine)
By Pass
Misuratore di vuoto MKS
Flussimetro
Reattore
Elettrodi
Campana di quarzo
Riscaldatore
R.F. (13.56 MHz)
Pompa rotativa Alcatel
- 22 -

Fig. 2.1)

For every type of G.D. equipment there is a characteristic optimization of the fundamental parameters as those specified before, in general however it is possible to make a schematic, as for instance the one in Fig. 2.2), for what the flow and the pressure pertains.

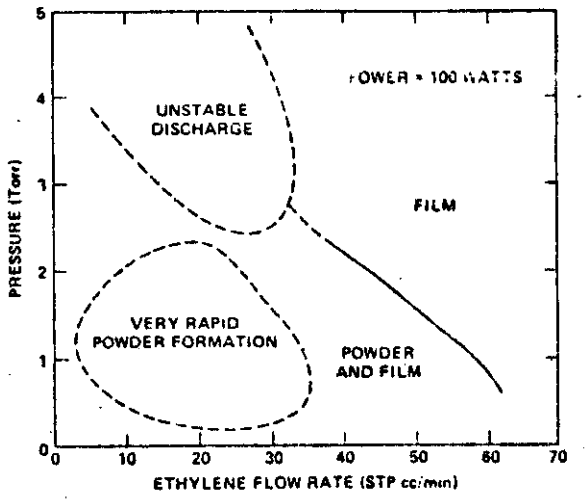

Fig. 2.2) Schematic drawing showing the pressure and flow optimal conditions for the formation of the film in the G.D.[1] reactor.

The hydrogen content of the material can be in some way monitored by acting on the flow, on the pressure and on the temperature.

A "doping" gas as phosphine (PH_3) or diborane (B_2H_4) can be mixed with the silane gas in order to get samples doped n or p, respectively.

A pressure of the gases between 0.5 and 1 torr has been used in the reactor for the growth of our samples and a light influence of this has been noticed on the speed of growth (by increasing the pressure the "rate" increased).

The gases flow has been maintained in the interval that goes from 4 to 10 cm^3 per minute; it also has shown influence on the speed of growth, even if not marked, but at its lower values a greater homogeneity of the samples corresponded.

The temperature of the substrates has been kept in the range 220-300 ºC while the discharge power was of the order of 0.3 W/cm^2.

The choice of the aforesaid values is the result of a series of tests and controls of the properties of the obtained films and devices by the aid of optical and transport techniques effected in connection with the rest of the activity of the research group.

The results are in accordance with what the literature reports. For instance in the Knights'

paper[2] it is reported that the hydrogen content of the films decreases very much at growth temperature above 400 ºC.

We noticed that for a discharge power higher than the reported one, the samples were not uniform.

For a good adherence of the material deposited on the substrates an accurate cleaning was necessary, therefore every time we degreased them first by trichloroethylene, then by hot methylic alcohol and by ultrapure acetone, and finally the removal of possible solid particles was favored by using an ultrasound bath.

The cleaning of the quartz bell resulted quite important for the realization of a good material. In a first trial this has been obtained by using NaOH dissolved in warm water. However by this way the G.D. deposited material resulted contaminated by sodium. The drawback has been eliminated by modifying the cleaning procedure: to remove the traces of the amorphous silicon remained by the precedent depositions the mixture of HF and HNO_3 has been used in proportions of 1 to 2 respectively, followed by a rinsing with acetone and then with distilled water and finishing by drying it at 120 ºC in an electric oven. However before growing the material, in order to avoid a still possible contamination from the reactor walls, a deposit of a first layer of silicon has been effected on them to bury the extraneous species, followed by a degassing procedure by heating up to ≅ 200 ºC for a hour and by contemporary pumping down by the rotary pump. This has been crucial for the attainment of a good vacuum in the system before the introduction of the discharge gases.

BIBLIOGRAPHY

General: F. Llewellyn-Jones, “The Glow Discharge”, Wiley and Sons, N.Y. (1966)

1 H. Kobayashi - A.T. Bell - M. Shen, J. Appl. Polym. Sci. **17**, 885 (1973)

2 J. Knights - R.J. Nemanich - G. Lucovsky, J. Non Cryst. Sol. **32**, 393 (1979)

CHAPTER III

“IDROGENATED AMORPHOUS SILICON-CARBIDE”

3.1 AMORPHOUS SILICON-CARBIDE PROPERTIES AND REALIZATION

The first realization of the hydrogenated amorphous silicon-carbide (a-SiC:H) as well as the first characterization of such a material dates from 1977 to the work of D.A. Anderson and W.E. Spear[1].

In that occasion to realize the material the glow-discharge with the mixture of the SiH_4 and C_2H_4 gases it has been used, with the substrate temperature kept at around 300 ºC, the gas pressure in the reactor between 0.4 and 0.8 torr and a flow of a few s.c.c.m. (cm^3 per minute, standard). Under such conditions Anderson has experimented a growth of the material around 50 Å/min, slightly lower than the amorphous silicon got under the same conditions.

In Fig. 3.1) the result of the first analyses of different samples effected by the two researchers is presented; it shows the percentage of carbon in the material obtained by varying the silane and ethylene mixtures.

Contemporary to the increase of carbon contained in the material a diminution of the density has been noticed by R.S. Sussmann and R. Ogden[2], therefore they advance the hypothesis that this is caused by an increase of the concentration of hydrogen. They have also done an analysis of the infrared absorption of the a-SiC:H samples grown at different temperatures and the result is shown in Fig. 3.2), where as the temperature of deposition increases the absorption bands related to the groups Si-C, Si-H and C-H reduce, showing that the incorporation of carbon and hydrogen decreases as the substrate temperature increases.

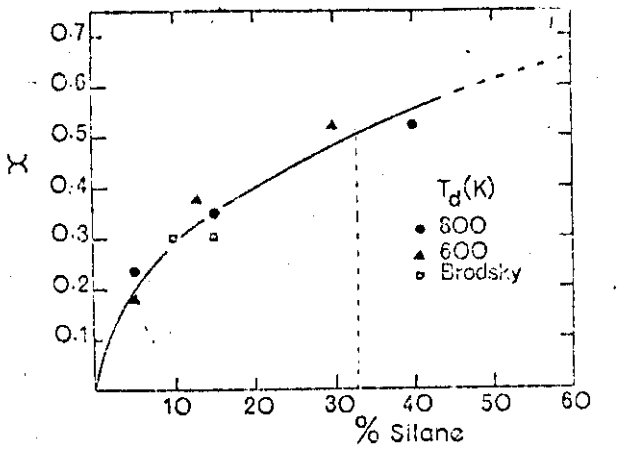

Fig. 3.l) Behavior of the composition parameter x in the silicon-carbide films (Si_xC_{1-x}) as a function of the silane volume percentage used in the samples preparation.

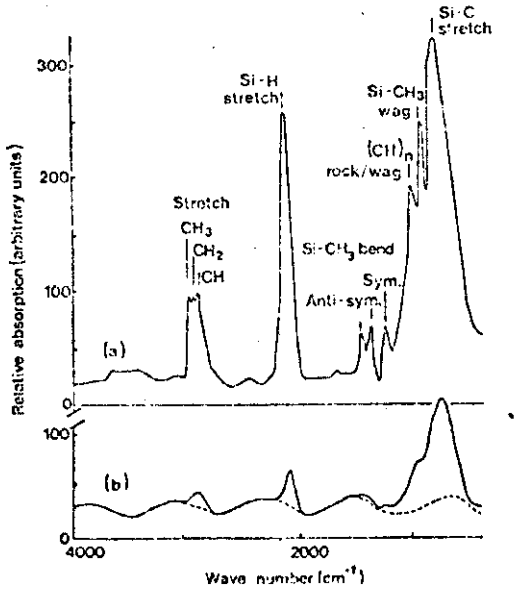

Fig. 3.2) Infrared absorption of the films with similar thickness deposited at (a) 30ºC and (b) 300ºC.

For what the optic properties of the amorphous silicon-carbide concerns, a lot of measurements of light absorption of the samples containing different percentages of carbon have been done. The most interesting results are from the analysis of the "optical gap" ($E_{g_{opt}}$). This parameter does not coincide with the mobility gap, but it is tightly connected to it, being in substance the energetic difference between the beginning of the conduction and valence band tails.

By assuming parabolic energy bands in K and the matrix elements of the optical transition independent from the energy, this formula[8] for the absorption coefficient of the amorphous silicon can be adopted:

$$3.1) \qquad \alpha = \frac{B}{h\nu}\left(h\nu - E_{gopt}\right)^2,$$

where B is a constant which takes into account the characteristics of the material (usually $B \sim 10^5$ - $10^6\ eV^{-1}cm^{-1}$).

Now it is clear that if we construct a $(\alpha h\nu)^{1/2}$ vs. $h\nu$ graphic and linearly extrapolate it to $(\alpha h\nu)^{1/2} = 0$, right the $E_{g_{opt}}$ is obtained. This is what has been done by Sussmann and Ogden and from the analysis of their experimental results, a big increase of the gap when increasing the x parameter of the a-Si_xC_{1-x}:H is noticed, as Fig. 3.3) shows.

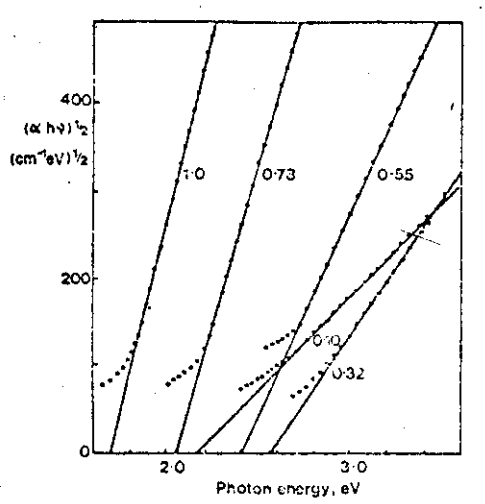

Fig. 3.3) Linear behavior of the absorption coefficient in the $(\alpha h\nu)^{1/2}$ vs $h\nu$ frame, in order to get $E_{g_{opt}}$ in accordance with Eq. 3.1). The composition parameter x is shown for each curve.

Evidently the possibility to suite the width of the forbidden gap by simply acting on the concentration of carbon exists with this particular material. Indeed there is a maximum value of it, as it results from Fig. 3.4).

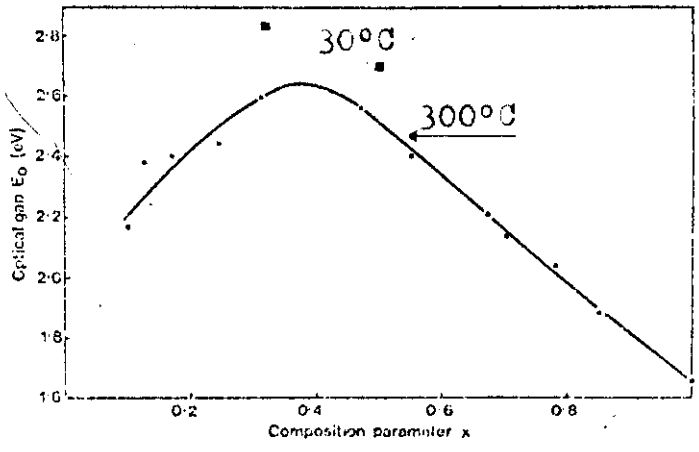

Fig. 3.4) $E_{g_{opt}}$ behavior by the composition parameter x.

As it can be noticed, there is also a strong dependence from the temperature of deposition. It is possible to see better this phenomenon from the of Anderson and Spear's analysis illustrated in Fig. 3.5).

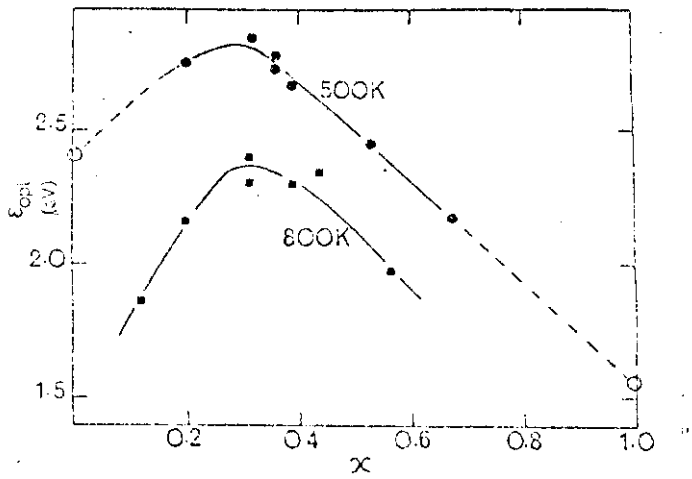

Fig. 3.5) $E_{g_{opt}}$ behavior by the composition parameter x for the samples deposited at 500 K and 800 K. The white dots refers to the a-C and a-Si samples grown at 500 K.

This big influence of the temperature could be bound to a diminution of the content of hydrogen, confirming what written in advance.

Still, following the material analysis done by Anderson and Spear, some information on the d.c. conductivity of the amorphous silicon-carbide can also be got.

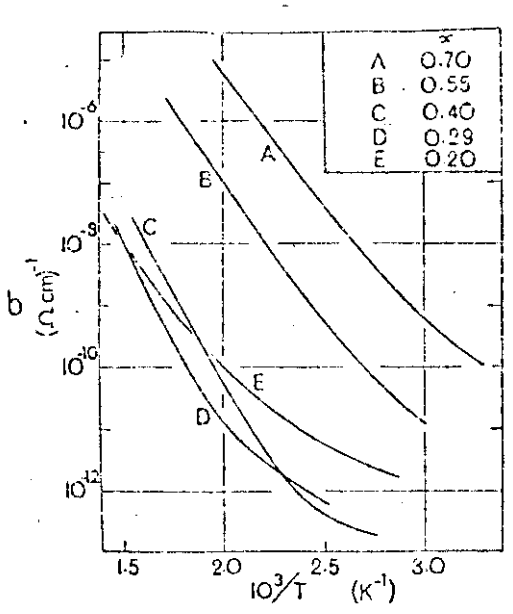

Fig. 3.6) Temperature vs. d.c. conductivity of silicon-carbide deposited by the G..D. at 800 K with the shown stoichiometric compositions.

They made measurements under high temperature conditions in an interval that went from 300 to 700 K, this because they did not get appreciable values at lower temperatures.

In figure 3.6) the behavior of the conductibility when varying the temperature is shown. Under these conditions it is possible to write:

3.2) $$\sigma = \sigma_0 \exp\left(-\frac{\varepsilon_\sigma}{KT}\right)$$

where ε_σ is the activation energy obtained from the graph.

From the experimental data got by the two researchers the influence of the carbon percentage present in the material on all the conduction characteristics is evident. Particularly from Fig. 3.7) can be noticed that a value of the stoichiometric parameter x exists around 0.3 for which there is the highest activation energy ε_σ, a saturation of the pre-exponential factor σ_0 dependent from the conduction mechanism, and the lowest conductivity.

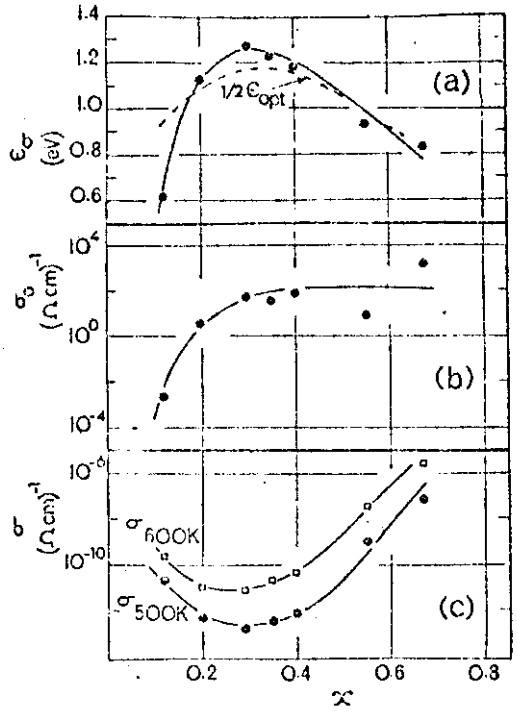

Fig. 3.7) Conductivity parameters behaviors got form the high temperature zones in the curves of Fig. 3.6) as a function of the film composition x. (a) activation energy ε_σ; (b) pre-exponential factor σ_0; (c) conductivity value σ at 500 and 600 K.

In Fig. 3.7a) it is interesting to compare the variation of the activation energy as a function of x (Si_xC_{1-x}) with the behavior of $E_{g_{opt}}$ gotten through the data of Fig. 3.5). As it can be noticed for

x > 0.2 ε_σ has a similar behavior, while contemporary σ_0 saturates to 10^{-2} $(\Omega cm)^{-1}$ as it is visible in Fig. 3.7b). This seems to be a symptom of an extended states conduction mechanism and this is reasonable being under high temperature conditions. Instead for x < 0.2 a deviation of ε_σ by the behavior $\frac{E_{gopt}}{2}$ is noticed, which seem to be due to the presence of a different mechanism of conduction, as for instance a hopping between localized states in the gap of mobility.

3.2 COMPARISON BETWEEN THE a–SIC:H MATERIAL OBTAINED BY SIH_4 AND C_2H_4 MIXING AND THE ONE OBTAINED BY SIH_4 AND CH_4 MIXING.

So far we have studied the characteristics of the hydrogenated silicon-carbide in a qualitative way, focalizing particularly onto the material obtained by ethylene and analyzed by Anderson and Spear.

More recent works[3] have shown the feasibility of the hydrogenated silicon-carbide by using the methane in place of ethylene.

The comparison between the a-SiC:H got with the mixture silane-ethylene and the one got with silane-methane underlines the different carbon concentration in the material with the same dilution of the two gases, as it can be seen in Fig. 3.8), that brings the results obtained by Hamakawa[3]

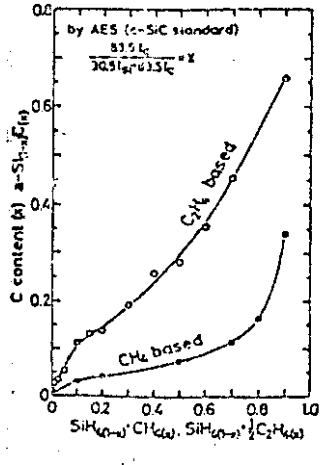

Fig. 3.8) Comparison between the a-SiC:H carbon content and the G.D. gas mixing composition for the samples based on ethylene and methane. (Now the stoichiometric parameter x refers to carbon).

It is evident that the amorphous silicon-carbide obtained by the ethylene contains a greater percentage of carbon and this seems related to the way it is incorporated in the matrix of silicon.

Contemporary, from the comparison of the optical gaps obtained for the materials realized with the two types of mixtures, it is noticed that by using SiH_4 + C_2H_4 greater $E_{g_{opt}}$ results, as shown in Fig. 3.9).

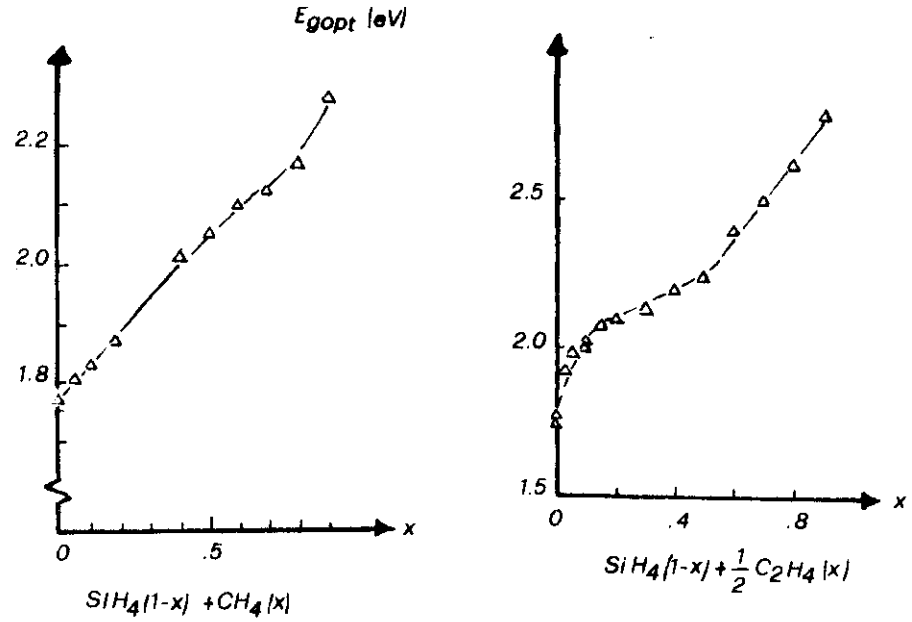

Fig. 3.9)

To deeply analyze the problem of the carbon incorporation we can refer to an interesting study of the structure of the amorphous silicon-carbide carried on by the researchers of the Hamakawa's group at the University of Osaka. They suggest a comparison in the infrared absorption between the material grown by using ethylene and the one grown by using methane. In Fig. 3.10) it can be noticed that in the silicon-carbide based on ethylene the Si-CH_3 bonds do not almost exist, whose absorption bands are instead well visible in the spectrum of the one based on methane.

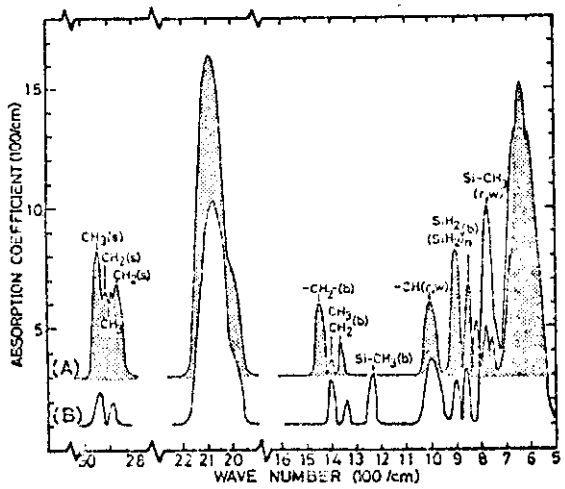

Fig. 3.10) Infrared spectrum of the a-SiC:H based on ethylene (A) and on methane (B).

The peaks of the Si-CH_3 (bending) and of the Si-CH_3 (rocking e wagging) are located at 1250 and 780 cm^{-1} , respectively, as from the work of Wieder and coworkers[5].

The absorption peaks located at 1450, to 2870 and 2910 cm^{-1} correspond to the vibrational modes related to the groups CH_2 (b) and CH_2 (stretching)respectively; these last are present only in the a-SiC:H realized with ethylene. From this Hamakawa deduces that the carbon incorporation in the amorphous silicon obtained by this way happens through ethylic groups (C_2H_5), and through methylic groups (CH_3) in the a-SiC:H in the a-SiC:H obtained by methane. In Fig. 3.11) a model of the structure of the chemical bonds for the two cases is shown.

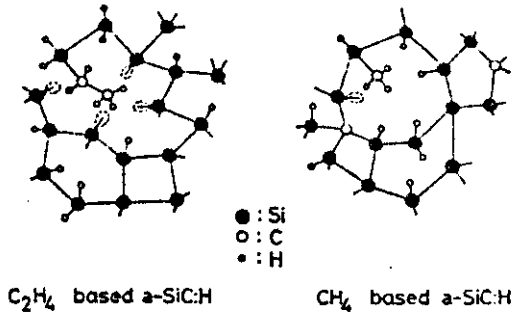

Fig. 3.11) Model of the chemical bond structure in the hydrogenate amorphous silicon-carbide matrix. (left) a-SiC:H based on ethylene; (right) a-SiC:H based on methane.

On this last type of material it is interesting to notice that if the content of methane in the discharge mixing increases, the absorption band placed at 2000 cm^{-1} has the tendency to reduce, while contemporary the band at 2090 cm^{-1} rise up, as it is shown in Fig. 3.12). The Si-H (s) vibrational mode is situated at 2000 cm^{-1} [6], but it is also well known that this tends to move toward bigger wave-numbers[5] if some carbon binds to the silicon; such a move is due to the different electronegativity of the carbon in comparison to the silicon. In fact taking as a reference the work of Lucovsky[7] on the molecular vibration frequencies, and by replacing 1 or 2 first neighbors of carbon with the silicon: 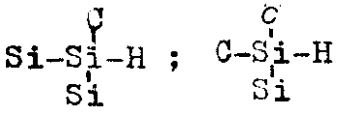 , a value around 2090 cm^{-1} can be obtained for the wave-number.

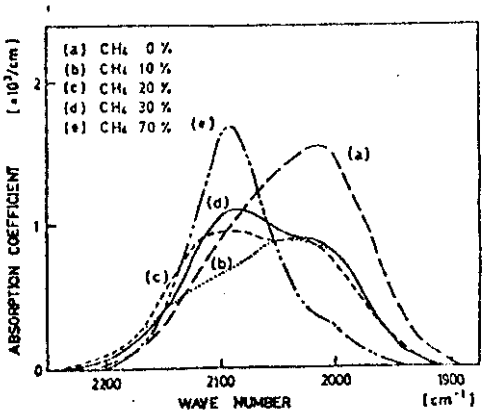

Fig. 3.12) Stretching absorption energy mode of the a-SiC:H film grown at 250ºC.

From this it follows that the increase of the 2090 cm^{-1} band corresponds really to an increase of the bound carbon.

In conclusion, on the basis of what has been seen, to get the best silicon-carbide alloy in which the tetraedrical structure is preserved the methane must be used.

BIBLIOGRAPHY

1 D.A. Anderson - W.E. Spear, Phil. Mag. **35**, 1 (1977)

2 R.S. Sussmann – R. Ogden, Phil. Mag. **44**(b), 137 (1981)

3 Y. Tawada - M. Kondo - H. Okamoto - Y. Hamakawa, Proc. 9th Int. Conf. Am. Liq. Semic., Grenoble (1981)

4 Y. Tawada - E. Tsuge - M. Kondo - H. Okamoto - Y. Hamakawa, J. Appl. Phys. **53**(7), (1982)

5 H. Wieder - M. Cardona - C.R. Guerrieri, Phys. Status Sol. B **92**, 99 (1979)

6 M.H. Brodsky - M. Cardona - J.J. Cuomo, Phys. Rev. B **16**, 3556 (1977)

7 G. Lucovsky, Solid State Comm. **29**, 571 (1979)

8 E.A. Davis – N.F. Mott, Phil. Mag. **22**, 913 (1970)

CHAPTER IV

“SCHOTTKY BARRIER PROFILE”

4.1 INTRODUCTION

The experience acquired so far in the field of the rectifier devices realized through metallic contacts on semiconductors take us to adopt the theory of Schottky (1939) according to which the potential barrier is determined by a uniform space-charge due to the ionized impurities. For this reason these devices are called “Schottky diodes.”

Let us define “work function” the energy necessary to remove an electron from the Fermi level and to bring it to the vacuum level, the limit of the free space.

Let us consider a Schottky diode whose semiconductor is n doped, that is with shallow impurities of the donor type; the potential barrier, that will be indicated by V_{do}, and the relative band bending, caused by the difference between the work functions of the semiconductor and the metal, creates a region in which there are no conduction electrons, as it happens in a p-n junction, that is just called “exhaustion layer” or “space-charge layer” or simply “barrier layer”, and it will be indicated by *W*.

Instead the barrier viewed from the semiconductor to the metal, that we will be indicated by ϕ_b for the electrons and ϕ_h for the holes, comes from the difference between the metal work function ϕ_M and the semiconductor electronic affinity χ_s :

$$\phi_b = \phi_M - \chi_s \quad ; \quad \phi_h = \chi_s + E_g - \phi_M$$

where for “electronic affinity” we intend the necessary energy to remove an electron from the bottom of the conduction band and to take it to the vacuum level.

In practice however it is often noticed that ϕ_b is almost independent from the work function of the metal and this is explained by Bardeen (1947) in terms of existence of the semiconductor surface states caused by the interruption of the bonds, as also by contaminations.

This can be understood by considering a Schottky barrier device with the bands schematized in Fig. 4.1), with the realistic presence of a thin (10 - 20 Å) layer of oxide and supposing to have surface states. The quantity $q\phi_o$ indicates the “neutrality level” at the surface, that is the energetic limit up to which the surface states are filled when it is electrically neutral.

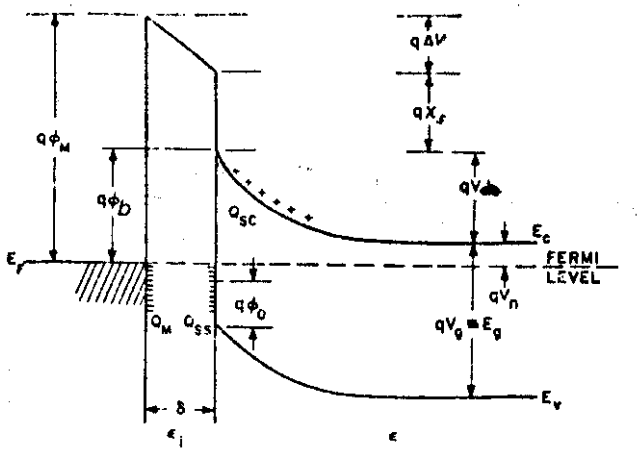

Fig. 4.1) Energy level diagram of a metal/n-doped semiconductor junction. The symbols are explained in the text.

Let us assume a step like Fermi distribution function and a surface density of states D_s constant between ϕ_o and the Fermi level, then the surface charge density will be:

$Q_{ss} = -q\, D_s\, (E_g - q\phi_b - q\phi_o)$,

The space-charge that develops in the semiconductor exhaustion layer will be:

$Q_{sc} = q\, N_B\, W$, if in this case N_B is the density of the donor impurity.

Now, by indicating the exhaustion layer thickness by the expression that will be explained later:

$$W = \left[\frac{2\varepsilon}{qN_B} \left(V_{do} - \frac{KT}{q} \right) \right]^{1/2}$$, where ε is the semiconductor permittivity,

$$Q_{sc} = \left[2qN_B\varepsilon \left(V_{do} - \frac{KT}{q} \right) \right]^{1/2}$$;

and then, as the height of the internal barrier is equal to:

$V_{do} = \phi_o - V_n$ $\qquad (V_n = E_c - E_f)$:

4.1) $$Q_{sc} = \left[2\,\varepsilon\, qN_B \left(\phi_b - V_n - \frac{KT}{q} \right) \right]^{1/2}$$.

By summing Q_{ss} and Q_{sc} we get the total semiconductor charge, which should be equal and opposite to the one created in the metal:

4.2) $Q_M = -(\, Q_{ss} + Q_{sc})$, for which the potential drop ΔV on the thin oxide layer at the interface can be obtained from the Gauss theorem:

4.3) $\frac{\Delta V}{\delta} = -\frac{Q_M}{\varepsilon_i}$, with ε_i equal to the interface oxide permittivity and δ its thickness.

However from the figure 4.1) it is seen that:

4.4) $q\,\Delta V = q\phi_M - \mathrm{q}\,(\phi_b + \chi)$.

By combining now the Eq.s 4.1), 4.2), 4.3) e 4.4) the following expression is obtained:

4.5)

$$q\phi_b = q\left[c_2(\phi_M - \chi) + (1 - c_2)\left(\frac{E_g}{q} - \phi_0\right) - \Delta\phi\right] + \left\{\frac{c_2^2 c_1}{2} - c_2^{3/2}\left[\begin{array}{l} c_1(\phi_M - \chi) + (1 - c_2)\left(\frac{E_g}{q} - \phi_0\right)\frac{c_1}{c_2} - \\ \frac{c_1}{c_2}\left(V_n + \frac{KT}{q}\right) + \frac{c_2 c_1^2}{4} \end{array}\right]^{1/2}\right\}$$

where:

$$c_1 = \frac{2q\varepsilon\, N_B \delta^2}{\varepsilon_i^2} \quad \text{and} \quad c_2 = \frac{\varepsilon_i}{\varepsilon_i + q^2\delta\, D_s} .$$

For $\varepsilon \approx 10\varepsilon_0$; $\varepsilon_i = \varepsilon_0$ (as the thinness of the oxide layer permits); $N_B < 10^{18}$ cm^{-3}, we get $c_1 \cong$ 10 mV, for which the term between braces results lower than the first term and it can be then neglected to write:

4.6) $$q\phi_b = \frac{\varepsilon_i}{\varepsilon_i + q^2\delta\, D_s} q(\phi_M - \chi) + \left(1 - \frac{\varepsilon_i}{\varepsilon_i + q^2\delta\, D_s}\right)(E_g - q\phi_0) .$$

If now the density of the surface states $D_s \to \infty$, then:

4.7) $q\phi_b \Rightarrow (E_g - q\,\phi_0)$, that is the barrier tends to a value in which ϕ_M does not appear, but it has a direct dependence on the semiconductor gap; while if $D_s \to 0$:

4.8) $q\phi_b \Rightarrow \mathrm{q}(\phi_M - \chi)$, that is the ideal case expression.

4.2 BEHAVIOR OF THE POTENTIAL IN THE SCHOTTKY BARRIES

To face a theory of the transport in the metal-semiconductor junction devices it is necessary to study the behavior of the electric field and the potential in such diodes.

For a simple unilateral step junction with a charge density $\rho = qN_B$ for $x < W$ and $\rho \cong 0$ for $x > W$ (N_B is the concentration of the ionized impurities, that we will suppose donor like), the Poisson equation, onlyy for one-dimension for simplicity, becomes:

4.9) $$\frac{-\partial^2 V(x)}{\partial x^2} = \frac{\partial E(x)}{\partial x} = \frac{\rho(x)}{\varepsilon} = q\frac{p(x) - n(x) + N_B^+(x)}{\varepsilon}$$

where $p(x)$ and $n(x)$ are the electron and hole concentration respectively, in the generic position x.

For a junction metal/n-doped semiconductor, with the origin of the coordinates in the point of contact of the two materials [see Fig. 4.2)], and by making use of the "exhaustion layer" approximation (p - n ≅ 0 for 0 <x <W), it will be written:

4.10) $$\frac{\partial E(x)}{\partial x} = \frac{q}{\varepsilon} N_B^+(x) \ .$$

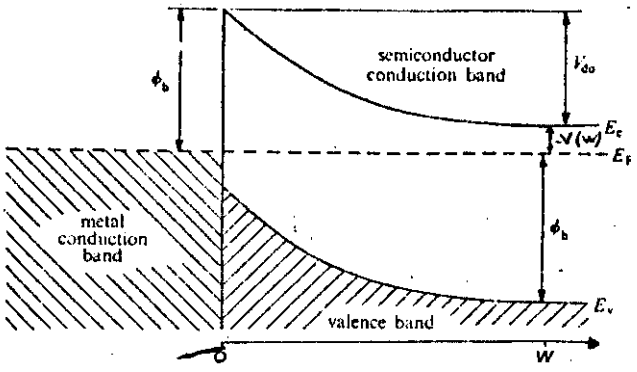

Fig. 4.2) Schottky barrier between metal and n-type semiconductor without polarization.

To get the behavior of the electric field as a function of the depth x, it is necessary to integrate the 4.10) between W and x, that is in the space-charge zone. For simplicity we will suppose that $N_B^+ = N_B = \text{cost}$; then for 0 <x <W it will result that:

4.11) $E(x) = q\frac{N_B}{\varepsilon}(x - W)$, which, integrated again, gives the potential behavior referred

to the Fermi level of the metal:

4.12) $V(x) = q\frac{N_B}{\varepsilon}\left(Wx - \frac{x^2}{2}\right) - \phi_b$, having here neglected the effect of the force-image.

From the 4.12) the internal potential barrier V_{do} can be obtained, being $V_{do} = \phi_b + V(W)$:

4.13) $V_{do} = q\frac{N_B W^2}{2\varepsilon}$; carrying on, the height of the exhaustion layer can be drawn:

4.14) $W = \left|\frac{2\varepsilon}{qN_B}\left(V_{do} - V - \frac{KT}{q}\right)\right|^{1/2}$.

In 4.14) also the term of the potential V of the possible polarization (> 0 for the direct one and < 0 for the inverse one) appears as well as the contribution due to the electric field coming from to the mobile carriers (KT/q).

However everything is valid for crystalline semiconductors.

If we consider the amorphous silicon, the structure of the reasoning is rather different.

Several studies and theoretical models exist on the matter, one of the most interesting of which is the Shur-Cubatyi-Madan's [1].

Following this, we can approximate the density of states in the amorphous silicon forbidden gap by this way:

4.15) $g(E) = g_{\min}\cosh\left(\frac{E}{E_{ch}}\right)$, in which the energy E is measured starting from the center of the gap, where $g = g_{min}$, E_{ch} is a characteristic energy that takes into account the goodness of the material together with g_{min} . Typical values are: $E_{ch} = 10^{-1}$eV, $g_{min} = 10^{16}$eV^{-1}cm^{-3}.

This type of approximation results to be very close to real, as it can be observed by the comparison of Fig. 4.3).

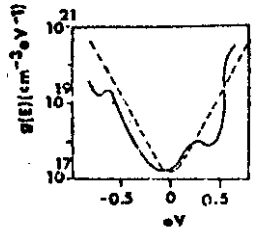

Fig.4.3) Comparison between the analytical expression of $g(E)$ and the real density of state measured by W. Spear and P.G. Le Comber[2].

By expressing the 4.15) in exponential terms:

$$g(E) = \frac{g_{\min}}{2}\left(\exp\left(- \frac{E}{E_{ch}} \right) + \exp\left(\frac{E}{E_{ch}} \right) \right) ;$$

the acceptor like localized states will be described by the first term, that we will call g_p , while the donor like by the second term g_n , that is:

4.16) $$g(E) = \frac{g_{\min}}{2}\left(g_p(E) + g_n(E) \right) .$$

By knowing the values that E_{ch} assumes (100 meV if four time greater than KT at room temperature), we make a negligible error by approximating the Fermi function by a step. Under these conditions the charge density of the donor and acceptor states will be given respectively by:

4.17) $$p^+ = \int_{E_f}^{E_{g/2}} g_n(E)\, dE = \frac{E_{ch}\, g_{\min}}{2}\left(\exp\left(\frac{X_g}{2} \right) - \exp(X_f) \right)$$

4.18) $$n^- = \int_{-E_{g/2}}^{E_f} g_p(E)\, dE = \frac{E_{ch}\, g_{\min}}{2}\left(\exp\left(\frac{X_g}{2} \right) - \exp(- X_f) \right)$$

where $X_g = \frac{E_g}{E_{ch}}$ and E_g is the forbidden energy gap, while X_f is the deviation of the Fermi level from its position in the intrinsic case: $X_f = \frac{E_f - E_{f0}}{E_{ch}}$; here E_{f0} corresponds to zero energy.

Supposing the contribution of the free charges negligible, the density of net charge will come from 4.17) and 4.18):

4.19) $$p^+ - n^- = - g_{\min} E_{ch} \sinh X_f .$$

For the charge neutrality, in case the material is doped with a donor concentration N_D, and also by assuming that at room temperature $N_D \cong N_D^+$:

4.20) $p^+ - n^- + N_D = 0$, therefore the relative Fermi level displacement will be:

4.21) $$X_f = \sinh^{-1}\left(\frac{N_D}{E_{ch}\, g_{\min}} \right) = \sinh^{-1}(\eta) ,$$

where we indicated by

4.22) $\eta = \frac{N_D}{E_{ch}\, g_{\min}}$ the nondimensional doping density.

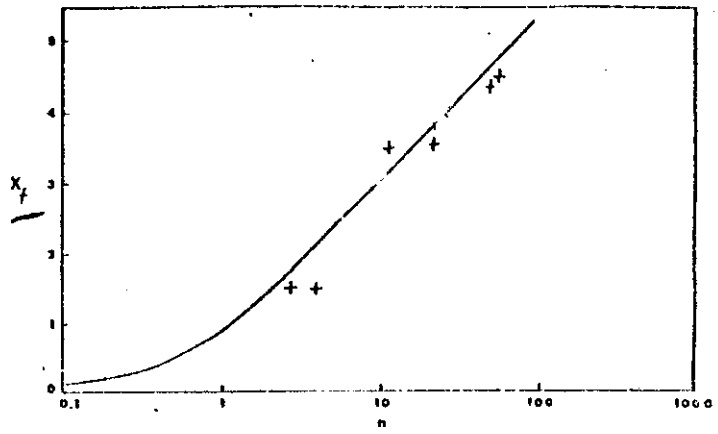

Fig.4.4) Nondimensional Fermi level X_f as a function of the doping density. The data comes from Spear et al. [2].

In figure 4.4) right the 4.21) behavior is shown in comparison to the experimental data of Spear. As it is seen in 4.21) and 4.22), to have an effective doping, the density of states in the gap must be minimized, which means that it is easier to dope a good material then a bad one. This confirms what said in Chapter I about the doping in the amorphous material.

To calculate the behavior of the potential barrier, we must start, as usual, from the Poisson equation:

4.23) $\frac{1}{q}\frac{\partial^2 E_c}{\partial z^2} = \rho(E_c)/\varepsilon_0\varepsilon$, where E_c is the conduction band minimum, z is the spatial coordinate with origin where $E_0 - E_{cb} = (3/2)KT$, E_{cb} is the energy position of the conduction band far from the barrier, ε is the relative permittivity of our material and $\rho(E_c)$ is the density of the space-charge. In our case, by using the 4.19):

4.24) $\rho(E_c) = qN_D + q(p_+ - n_-) = qN_D - qg_{min}E_{ch}\sinh(X_f - X_c)$

with $X_c(z) = \frac{E_c(z) - E_{cb}}{E_{ch}}$.

Again, by substituting $f = \frac{1}{q}\frac{\partial E_c}{\partial z}$ and by taking advantage of the side condition $f = 0$, that is the electric field is null when $E_c(z) = E_{cb} = 0$, the 4.23) can be integrated in energy to get:

4.25) $f = \left(\frac{2}{\varepsilon_0\varepsilon q}\int_0^{E_c}\rho(E_c')dE_c'\right)^{1/2}$; by writing this in terms of the coordinate z and then integrating in energy:

4.26) $$z(E_c) = \int_{E_T}^{E_c} \frac{(\varepsilon_0 \varepsilon / 2q)^{1/2}}{\left(\int_0^{E_c'} \rho(E_c'') dE_c'' \right)} dE_c' \quad .$$

To have taken as the lower extreme $E_T = E_{cb} + 3/2\ KT$ simply means to have lifted the lower limit of integration, this because with $E_T = 0$ the barrier in an intrinsic material would extend to the infinity, as it will be seen later in the 4.30).

From the 4.24) it comes out:

4.27) $$\int_0^{E_c} \rho(E') dE' = qN_D E_c + qg_{\min} E_{ch}^2 \left(\cosh(X_f - X_c) - \cosh(X_f) \right) \quad .$$

By using the coordinate $Y = \frac{z}{z_0}$, where:

4.28) $z_0 = \left(\frac{\varepsilon_0 \varepsilon}{q^2 g_{\min}} \right)^{1/2}$ is a normalization length analogous to the Debye length, by replacing the 4.27) in the 4.26), we get:

4.29) $$Y = (1/2)^{1/2} \int_{X_T}^{X_c} \frac{dX_c'}{\left(\eta X' + \cosh(X_f - X_c') - \cosh(X_f) \right)^{1/2}}$$

where again $X_T = \frac{E_T}{E_{ch}}$ is nondimensional.

For an intrinsic material $\eta = 0$, therefore the 4.29) becomes:

4.30) $$Y = 1/2 \int_{X_T}^{X_c} \frac{dX_c'}{\left(\frac{1}{2} (\cosh(X_c') - 1) \right)^{1/2}} = \ln\left(\tanh\left(\frac{X_c}{4} \right) \right) - \ln\left(\tanh\left(\frac{X_T}{4} \right) \right)$$

which gives the behavior of the minimum of the conduction band when varying the distance from the barrier.

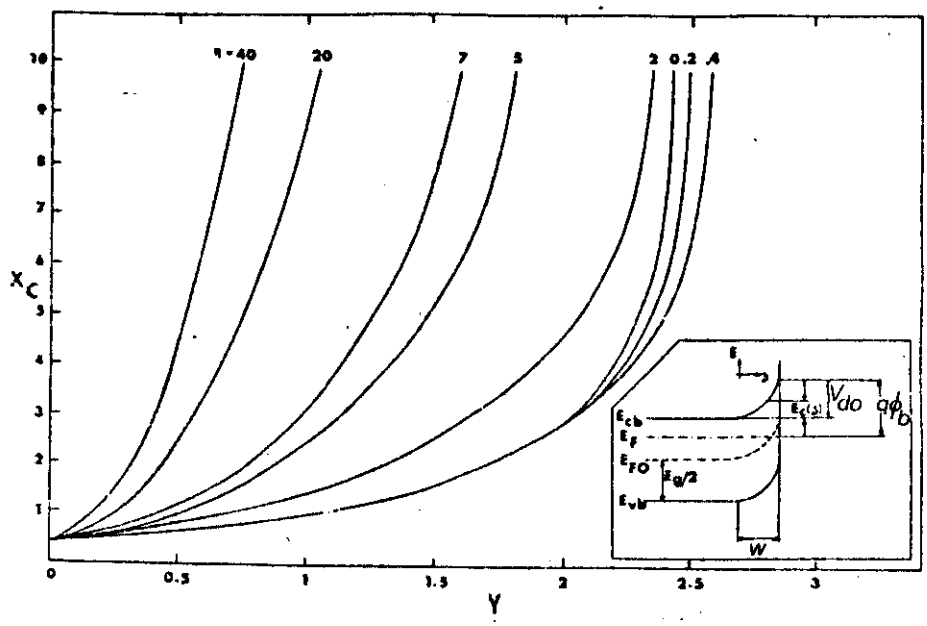

Fig. 4.5) Profile of the Schottky barrier. η is the doping density. The insert shows the qualitative profile of the Schottky barrier. The length of the barrier is expressed by W as usual.

In figure 4.5) such a behavior is shown, together with a band schematic of the Schottky barrier device.

The width of the barrier $W = z_0 Y_b$ can be drawn by Eq. 4.30) by substituting X_c , with

$$X_b = q\frac{V_{do}}{E_{ch}} = \frac{\phi_b - (E_{cb} - E_f)}{E_{ch}} .$$

Eq. 4.30) can be also written in terms of X_c at the first member:

4.31) $\tanh\frac{X_c}{4} = \left(\tanh\frac{X_T}{4}\right)\exp(Y)$, which can be approximated by a behavior like:

4.32) $X_c = cost \cdot \exp(Y)$ only in the case in which $X_c \ll 4$, i.e. $E_c - E_{cb} \ll 4E_{ch} \cong 400$ meV in the a-Si:H case, as calculated by Shur.

This initial exponential behavior can be noticed in Fig. 4.5) for $X_c \ll 4$.

BIBLIOGRAPHY

General: S.M. Sze, “Physics of Semiconductor Devices”, John Wiley and Sons Inc., N.Y. (1969)

1 M. Shur - W. Czubatyj - A. Madan, Sol. En. Mat. **2**, 349 (1980)

2 W. Spear - P.G. Le Comber, Phil. Mag. **33**(6), 935 (1976)

CHAPTER V

“TRANSPORT IN THE SCHOTTKY BARRIER DEVICES”

5.1 THERMIONIC E DIFFUSION THEORIES

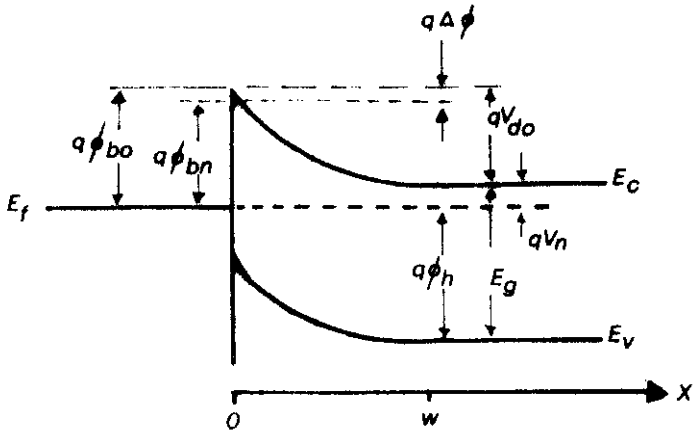

Fig. 5.l) Band schematic of a Schottky barrier.
ϕ_h : potential barrier for holes;
ϕ_{bn} : potential barrier for electrons from M to S;
ϕ_{bo} : asymptotic value of ϕ_{bn} at null electric field;
V_{do} : potential barrier for electrons from S to M;
$\Delta\phi$: barrier lowering caused by the force image;
W : exhaustion layer.

In the Schottky barrier devices, unlike what happens in the p-n junction ones, the transport mechanism of the current is dominated by the majority carriers.

There are various ways to describe such a mechanism, two of which will be examined here:

- the thermionic emission theory due to H.A. Bethe[1] , and
- the Schottky theory of the isothermal diffusion[2].

The theory of Bethe, making reference to the one-dimensional model of figure 5.1), assumes that $q\phi_{bn} \gg KT$, while it neglects the electronic collisions in the exhaustion layer W.

The current that goes from the semiconductor to the metal is immediately obtained from the thermionic emission theory:

$$J_{S\to M} = \frac{qn\left(m^*\right)^{3/2}}{\left(2KT\pi\right)^{3/2}} \int_{-\infty}^{+\infty} dv_y \int_{-\infty}^{+\infty} dv_z \int_{-\infty}^{+\infty} v_x \exp\left(\frac{-m^*\left(v_x^2 + v_y^2 + v_z^2\right)}{2KT}\right) dv_x = \tag{5.1}$$

$$qn\left(\frac{KT}{2\pi\, m^*}\right)^{1/2} \exp\left(\frac{-m^*\left(v_{ox}\right)^2}{2KT}\right)$$

where m^* is the effective mass of the electrons and v_{ox} is the minimum velocity necessary to

overcome the barrier; this is easily calculable from the energetic balance:

5.2) $$\frac{1}{2}m^{*}v_{ox}^{2} = q(v_{do} - v)$$

$v > 0$ for the direct polarization;

$v < 0$ for the inverse polarization.

The majority carriers concentration n under equilibrium is obtained through the statistic of Boltzmann:

5.3) $$n = N_c \exp\left(-\frac{E_c - E_f}{KT}\right), \text{ con } N_c = 2\left(\frac{2\pi m^{*} KT}{h^2}\right)^{3/2}.$$

Let us take into account now:

5.4) $$qV_{do} = q\phi_{bn} + q\Delta_f - qV_n \text{ , where:}$$

5.5) $$qV_n = E_c - E_f .$$

By substituting the two Eq.s 5.2) and 5.3) in the 5.1), we get:

$$J_{S\to M} = \frac{4\pi m^{*} K^2}{h^3} T^2 \exp\left(-\frac{q\phi_{bn} + q\Delta\phi}{KT}\right)\exp\left(\frac{qV}{KT}\right),$$

but neglecting the charge-image effect and putting: $A^{*} = \frac{4\pi qm^{*} K^2}{h^3}$, which coincides with the constant of Richardson for the thermionic emission in the vacuum when free electrons are considered ($m^{*} = m_e$), we have:

5.6) $$J_{S\to M} = A^{*}T^2 \exp\left(-\frac{q\phi_{bn}}{KT}\right)\exp\left(\frac{qV}{KT}\right).$$

To get the current density in the opposite direction it is enough to notice that the height of the barrier for the electrons from the metal to the semiconductor in the ideal case is independent from the applied voltage, from which, having it to be equal to the one flowing from the semiconductor to the metal under conditions of thermal equilibrium, i.e. $V = 0$, it happens that:

5.7) $$J_{M\to S} = -A^{*}T^2 \exp\left(-\frac{q\phi_{bn}}{KT}\right).$$

In order to get the total current density, it is enough to sum the two Eq.s 5.6) e 5.7):

5.8) $$J = A^{*}T^2 \exp\left(-\frac{q\phi_{bn}}{KT}\right)\left(\exp\left(\frac{eV}{KT}\right) - 1\right) = J_{ST}\left(\exp\left(\frac{eV}{KT}\right) - 1\right)$$

by having set:

$$J_{ST} = A^{*} T^2 \exp\left(-\frac{q\varphi_{bn}}{KT}\right)$$: "thermionic inverse saturation current density".

As it easily appears, the behavior as a function of the voltage is the same of the p-n junction.

The theory of Schottky for the diffusion bases itself on the assumptions that the height of the barrier ϕ_{bn} is much greater than *KT,* that the density of the carriers at $x = 0$ and $x = W$ is the same of the equilibrium and therefore it is not altered by the current, and finally that the semiconductor is not so much doped to be degenerate.

Starting then from the "current density equation" still one-dimensional for simplicity and still making reference to the majority carriers, in our case the electrons:

5.9) $$J_{xn} = J = q\left(\mu_n n(x) E + D_n \frac{\partial n(x)}{\partial x} \right) = qD_n \left(- \frac{q}{KT} n(x) \frac{\partial \psi(x)}{\partial x} + \frac{\partial n}{\partial x} \right)$$, where

$D_n = \frac{KT}{q} \mu_n$ is the "diffusion constant" or "Einstein constant" and μ_n is the electron mobility.

However we know that under the working conditions the current density in the exhaustion layer does not depend on the position *x,* for which, by using $\exp\left(- \frac{q\varphi(x)}{KT} \right)$ as the integrating factor, the 5.9) can be integrated in the following way:

$$J \int_0^W \exp\left(- q \frac{\psi(x)}{KT} \right) dx = qD_n \int_0^W \left(- q/KT \, n(x) \frac{\partial \psi(x)}{\partial x} + \frac{\partial n(x)}{\partial x} \right) \exp\left(- \frac{q\psi(x)}{KT} \right) dx =$$

$$qD_n \int_0^W \left(n(x) \frac{\partial}{\partial x} \exp\left(- q \frac{\psi(x)}{KT} \right) \right) = qD_n \left(n(x) \exp\left(- q \frac{\psi(x)}{KT} \right) \right) \Big|_0^W$$

and from it:

5.10) $$J = \frac{qD_n \left(n(W) \exp\left(- q \frac{\psi(W)}{KT} \right) - n(0) \exp\left(- q \frac{\psi(0)}{KT} \right) \right)}{\int_0^W \exp\left(- q \frac{\psi(x)}{KT} \right) dx} .$$

Now, by making use of the side conditions:

$$n(0) = N_c \exp\left(- \frac{E_c(0) - E_f}{KT} \right) = N_c \exp\left(- q \frac{\phi_{bn}}{KT} \right)$$

$$n(W) = N_c \exp\left(- \frac{E_c(W) + E_f}{KT} \right) = N_c \exp\left(- q \frac{V_n}{KT} \right)$$

$q\psi(0) = -q\,\phi_{bn}$

$q\psi(W) = -qV_n - qV$

for the 5.10) we get:

5.11) $$J = qD_n \left(N_c \exp\left(\frac{qV}{KT} \right) - N_c \right) \Big/ \left[\int_0^W \exp\left(- q \frac{\psi(x)}{KT} \right) dx \right] .$$

We already know the behavior of the potential $\psi(x)$ in the Schottky barriers, so we can look for a solution of the 5.11) in the crystalline simpler case:

$$J = qN_c D_n \left(\exp\left(\frac{qV}{KT} \right) - 1 \right) \Bigg/ \left(\int_0^W \exp\left(\frac{q^2 N_D}{\varepsilon KT} \left(\frac{x^2}{2} - Wx \right) \right) \exp\left(\frac{q\phi_{bn}}{KT} \right) dx \right) =$$

$$qN_c D_n \left(\exp\left(\frac{qV}{KT} \right) - 1 \right) \exp\left(- \frac{q\phi_{bn}}{KT} \right) \Bigg/ \left(\exp\left(- \frac{q^2 N_D W^2}{2KT} \right) \cdot \int_0^W \exp\left(\frac{q^2 \left(x - W^2 \right) N_D}{2KT\varepsilon} \right) dx \right)$$

If we remember now the expression of the exhaustion length W in terms of V and V_{do} , we can replace it at the denominator, and then an approximate solution is:

5.12)
$$J \cong \frac{q^2 D_n N_c}{KT} \left(\frac{q(V_{do} - V) 2N_D}{\varepsilon} \right)^{1/2} \exp\left(- \frac{q\phi_{bn}}{KT} \right) \cdot \left(\exp\left(\frac{qV}{KT} \right) - 1 \right) \Bigg/ \left(1 - \exp\left(- \frac{2q(V_{do} - V)}{KT} \right) \right)$$

One of the hypotheses adopted in the handling of the Schottky theory is that qV_{do} is much greater than KT, for which the exponential at the denominator of 5.12) can be neglected respect to 1, to arrive to:

5.13) $$J_D = J_{SD} \left(\exp\left(\frac{qV}{KT} \right) - 1 \right)$$

where $J_{SD} = \frac{q^2 D_n N_c}{KT} \left(q \frac{(V_{do} - V) 2N_D}{\varepsilon} \right)^{1/2} \exp\left(- \frac{q\phi_{bn}}{KT} \right)$ is the "inverse saturation diffusion current density".

We note that also the 5.13) is the ordinary J-V equation of the rectifying device and it is similar to the 5.8), with the difference however that J_{SD} varies with the voltage and J_{ST} is also more sensitive to the temperature than this one.

5.2 THERMIONIC EMISSION AND DIFFUSION THEORIES COMBINED[4]

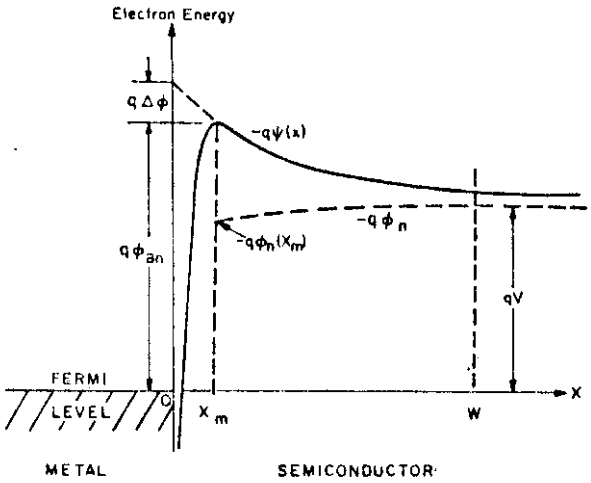

Fig. 5.2) Electronic potential energy of the metal-semiconducor junction.

If the behavior of the potential is analyzed between $x = 0$ and $x = W$, as it is schematized in Fig. 5.2), a theory of the transport can be built that combines the two phenomenons of the thermionic emission and the diffusion previously discussed, by basing onto the possible energetic states where the carrier can be found in, the electron in our case.

The figure put in evidence the effect due to the charge image on the potential of the electron as it approaches to the metal.

By introducing the "quasi Fermi level" ($-q\phi_n$) the expression of the density of the electrons in the generic point x will be:

5.14) $$n(x) = N \exp(-q(\phi_n(x) - \psi(x))/KT) .$$

Consequently we will speak of quasi-Fermi level also for the current density of the electrons. If μ_n is the electron mobility:

5.15) $$J = -q\mu_n n \frac{d\phi_n}{dx} .$$

However this argumentation is possible only where the potential energy does not vary too quickly within the mean free path of the electrons, that is only for $x > x_m$ in our scheme, otherwise the quasi-Fermi level cannot be used.

Anyway in order to continue our study, we can schematize the path between $x = 0$ and $x = x_m$

as the recombination layer for the electrons and we can describe the charge flow at $x = x_m$ by an effective velocity of recombination "v_R", so that:

$J = q(n(x_m) - n_0)v_R$, where n_0 is the electronic concentration of quasi-equilibrium, what it would be if the equilibrium conditions could be reached without altering the height or the position of the maximum of the potential energy. Then, by referring to the Eq. 5.14):

$$n_0 = N_c \exp\left(-\frac{q\phi_{bn}}{KT}\right) \text{, as also:}$$

$$n(x_m) = N_c \exp\left(-q\frac{\phi_n(x_m) - \psi(x_m)}{KT}\right) = N_c \exp\left(-\frac{q\phi_n + q\phi_{bn}}{KT}\right)$$

$$5.16) \quad J = qN_c v_R \exp\left(-\frac{q\phi_{bn}}{KT}\right)\left(\exp\left(-q\frac{\phi_n(x_m)}{KT}\right) - 1\right) .$$

Still the expression $\exp(-q\phi_n(x_m)/KT)$ can be obtained by 5.14) and 5.15):

$$-\frac{J}{q\mu_n \frac{d\phi_n}{dx}} = N_c \exp\left(-q\frac{\phi_n(x) - \psi(x)}{KT}\right) ;$$

$$(-J/q\mu_n N_c)\exp\left(-q\frac{\psi(x)}{KT}\right) = \frac{d\phi_n(x)}{dx}\exp\left(-\frac{q\phi_n(x)}{KT}\right) .$$

Integrating now between the extremes discussed above (x_m and W), and by remembering that J is independent of the position:

$$-\frac{J}{q\mu_n N_c}\int_{x_m}^{W}\exp(-q\psi(x)/KT)dx = \int_{x_m}^{W}\frac{d\phi_n}{dx}\exp(-q\phi_n(x)/KT)dx ;$$

$$-\frac{KT}{q}\int_{x_m}^{W}\frac{d}{dx}\exp(-q\phi_n(x)/KT)dx = \frac{-J}{q\mu_n N_c}\int_{x_m}^{W}\exp(-q\psi(x)/KT)dx .$$

However, from how we chose the reference, $\phi_n(W) = -V$, and therefore:

$$5.17) \quad \exp(-q\phi_n(x_m)/KT) = \exp(qV/KT) - \frac{J}{\mu_n N_c KT}\int_{x_m}^{W}\exp(-q\psi(x)/KT)dx .$$

Eq. 5.16) can be expressed as:

$$J = qN_c v_R \exp(-q\phi_{bn}/KT)\left(\exp(qv/KT) - \frac{J}{\mu_n N_c KT}\int_{x_m}^{W}\exp\left(-\frac{q\psi(x)}{KT}\right)dx - 1\right) =$$

$$qN_c v_R \exp\left(-\frac{q\phi_{bn}}{KT}\right)\left(\exp\left(\frac{qV}{KT}\right) - 1\right) - qv_R J/(\mu_n KT)\int_{x_m}^{W}\exp\left(-q\frac{\psi(x) + \phi_{bn}}{KT}KT\right)dx ;$$

$$J\left(1+\frac{qv_R}{\mu_n KT}\right)\int_{x_m}^{W}\exp\left(-q\frac{\psi(x)+\phi_{bn}}{KT}\right)dx = qN_c v_R \exp\left(-\frac{q\phi_{bn}}{KT}\right)\cdot\left(\exp(qV/KT)-1\right)\ ;$$

5.18) $$J = \frac{qN_c v_R \exp(-q\phi_{bn}/KT)(\exp(qV/KT)-1)}{1-v_R/v_D}$$

by having indicated with

$$v_D = \frac{KT\mu_n}{q\int_{x_m}^{W}\exp\left(-q\frac{\psi(x)+\phi_{bn}}{KT}\right)dx}$$ the effective diffusion velocity of the electrons between W and x_m, by remembering that $\mu_n = \frac{qD_n}{KT}$.

Coming back for a moment to the velocity of recombination, it is easy to notice that in case that no electrons return from the metal, except those associates to the current density qn_0v_R previously seen, the semiconductor is a thermionic emitter and in case of a Maxwellian electronic distribution it results that: $v_R = \frac{A^*T^2}{qN_c}$, where A^* is the famous effective constant of Richardson.

From the 5.18) it is seen that if $v_D \gg v_R$, the process of thermionic emission prevails, if on the contrary $v_R \gg v_D$, the process of diffusion prevails.

The difference between the thermionic emission and the diffusion theories can be understood in a qualitative view by observing the different behavior of the quasi-Fermi level at the interface between the semiconductor and the metal:

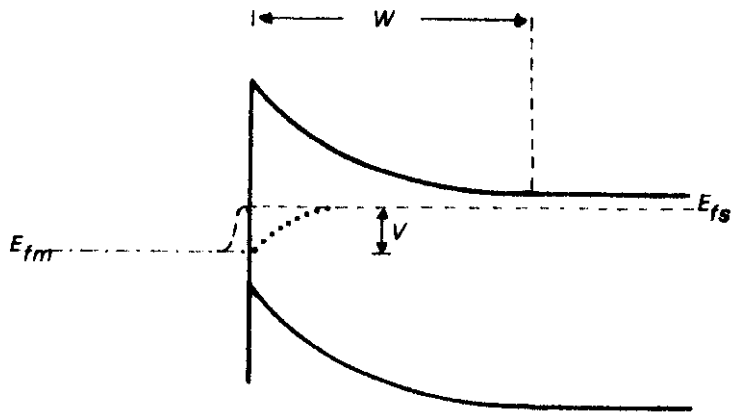

Fig. 5.3) Quasi-Fermi level at the metal-semiconductor interface.
…..… diffusion theory.
------- thermionic emission theory.

In the case of the diffusion theory, by assuming again that the electron concentration near the metal-semiconductor interface is not influenced by the possible polarization, the quasi-Fermi level, after a gradual decay in the space-charge zone, lines up with the Fermi level of the metal, as illustrated in Fig. 5.3).

Instead in the case of the thermionic emission theory, the “hot” electrons penetrate in the metal from the semiconductor and lose their energy down to the thermal equilibrium by colliding with the conducting electrons and with the lattice, therefore in such a case the quasi-Fermi level decays to the Fermi level of the metal only after it is penetrated into it.

A way to put the basis for the diffusive theory of the transport also comes by assuming the width W of the barrier greater than the mean free path of the charged carriers, so that they experience numerous collisions in the barrier zone; generally in the amorphous materials the mean free path of the electrons is rather small, therefore this condition is always verified. This brings to conclude that in the Schottky barrier devices realized with amorphous semiconductors the diffusive rather than the thermionic theory of the transport must be applied [5,6].

5.3) DEVIATION FROM THE IDEALITY

We have seen so far that the equation that connects the current to the voltage in a Schottky barrier diode has the same form of a p-n diode one.

In the ideal case it can be written then:

5.19) $I = I_s\,(\exp(eV/KT) - 1)$.

Indeed there are many phenomenons that make the real *I-V* characteristic to deviate from the 5.19) that forces to adopt an equivalent circuit for our device as the one of Fig. 5.4).

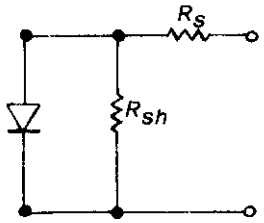

Fig. 5.4) Generic diode equivalent circuit, which shows the "real" characteristics. R_s = series resistance; R_{sh} = shunt resistance.

Then on this basis the real *I-V* characteristic will be written:

5.20) $I = I_s \exp\left(e\left(V - IR_s\right)/\left(nKT\right) - 1\right) + \left(V - IR_s\right)/R_{sh}$

where *n* is the "ideality factor" of the diode.

In the meanwhile we take into consideration right *n*, by saying that it has value 1 for an ideal diode; a deviation from the unity can be the consequence of a dependence of the height of the barrier ϕ_b by the polarization voltage, for instance because of the force image, that indeed in the amorphous silicon is negligible, or for the presence of an oxide at the metal-semiconductor interface as shown in figure 5.5).

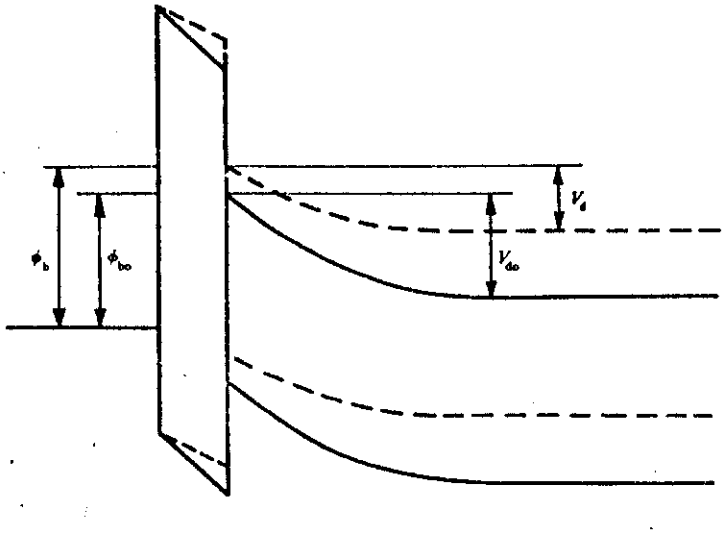

Fig. 5.5) Schottky barrier with an interface layer.
_____ no polarization;
--------- direct pol.^{n} .

Both these phenomenons in fact increase ϕ_b in the situation of direct polarization, in a way that as the voltage increases, the current increases more slowly than it would in the ideal case and this corresponds right to $n > 1$.

To visualize this process we depart from the current-voltage characteristic as it comes from the thermionic theory of the transport:

5.22) $\phi_b(V) = \phi_{bo} + \beta V$, having called ϕ_{bo} the barrier in absence of polarization.

Then the 5.21) will be modified in:

5.23)
$$J = A^* T^2 \exp\left(\frac{-q\phi_{bo}}{KT}\right)\exp\left(\frac{-qV\beta}{KT}\right)\left(\exp(qV/KT) - 1\right) =$$
$$J_0 \exp\left(\frac{-qV\beta}{KT}\right)\left(\exp\left(\frac{qV}{KT}\right) - 1\right) = J_0 \exp\left(\frac{-qV\beta}{KT}(1-\beta)\right) - \exp\left(\frac{-qV\beta}{KT}\right) .$$

If we put now:

5.24) $1 - \beta = 1/n$, that is $\beta = 1 - 1/n$

5.25) $J = J_0 \exp(qV/(nKT))(1 - \exp(-qV/KT))$.

This is the true equation that binds current and voltage in a Schottky barrier device when it depends on the applied voltage. When however we are under the condition in which $V > \frac{3KT}{q}$, the 5.25) can be simplified in:

5.26) $J \approx J_0 \exp(qV/(nKT))$, that is the same expression of the real characteristic of a p-n

junction under the same conditions, where however in that case n keeps into account only the recombinant processes. In effects the recombination phenomenons in the exhaustion layer for the Schottky barriers [see fig. 5.6)] are not appreciable, especially when the barrier ϕ_b is not much greater than half of the gap[7], therefore the relative barrier for the injection of the holes results very big.

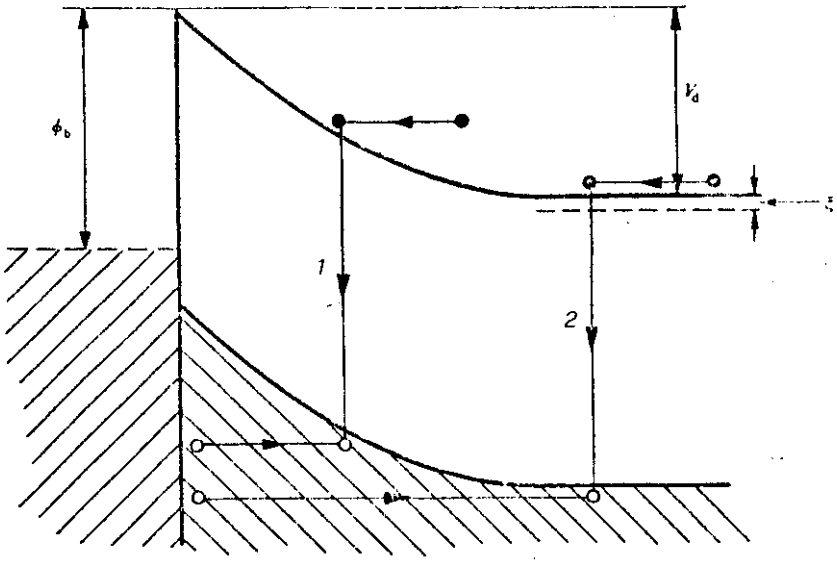

Fig. 5.6) Recombination mechanism in a Schottky barrier.
1: space-charge zone recombination;
2: neutral zone recombination ("holes injection").

An effect on n similar to that caused by a layer of oxide can also come from a "tunneling" process through the barrier V_{do}. The layer of oxide that in direct polarization increased the effective ϕ_b has right the contrary effect in inverse. From this results that no saturation can be reached, as it is shown in Fig. 5.7).

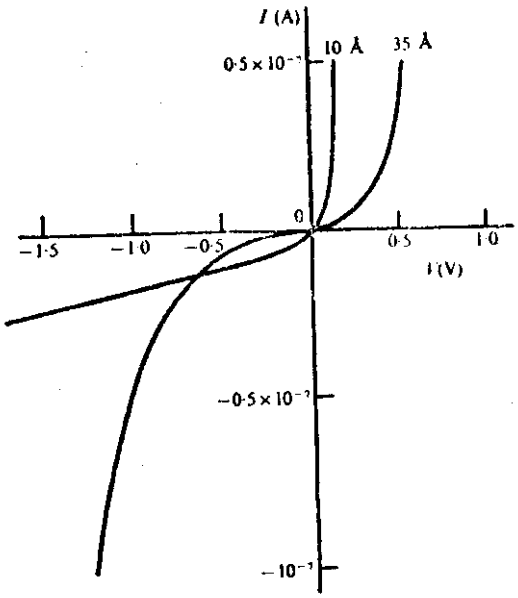

Fig. 5.7) Inverse characteristic of a Schottky diode with the oxide interface layers having different thickness.

An analogous behavior of the inverse current can happen because of the generation of electron-hole couples in the barrier zone "*W*", especially in semiconductors with great forbidden gaps and short life-times such as the amorphous silicon. It is clearly proportional to the width of *W,* therefore by knowing as it varies with the voltage, it is possible to recognize it in the graphic of the inverse *I*(*V*).

The "serial resistance" that appears in the 5.20) derives from a bad realization of the contacts on the device itself, or from a contribution of "sheet resistance" if the evaporated metals are very thin, or again, as in our case, from the high-resistance material as the amorphous silicon is. Its presence in the device is evidenced by the graph "ln *I*(*V*)" through the bending noticed at high direct polarizations [see Fig.5.8)].

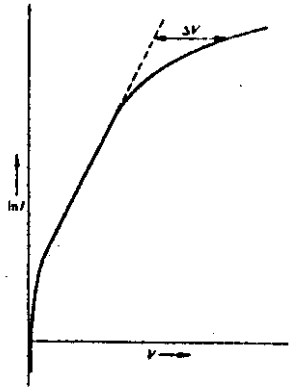

Fig. 5.8) Current/voltage characteristic of a diode showing the serial-resistance effect; ΔV is the potential drop on it.

The eventual "shunt" considered in 5.20) influences the interval of the linear $I(V)$ characteristic around the origin; in fact the current there, instead of remaining null before the knee, could grow with a linear dependence on the voltage [see fig.5.9)] right because of the shunt, the angular coefficient giving $1/R_{sh}$.

In the case of the amorphous a $R_{sh} \neq \infty$ originates from the presence of holes in the less homogeneous film, as well as from a tunnel current in the superficial zones of the devices where the field is more intense and the barrier thinner. This phenomenon hinders the inverse saturation too.

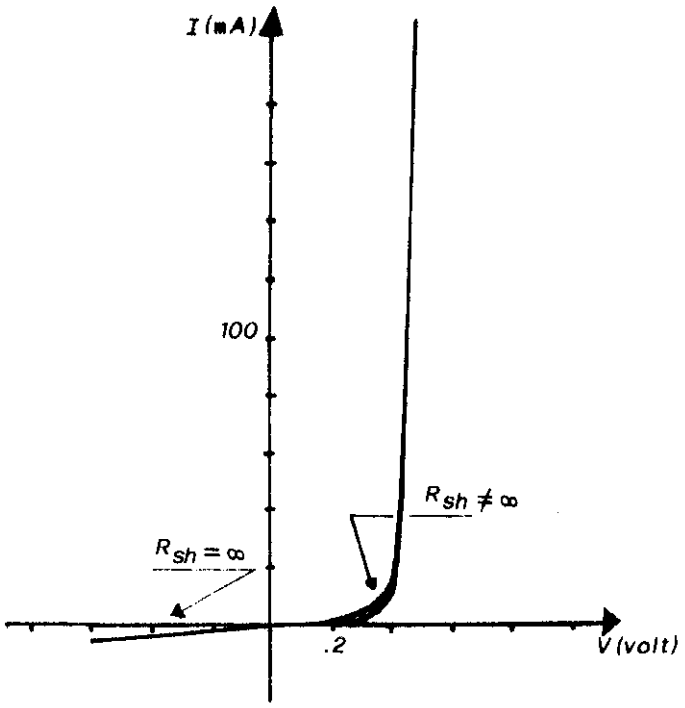

Fig. 5.9) Theoretical $I(V)$ characteristic with the "shunt" resistance effect.

BIBLIOGRAPHY

General E.H. Rhoderick, “Metal-semiconductor contacts”, Clarendon Press - Oxford (1978)

1 H.A. Bethe, “Theory of the Boundary Layer of Crystal Rectifiers’, MIT Radiation Lab. Rep. **43**, 12 (1942)

2 W. Schottky, Naturwiss. **26**, 843 (1933)

3 H.K. Henisch, “Rectifying Semiconductor Contacts’, Oxford Univ. Press, §7.5) (1957)

4 C.R. Crowell - S.M. Sze, “Current Transport in Metal-Semiconductor Barriers”, Sol. State Elect. **9**, 673, (1965)

5 C.R. Wronski - D.E. Carlson - R.E. Daniel, Appl. Phys. Lett. **29**(9), 602 (1976)

6 A. Madan - W.Czubatyi - J. Yang, Appl. Phys. Lett. **40**(3), 234 (1982)

7 C.R. Wronski, J. Appl. Phys. **41**(9), 3805 (1970)

CHAPTER VI

“PHOTOTRANSPORT IN THE AMORPHOUS SILICON SCHOTTKY BARRIER DEVICES”

To reach the equation that governs the phototransport in a junction we have to depart from the "current density equation", that will be written in the following for the electrons and for the holes in only one dimension:

6.1a) $$J_n = e\left(\mu_n nE + D_n \frac{dn}{dx}\right)$$

6.1b) $$J_p = e\left(\mu_p pE - D_p \frac{dp}{dx}\right)$$

here we indicate with μ_n and μ_p the mobilities, with n and p the concentrations of the electrons and the holes, with D the constant of diffusion and with E the electric field.

The first terms at second member of 6.1) represent the drift contribution to the current, while the second terms the one due to the diffusion of the carriers.

On the other hand the "continuity equation" tells us that:

6.2a) $$\frac{d\Delta n}{dt} = \frac{1}{e}\frac{dJ_n}{dx} - R + G$$

6.2b) $$\frac{d\Delta p}{dt} = -\frac{1}{e}\frac{dJ_p}{dx} - R + G$$

where with Δ_n and Δ_p the concentrations of the excess carriers are indicated, with R the term of recombination and with G the generation.

Therefore, for the electrons:

$$\frac{d\Delta n}{dt} = \mu_n \frac{d(nE)}{dx} + D_n \frac{d^2 n}{dx^2} - R + G \;;$$

in stationary condition: $\frac{d\Delta n}{dt} = 0$, and by remembering that $D = \frac{KT}{e}\mu$:

$$D_n\left(\frac{e}{KT}\frac{d(nE)}{dx} + \frac{d^2 n}{dx^2}\right) - R + G = 0 \;;$$

$$D_n \frac{d}{dx}\left(\frac{e}{KT}nE + \frac{dn}{dx}\right) - R + G = 0 \;.$$

Similarly for the holes:

$$D_p \frac{d}{dx}\left(\frac{dp}{dx} - \frac{e}{KT}pE\right) - R + G = 0 \;.$$

From the "Shockley-Read-Hall" equation[1] (valid for recombination through a single center) we know that the recombinant term is:

6.5) $$R = \frac{dn}{dt} = \frac{dp}{dt} = -\frac{np - n_i^2}{n\tau_p + p\tau_n} \;,$$

where n_i is the concentration of the carriers ($n = p \equiv n_i$) in the intrinsic case and with τ_n and τ_p the life times of the electrons and the holes.

It is evident now that if we insert the 6.5) in the 6.3) and in the 6.4), we will not get an analytical solution, but only a numerical one. However approximate methods exist in which simpler expressions for R are used.

Particularly one of these[2] is applied to the amorphous silicon and it implies that in such a material:

I) the recombination of the carriers happens through the recombination centers in the forbidden gap;

II) the density of the photo-generated carriers is greater than the one thermically generated: $np > n_i^2 = n_0 p_0$;

III) the electron density is greater than the holes one; assumption reasonable unless near to the surface.

By these assumptions the 6.5) becomes:

6.6) $R \cong -\frac{np}{n\tau_p + p\tau_n}$, which, if $\tau_p \sim \tau_n$ is taken, will be written:

6.7) $R = -\frac{p}{\tau_p}$.

By this way the process of the electron-hole recombination is governed by the density of the holes for a large part of the volume of the sample. The number of the recombination centers can be supposed constant along the whole sample so that to consider in this way also the recombination kinematics of the holes and to take in conclusion τ_p as a constant.

However to reach the solution of the transport equations 6.3) and 6.4), the road is very crooked and difficult and at last not suitable for an immediate comparison with the experience.

A good description of the spectral response can be gotten by neglecting this term of recombination; in effects this is permitted when the electric fields are high. By this way an analytical solution of the system of differential equations 6.3), 6.4) can be reached in a relatively simple way.

We see how it happens by following the work of Gutkowicz and coworkers[3].

Let us call:

6.8) $E = -\frac{dV}{dx} = V_0 \frac{df(x)}{dx}$, where V_0 is the maximum internal potential and $f(x)$ the potential profile.

6.9) $z = \frac{x}{L}; \quad N(z) = \frac{nD_n}{G_0 L}; \quad P(z) = \frac{pD_p}{G_0 L}$ will be the new variables where the thickness of the film of the amorphous silicon L, the constant of diffusion D and the flow of the photons incident on the surface ($x = 0$) G_0 have been put. Then we will have for the 6.3) the new expression:

6.10) $$\frac{G_0}{L}\frac{d}{dz}\left(\frac{dN}{dz} + \frac{eV_0}{KT}N\frac{df}{dz}\right) + G(z) = 0 \ ;$$

by expliciting then $G(z) = \alpha(\lambda)\, G_0\, g(z,\lambda)$ the 6.10) becomes:

6.11) $$\frac{d}{dz}\left(\frac{dN}{dz} + \varepsilon N\frac{df}{dz}\right) + \alpha(\lambda) L g(z,\lambda) = 0$$, where we put $\varepsilon = eV_0/KT$ and we called with $\alpha(\lambda)$ the absorption coefficient and with $g(z,\lambda)$ the absorption profile of the incident light.

Now the "absorptive" side conditions can be introduced, which are valid for ohmic or ideal metal-semiconductor contacts:

6.12) $N(z=0) = N(z=1) = P(z=0) = P(z=1) = 0$.

The 6.11) can be integrated for a first time between 0 and z, to get:

6.13) $$\frac{dN}{dz} + N\frac{df}{dz} - A^+ + \alpha L\int_0^z g(z')dz' = 0$$, with indicated by $A^+ = \left.\frac{dN}{dz}\right|_{z=0}$ a term that is proportional to the electron current density at the surface.

If this is multiplied by the factor $\exp(\varepsilon f)$:

$$\frac{dN}{dz}\exp(\varepsilon f) + N\frac{df}{dz}\exp(\varepsilon f) - A^+\exp(\varepsilon f) + \alpha L\exp(\varepsilon f)\int_0^z g(z')dz' = 0$$

we see that the first terms can be reduced to only one derivative:

$\frac{d}{dz}\left(N\exp(\varepsilon f)\right)$, for which if we integrate once again it remains:

6.14) $$N(z)\exp(\varepsilon f(z)) + \alpha L\int_0^z dz'\exp(\varepsilon f(z'))\int_0^{z'} g(z'')dz'' - A^+\int_0^z \exp(\varepsilon f(z'))dz' = 0 \ ;$$

from which:

6.15) $$N_z = \exp(-\varepsilon f(z))\left(A^+\int_0^z \exp(\varepsilon f(z'))dz' - \alpha L\int_0^z dz'\exp(\varepsilon f(z'))\int g(z'')dz''\right) .$$

The discourse is similar as it concerns the holes. With the usual choices we have:

6.16) $$\frac{d}{dz}\left(\frac{dP}{dz} - \varepsilon P\frac{df}{dz}\right) + \alpha(\lambda) L g(z,\lambda) = 0$$; such an expression can be integrated with the same side conditions:

6.17) $\frac{dP}{dz} - \varepsilon P\frac{df}{dz} - A^{+} + \alpha L\int_0^z g(z')dz' = 0$; having indicated by

$A^{-} = \left(\frac{dP}{dz}\right)\Big|_{z=0}$ a term proportional to the density of the current of the holes at the surface.

Then by multiplying all for the integral factor $\exp(-\varepsilon f)$, the 6.17) can be written:

$$\frac{d\left(P\exp(-\varepsilon f)\right)}{dz} + \alpha L\exp(-\varepsilon f)\int_0^z g(z')dz' - A^{-}\exp(-\varepsilon f) = 0 \ ;$$

and in conclusion from a further integration we get:

6.18) $$P(z) = \exp(\varepsilon f(z))\left(A^{-}\int_0^z \exp(-\varepsilon f(z'))dz' - \alpha L\int_0^z dz'\exp(-\varepsilon f(z'))\int_0^{z'} g(z'')dz'' \right) .$$

The integrating constants A^{+} ed A^{-} can be easily obtained from the side conditions $N(1) = 0$ and $P(1) = 0$ respectively:

$$0 = \exp(-\varepsilon f(1))\left(A^{+}\int_0^1 \exp(\varepsilon f(z))dz - \alpha L\int_0^1 dz\exp(\varepsilon f(z))\int_0^z g(z')dz' \right) ;$$

6.19) $$A^{+} = \alpha L\int_0^1 dz\exp(\varepsilon f(z))\int_0^z g(z')dz' \Big/ \int_0^1 \exp(\varepsilon f(z))dz$$; again:

$$0 = \exp(-\varepsilon f(1))\left(A^{-}\int_0^1 \exp(-\varepsilon f(z))dz - \alpha L\int_0^1 dz\exp(-\varepsilon f(z))\int_0^z g(z')dz' \right)$$; therefore

6.20) $$A^{-} = \alpha L\int_0^1 dz\exp(-\varepsilon f(z))\int_0^z g(z')dz' \Big/ \int_0^1 \exp(-\varepsilon f(z))dz .$$

By the adoption of the non-dimensional variables the equations 6.1) now will be written:

6.21a) $$J_n = eG_0\left(\varepsilon\frac{df}{dz}N + \frac{dN}{dz} \right)$$

6.21b) $$J_p = eG_0\left(\varepsilon\frac{df}{dz}P + \frac{dP}{dz} \right) .$$

Let us insert now the expressions of the found concentrations of electrons and holes:

$$J_n(z) = eG_0\left(\cancel{\varepsilon\frac{df}{dz}}N - \cancel{\varepsilon\frac{df}{dz}}N + \exp(-\varepsilon f(z)) \right)\left(A^{+}\exp(\varepsilon f(z)) - \alpha L\exp(\varepsilon f(z))\int_0^z g(z')dz' \right) ;$$

6.22) $$J_n(z) = eG_0\left(A^{+} - \alpha L\int_0^z g(z')dz' \right) .$$

$$J_p(z) = eG_0\left(\cancel{\varepsilon\frac{df}{dz}}P - \cancel{\varepsilon\frac{df}{dz}}P + \exp(\varepsilon f(z)) \right)\left(A^{-}\exp(-\varepsilon f(z)) - \alpha L\exp(-\varepsilon f(z))\int_0^z g(z')dz' \right) ;$$

6.23) $$J_p(z) = eG_0\left(\alpha L \int_0^z g(z')dz' - A^- \right) .$$

The total density of current can be now obtained from the sum of the 6.22) and 6.23), with the sign that competes by the chosen reference:

6.24) $-(J_n + J_p) = eG_0(A^- - A^+) = J_{tot}$.

As noticed, this is constant as the position z in the sample is changed as it must be, since the current has to be solenoidal.

Now it remains to give the correct values to the adopted constants. Wronski and coworkers set V_0 = 0.45 V following their previous experimental measurements; they assume an exponential profile of the potential in the exhaustion layer: $f(z) = \exp(-\delta Lz)$, with $\delta = 5 \cdot 10^{-4}$ cm^{-1} as they calculated it by capacitive measurements.

In the model adopted by Shur for the density of states in the gap of the amorphous silicon, we saw in Chapter IV that the potential behavior is acceptable for values smaller than 0.4 V, but Wronski in its article noticed that using also other reasonable potential profiles he got essentially the same results.

By neglecting the internal reflection of the back contact, that can have influence only in the long wavelengths zone, he placed $g(z,\lambda) = \exp(-\alpha(\lambda)Lz)$.

The Wronski's results are illustrated in the two Fig.s 6.1) and 6.2). Particularly from the 6.1) it is noticed that the maxima of the concentrations of the photogenerated electrons and holes are set in opposite positions, this because the electrons and the holes travel in opposite directions under the action of the electric field.

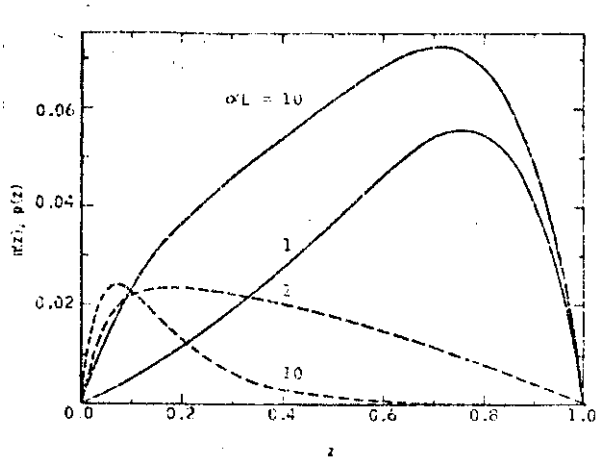

Fig. 6.1) Nondimensional electron and holes density as a function of the z position for two αL values.

In figure 6.2) the collection efficiency $\eta = \frac{J_{tot}}{eG_0}$ calculated by the described model is compared with the one of a Pd(≅100Å)/a-Si:H(≅2500Å) Schottky barrier device as obtained from the spectrum of the short-circuit current and corrected in order to take into account of the reflection from the Pd contact.

The η decrement at long wavelengths is mainly due to the diminution of the absorption coefficient in such a region.

Instead the decrement at short wavelengths is mainly due to the thermal diffusion of the electrons toward the front surface, that is in direction opposite to the field of the junction. This is due to the assumption of a totally absorptive [$n(z=0) = 0$] side condition.

It can be noted that the behavior of the $\eta(\lambda)$ well suits the experimental data.

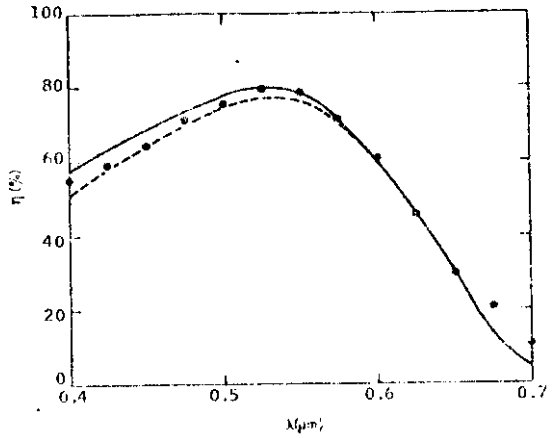

Fig. 6.2) Carriers collection efficiency η as a function of the wavelength; the hatches show the charge-image effect onto the theoretical behavior (continuous line). The points are the experimental data.

BIBLIOGRAPHY

1 J.L. Moll, “Physics of Semiconductors”, Mc Graw-Hill, New York (1964)

2 D. Gutkowicz-Krusin, Appl. Physics Lett. **52**(8), 5370 (1981)

3 O. Gutkowicz-Krusin - C.R. Wronski - T. Tiedje, Appl. Physics Lett. **38**(2), 87 (1981)

CHAPTER VII

“a–SiC:H - a–Si:H ETEROJUNCTIONS”

The etherojunctions are junctions between two semiconductors with different forbidden bands.

In the case of crystalline solids the origin of the band scheme of an ideal step etherojunction is described in the followings in the hypothesis that the material 1 with wider gap is of p type and the material 2 of n type.

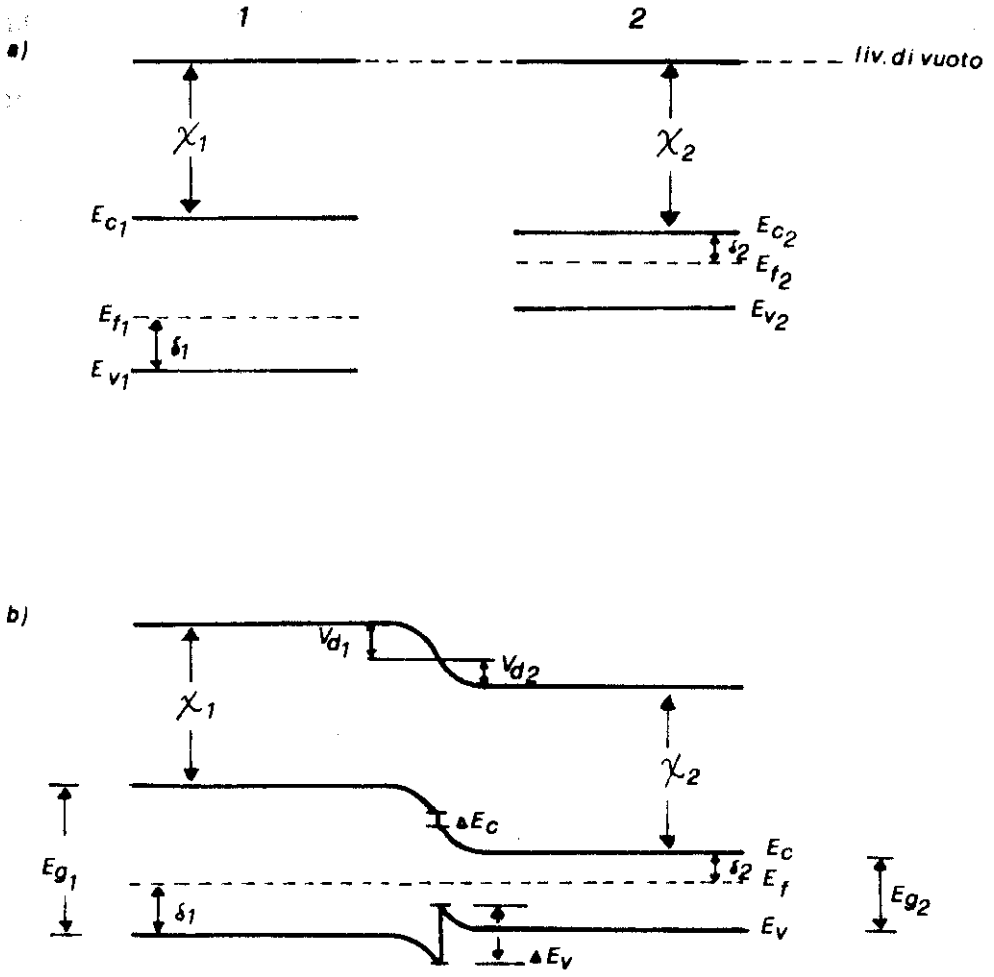

Fig. 7.1) Etherostructure construction.

In Fig. 7.la) the energy band schematics for two isolated semiconductors are shown; they are compared making the vacuum level as the reference.

When they are put on contact, the Fermi levels, that are indeed the chemical potentials of the two materials, have to line up for establishing the equilibrium. This extracts the electrons from the semiconductor 2 and accumulates them into the semiconductor 1, inducing the band bending:

7.1) $V_{d1} + V_{d2} = E_{f2} - E_{f1}$

The discontinuity expression ΔE_c in the conduction band is easily obtainable from the graphic:

7.2) $\Delta E_c = \chi_2 - \chi_1$.

For the discontinuity ΔE_v in the valence band the game is again simple, there is only the forbidden gap involved

7.3) $\Delta E_v = \chi_1 + E_{g1} - (\chi_2 + E_{g2}) = E_{g1} - E_{g2} - (\chi_2 - \chi_1)$.

The result coming from 7.2) e 7.3) is obvious:

7.4) $\Delta E_c + \Delta E_v = E_{g1} - E_{g2}$.

The etherojunctions between amorphous materials became important recently with the realization of a-Si_xC_{1-x}:H films that can be doped p or n and that have the height of the gap depending on the carbon content. It can reach up to 2.5 eV.

However it is rather difficult to construct an exact band model for these etherojunctions in order to understand the entity of the discontinuities in the valence and in the conduction bands.

An indirect way to understand the disposition of the bands has been adopted by Tawada, Hamakawa and coworkers[1] by analyzing the collection efficiency of the carriers (number of electron-holes couples accumulated at the contacts / number of incident photons) of their a-SiC:H(p) – a-Si:H(i) etherojunction p-i-n solar cells. They saw the collection efficiency at 400 nm wavelength practically doubled in comparison to an homojunction of the same type, while it was increased only of 20% at 550 nm and it was practically unchanged at higher wavelengths. Besides to the simple window-effect ought to the joint of two materials of different gaps, they claimed there was another important cause that justified such an increase: the presence of a barrier in the conduction band that stopped the back-diffusion of the electrons that were created with the holes in the intrinsic layer under the junction field.

The physical structure of the Tawada and Hamakawa device and the bands scheme adopted in their theory is shown in Fig. 7.2) together with the path of the carriers photogenerated in the exhaustion layer of the cell.

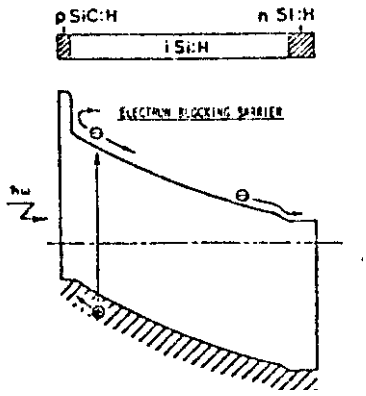

Fig. 7.2) Energy band profile of a heterojuction solar cell made by Tawada e Hamakawa by a-SiC:H (p) – a-Si:H (i).

The influence of the barrier that stops the electrons especially at lower wavelengths of the incident light is big, because the absorption at such a value of the photonic energy is high in this material and therefore it depletes the photons in a thickness next to the illuminated surface.

Again, from a spectral analysis Tawada and collaborators noticed that for the same type of silicon-carbide etherojunction devices obtained by ethylene instead of methane, the collection efficiency resulted rather lower; moreover, normalizing the maximum of the efficiency with that got with the other device, the spectrum coincided perfectly. Therefore they argued that the discontinuity in such a case was in the valence band, blocking the holes.

In Fig. 7.3) the comparison between the collection efficiencies of the homojunction and etherojunction silicon-carbide based amorphous p-i-n cells obtained by using methane or ethylene is shown.

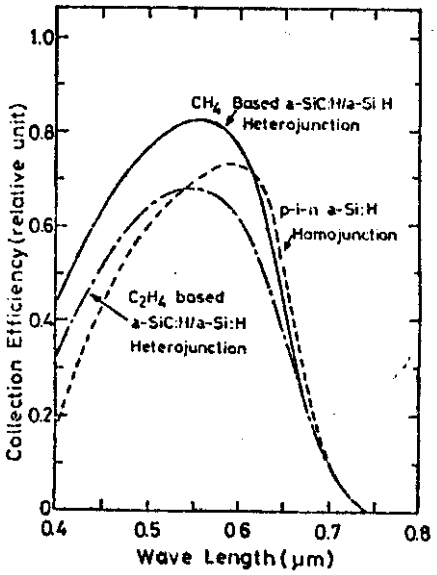

Fig. 7.3) Spectra of the collection efficiency for the etherojunction and homojunction solar cells, the p-i-n type.

A new use of the heterojunction properties is developed in the present Thesis work, with the aim to decrease the Schottky diodes saturation current and to get a spectral response manageable by the inverse polarization (see the following chapters).

BIBLIOGRAPHY

General: S.M. Sze, “Physics of Semiconductor Devices”, John Wiley and Sons Inc., N.Y. (1969)

1 Y. Tawada - K. Tsuge - M. Kondo - K. Nishimura - H. Okamoto - Y. Hamakawa, Proc. IVth Int. Phot. Sol. Ener. Conf. - Stresa, 698 (1982)

CHAPTER VIII

“EXPERIMENTAL RESULTS”

8.1 REALIZATION OF Pd/a–Si:H(i)/a–Si:H(n^+)/Cr SCHOTTKY BARRIER DEVICES

The schematic of Fig. 8.1) illustrates the succession of layers of material necessary for the realization of the Schottky barrier diode with the hydrogenated amorphous silicon.

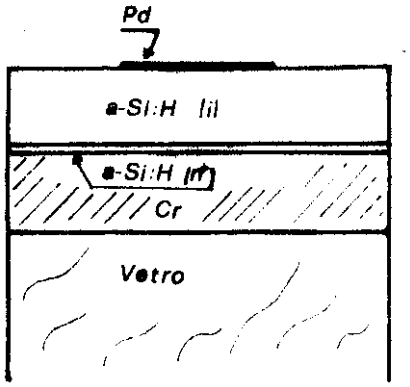

Fig. 8.l) Schematic not in scale of the succession of material layers composing our device.

On a glass substrate under a vacuum of di $l0^{-6}$ torr a layer of Cr (≅0.5 μm) is evaporated, which will act as the back contact. Later, everything is put into the G.D. deposition instrument, which it has been written of previously, and a first layer of heavily doped a-Si:H is deposited to make the chrome ohmic contact. For this purpose inside the reactor a mixture of SiH_4 + PH_3 flows in the 100 ÷ 1 ratio respectively together with H_2 where it represents the 90% of the total gas.

Under the following conditions: temperature of the substrate T_s = 250°C, pressure in the quartz bell p = 1 torr, gas flow ϕ = 10 sccm and power density w = (0.3 - 0.5) W/cm^2, it takes 5 minutes of discharge to get a thickness of material around 300 Å; this means 60 Å/min speed growth.

The next layer of intrinsic amorphous silicon is realized with a mixture of SiH_4 and H_2 (1 ÷ 9) under the same conditions as before, but for a longer time in order to get a layer of thickness between 3000 Å and l μm; in this case the velocity of deposition is slightly higher (75 Å/min).

Finally the grown sample is removed from the G.D. and put again in the evaporator under the vacuum for the deposition of the metal, that in our case is a semitransparent palladium (≅ 100 Å:

Transmission ≅ 60%) . The area of the device is 7 mm^2.

In Fig. 8.2) an *I-V* characteristic is shown with the effect of the sample contamination by the walls of the G.D. reactor, as explained in Chapter II. Near to a first "normal" behavior, even if affected by a strong R_s, there is a second exponential behavior that modulates the first one. This effect has been eliminated improving the cleaning of the system (see Chapt. II).

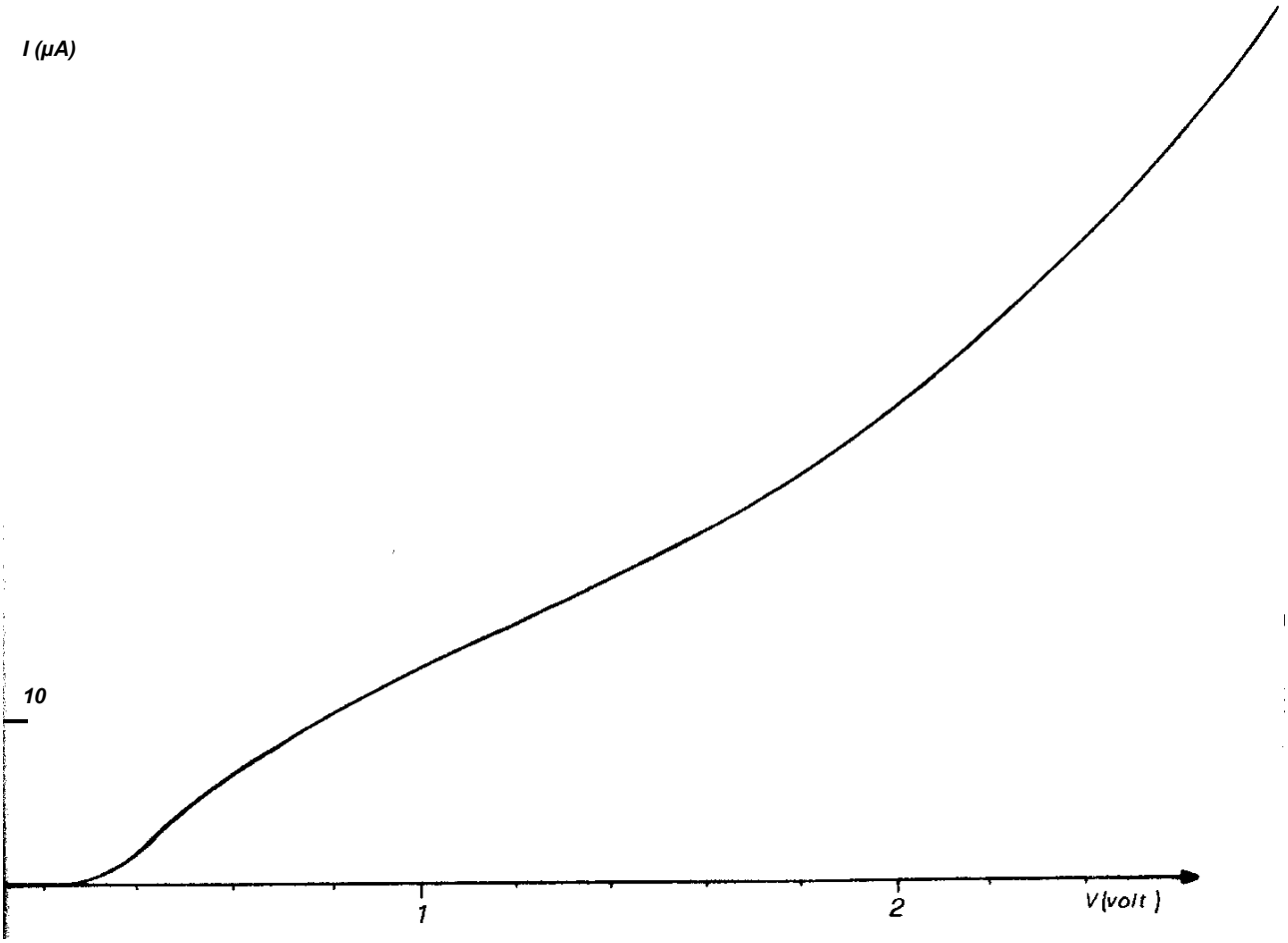

Fig. 8.2) Current-voltage characteristic of a Schottky barrier device realized by us on amorphous silicon. It illustrates the effect of the contamination of the material grown in the G.D. by the walls of the reaction chamber. This effect has also been noticed by others[1].

In these devices the optimal thickness of the intrinsic amorphous silicon layer was 3000 Å, because thicker champions showed a very strong series resistance that worsened the rectification ratio. This was due to the layer of material, in series to our device, not covered by the field of the junction. The very elevated resistivity(10^8-10^9 Ω·cm at room temperature) explained the size of the effect.

In Fig. 8.3) the effect of the series resistance on the *I-V* characteristic is shown. The value of

it (R_s) can be calculated by the angular coefficient of the straight line extrapolated at high direct polarizations: $\mathrm{tg}\alpha = 1/R_s$. In this case: $R_s = (570 \pm 20)\Omega$.

From the characteristic around the origin the presence of a small "shunt" is noticed: $R_{shunt} = (4.2 \pm 0.1)\cdot 10^4\ \Omega$.

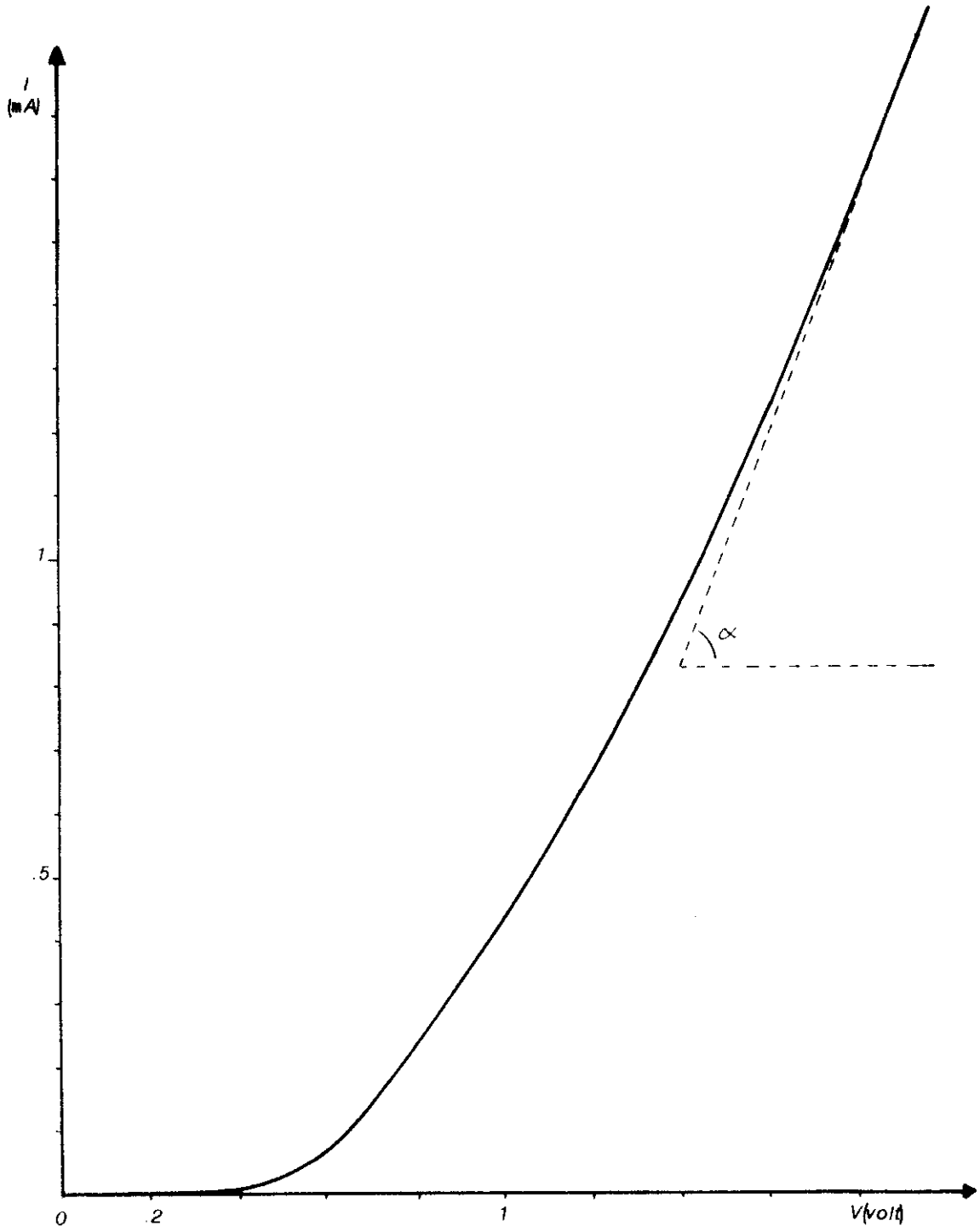

Fig. 8.3) *I-V* Characteristic showing the R_s effect and the method adopted for the calculation of it.

In Fig. 3.4) the behavior of ln $I(V)$ of the same sample is shown. As we know, the linear slope, that extends for two orders of magnitude of the current, comes from the fact that for V> 0.1 Volts the equation of the diode is essentially given by:

$I = I_0 \exp[(eV/(nKT)]$.

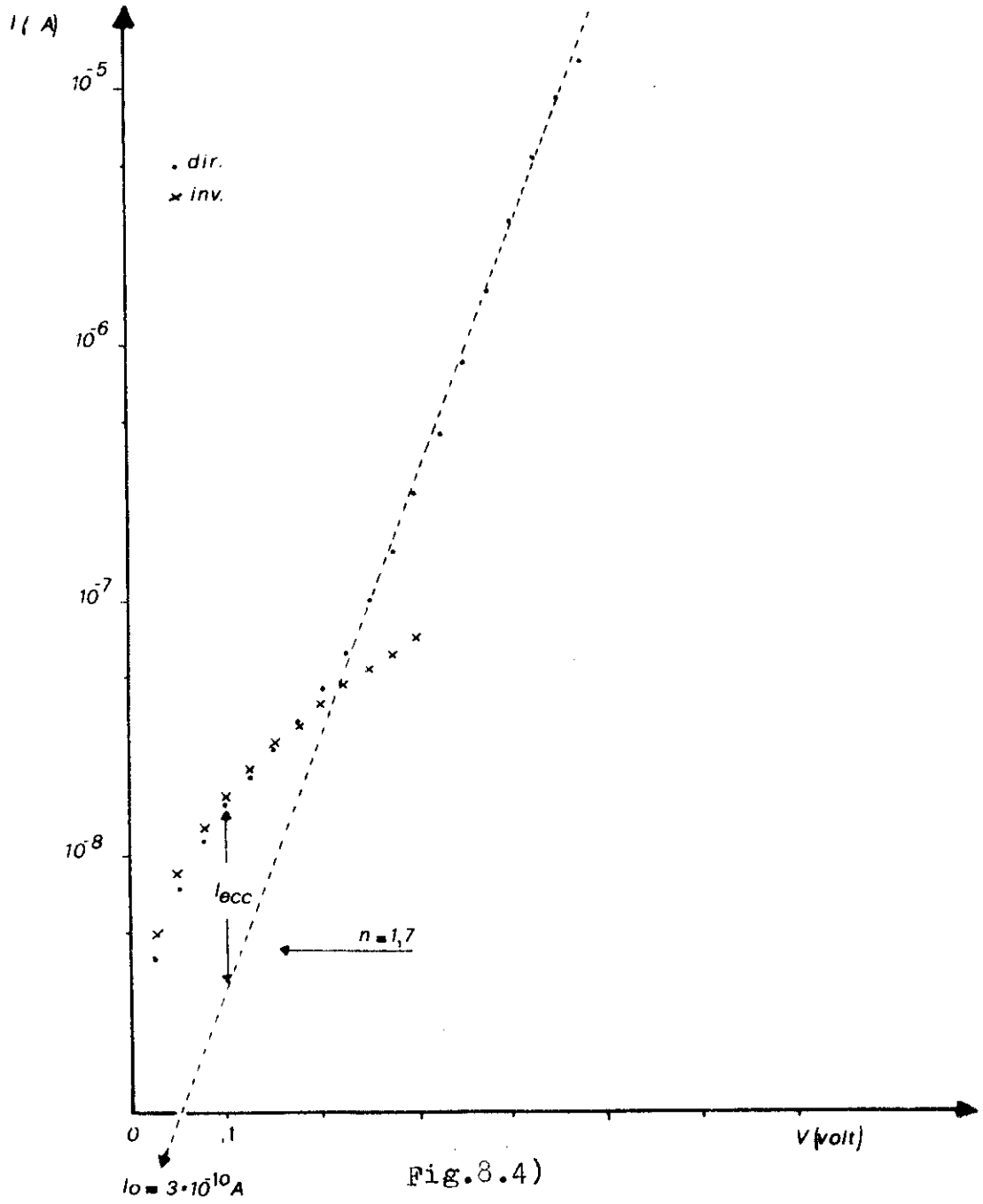

Fig.8.4)

From this semilogarithmic graphic the ideality factor "n" $\left(n = \frac{e}{KT}\frac{V}{\ln(I/I_0)} \right)$ and the saturation inverse current "I_0" ($I(V) = I_0$ when $V = 0$) can be extracted; in this case: $n = 1.7$ e $I_0 = 3\cdot10^{-10}A \Rightarrow J_0 = \frac{3\cdot10^{-10}}{7\cdot10^{-2}}$ A/cm^2 = $4.3\cdot10^{-9}$ A/cm^2. A first path of the inverse characteristic is shown there marked by the "x" symbols.

An analysis of the current has been effected on these samples while varying the temperature. In Fig. 8.5) such behavior is visualized. The variation of the series resistance appears immediate, which passes from about 800Ω at 280K to about 2KΩ at 220K; contemporary the R_{sh} increases too.

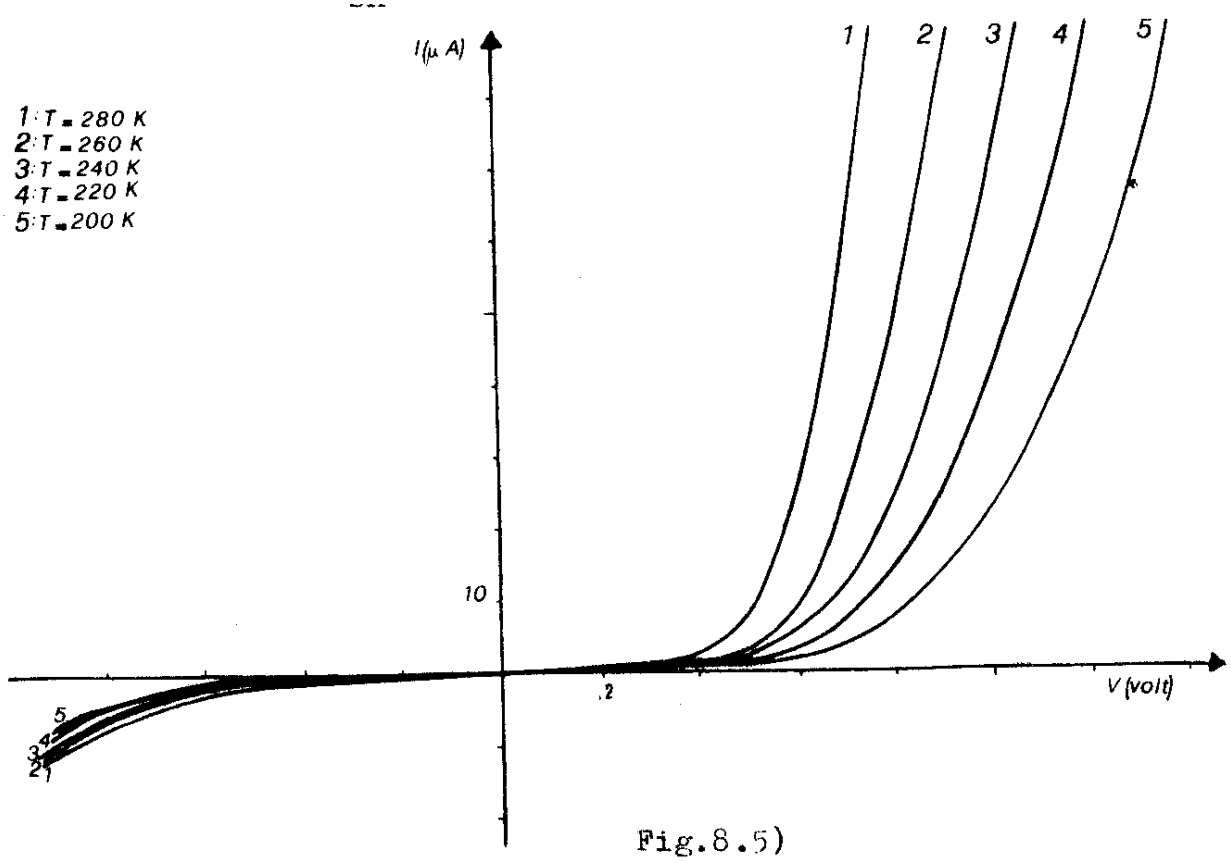

Fig.8.5)

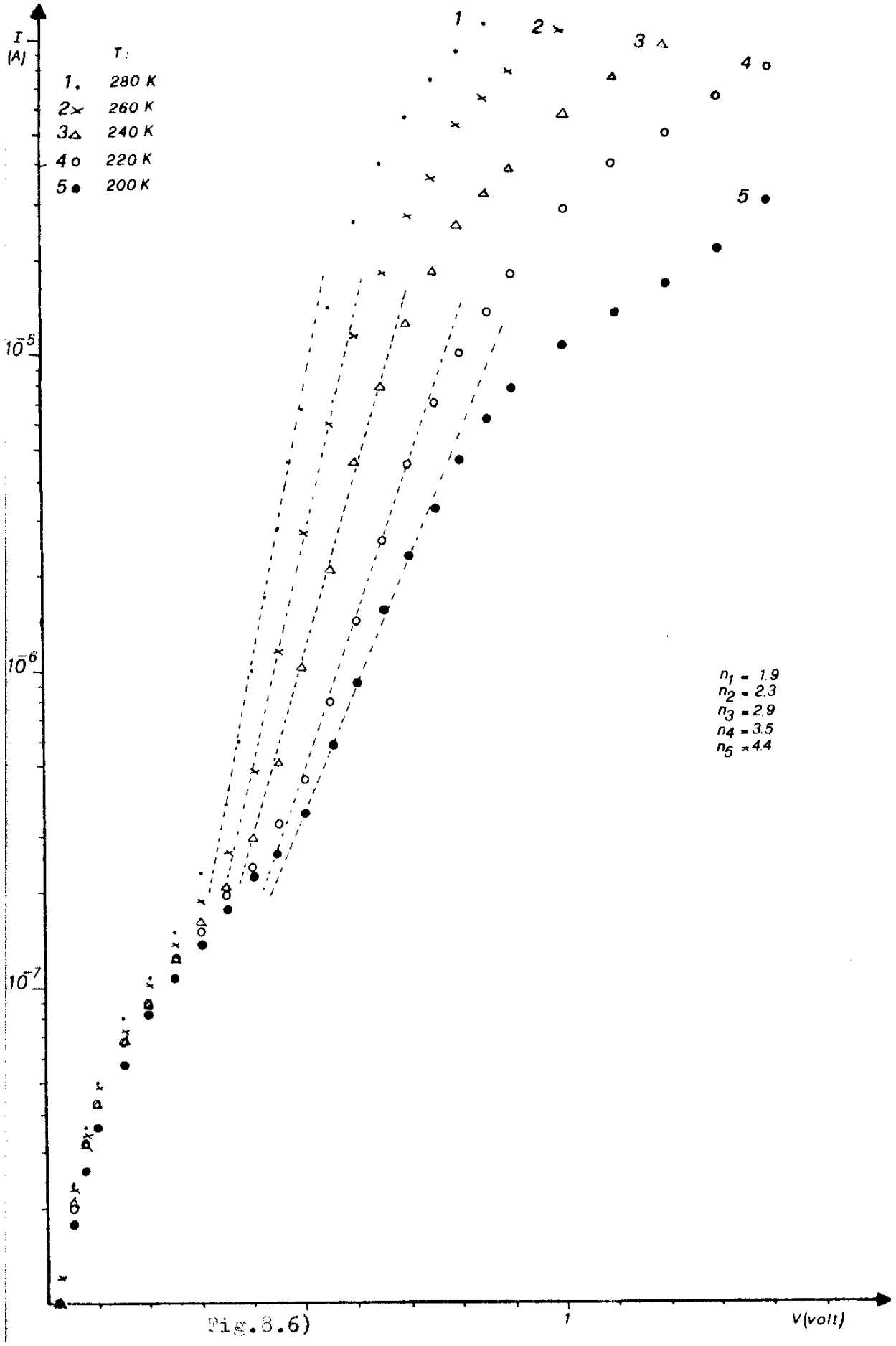
I (A)
T:
1. 280 K
2× 260 K
3△ 240 K
4○ 220 K
5● 200 K
10⁻⁵
10⁻⁶
10⁻⁷
1
2
3
4
5
n1 = 1.9
n2 = 2.3
n3 = 2.9
n4 = 3.5
n5 = 4.4
1
V(volt)

Fig.3.6)

In figure 8.6) the analysis in temperature is shown again, but this time in semilogarithmic scale to see the effect of it on the linear path. The variation of the slope is evident and this has consequences on the ideality factor of the diode.

The behavior of $n(T)$ can be seen in Fig. 8.7), that reports the values got by the graph 8.6).

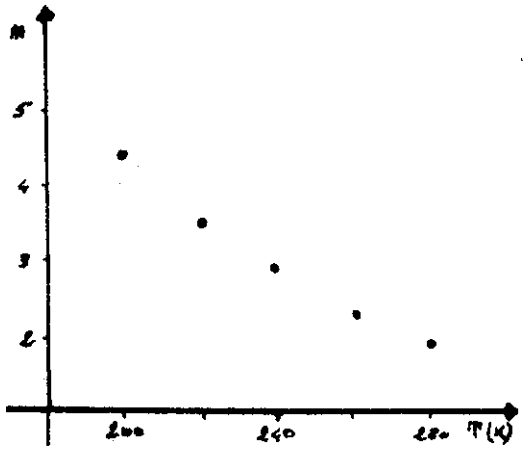

Fig. 8.7) Ideality factor as a function of the temperature for a sample of ours.

n increases notably as the temperature decreases; this behavior is already known both for the crystalline [2], and for the amorphous material devices[3].

8.2 SILICON-CARBIDE FILM GROWTH

On the basis of the conclusions of Chapter III we produced amorphous silicon-carbide by using a mixture of silane and methane in the G.D..

The adopted mixing ratios have been 7 parts of CH_4 and 3 of SiH_4, everything has been diluted in 9 parts of H_2. Under the same conditions of Hamakawa (see Chapt. III) for the pressure of the gases, for the temperature of the substrate, for the flow, and for the power, an incorporation of the l0% of carbon in the silicon structure should correspond to such a ratio.

In order to analyze the absorption vs. the wavelength on the sample produced by this way a spectrum in the visible and near infrared has been obtained through a spectrophotometer Cary.

By this way it was possible to build the graphic of $(\alpha h\nu)^{1/2}$ as a function of $h\nu$ with the aim again to get the optical gap. The result is shown in Fig. 8.8) with an $E_{g_{opt}}$ = 1.97 eV to be compared with what obtained with a a-Si:H sample grown under the same conditions, where $E_{g_{opt}}$ = 1.81 eV, that can be seen in Fig. 8.9).

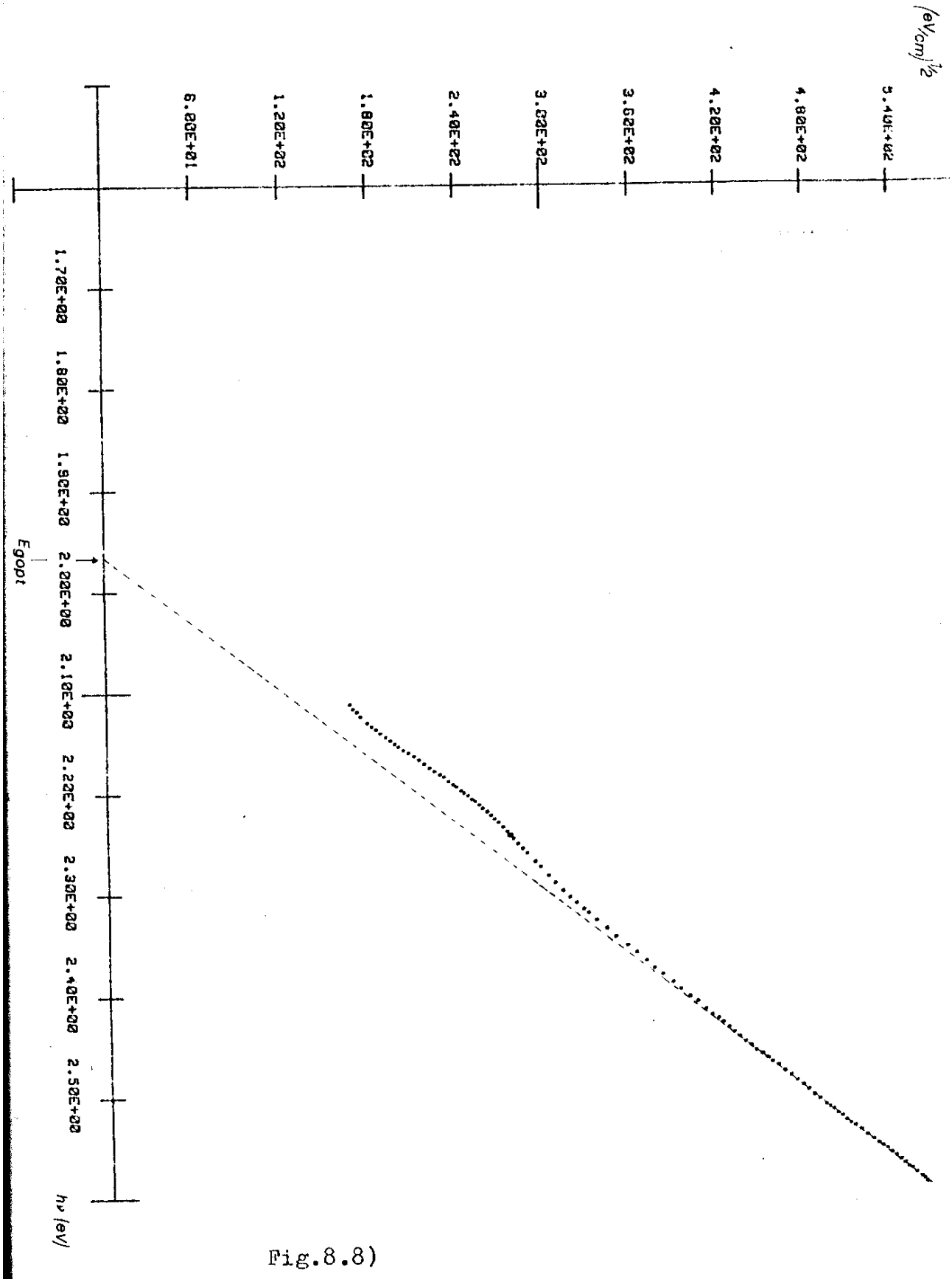
(eV/cm)^1/2
5.40E+02
4.80E+02
4.20E+02
3.60E+02
3.02E+02
2.40E+02
1.80E+02
1.20E+02
6.00E+01
1.70E+00
1.80E+00
1.90E+00
2.00E+00
2.10E+00
2.20E+00
2.30E+00
2.40E+00
2.50E+00
Egopt
hν (eV)

Fig.8.8)

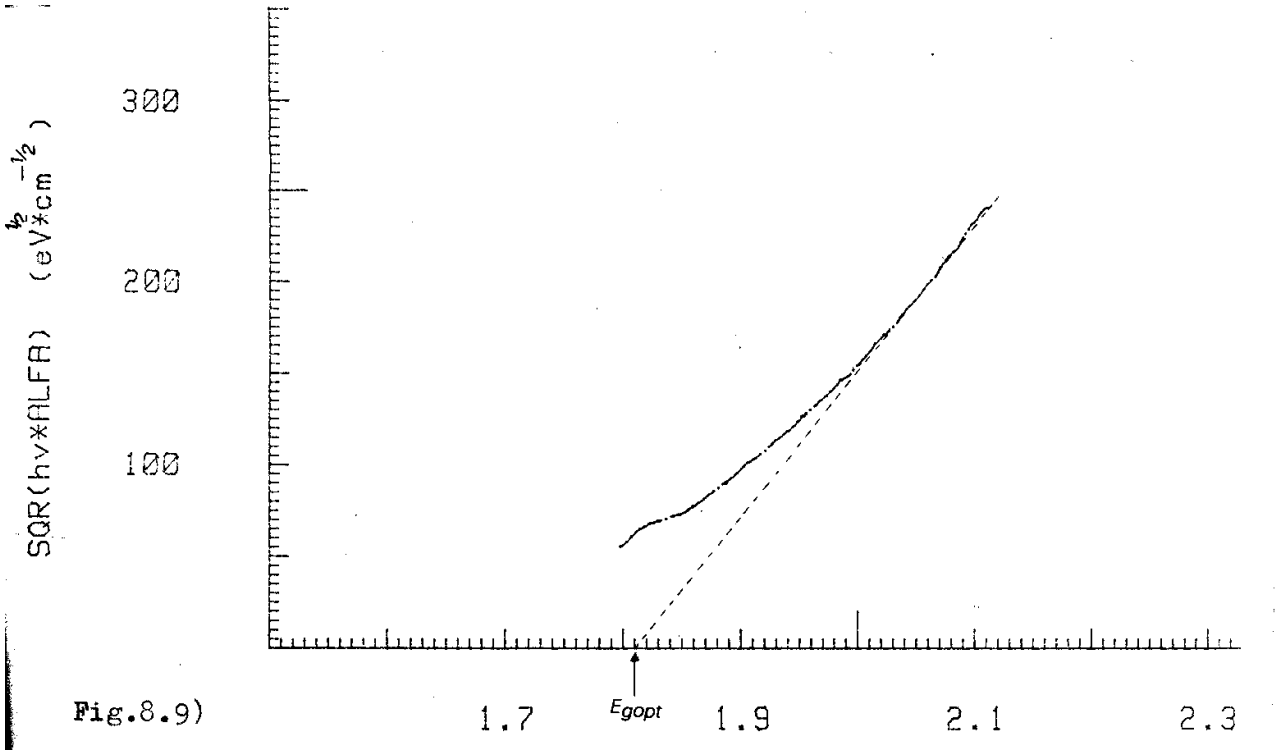

Fig.8.9)

Indeed from the absorption band located at 2090 cm^{-1} in the infrared spectrum of the sample, a small presence of bound carbon is deduced. The presence of recognizable bound oxygen is noticed also from the two big bands around 800 and 1000 cm^{-1}, perhaps right this element influenced the incorporation of the carbon. In Fig. 8.10) such a spectrum is shown with indicated the positions of the vibrations associated to the various bonds between silicon and carbon, silicon and hydrogen, silicon and oxygen, following what said by Wieder and cowokers[4].

Probably it is a bad vacuum in the G.D. chamber the caused of the unwanted oxygen incorporation. Unfortunately this does not allow us to distinguish the possible $Si-CH_3$ band at 780 cm^{-1} that should be present in the material got by methane, according to Hamakawa.

More recently the G.D. has been improved from the vacuum view point and in the new conditions the silicon-carbide has been realized with an infrared spectrum as the one shown in Fig. 8.11). There the typical bands of the $Si-CH_3$ groups appear clean. Anyway, if there is still an oxygen incorporation, it is small as small is the band at 1000 cm^{-1}. Unfortunately, for the time scheduling, all of our silicon-carbide devices have been gotten under the first conditions.

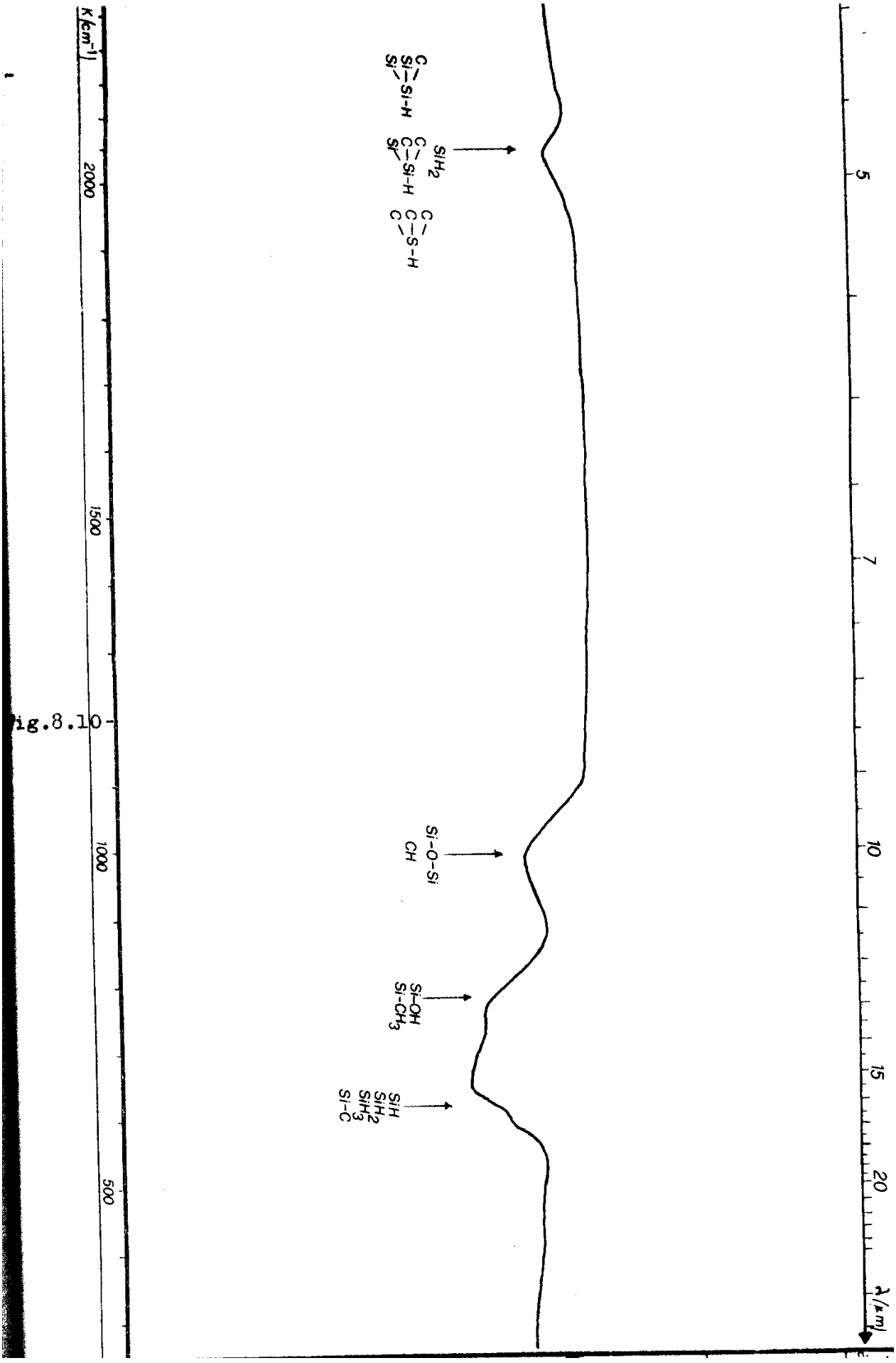
K(cm⁻¹)
2000
1500
1000
500
5
7
10
15
20
λ(μm)
SiH2
Si-O-Si
CH
Si-OH
Si-CH3
SiH
SiH2
SiH3
Si-C

Fig.8.10

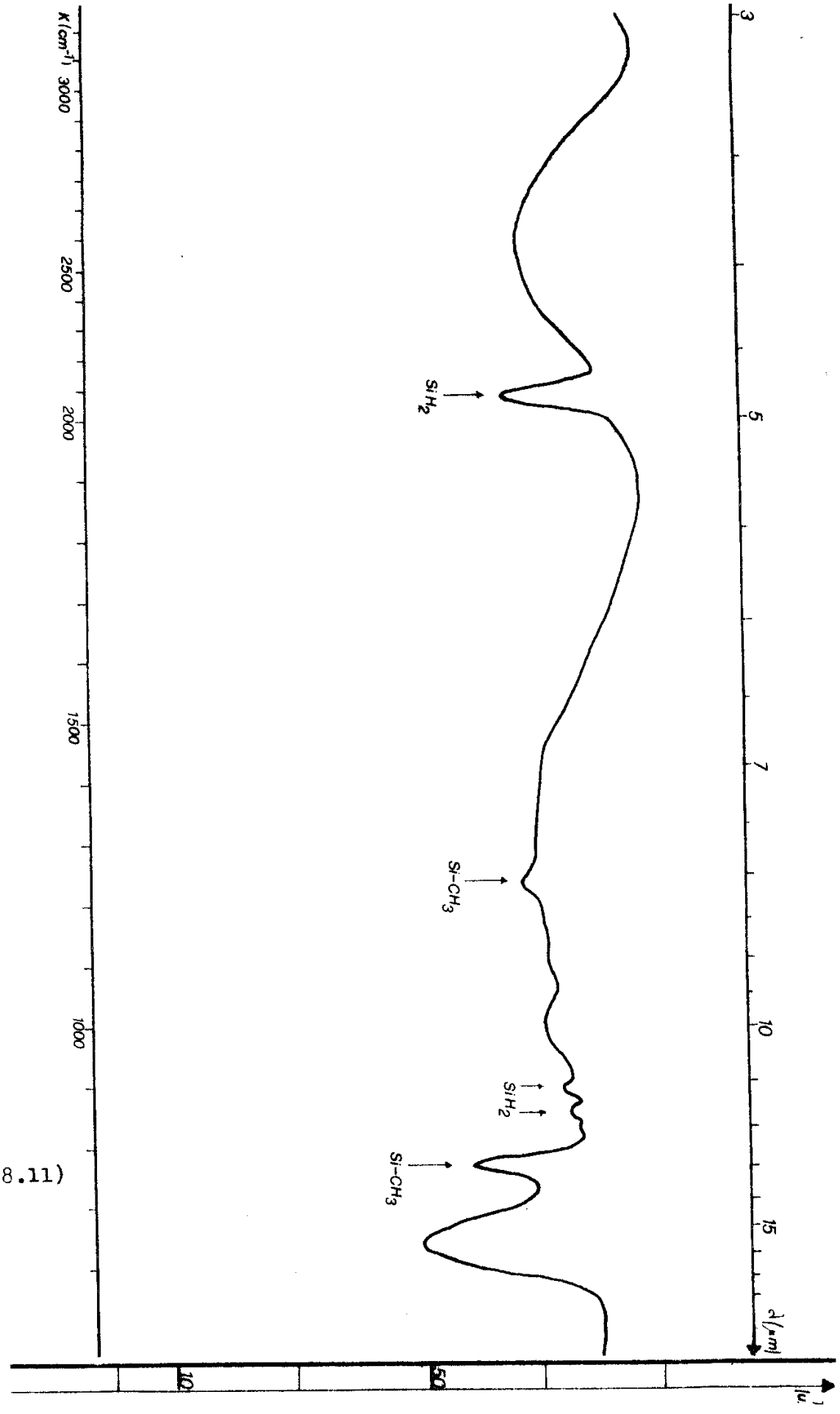
K(cm⁻¹)
3000
2500
2000
1500
1000
Si H2
Si-CH3
Si H2
Si-CH3
3
5
7
10
15
λ(μm)
10
50

Fig.8.11)

8.3 REALIZATION OF Pd/a–SiC:H(i)/a–Si:H(i)/a–Si:H(n^+)/Cr ETHEROSTRUCTURE DEVICES

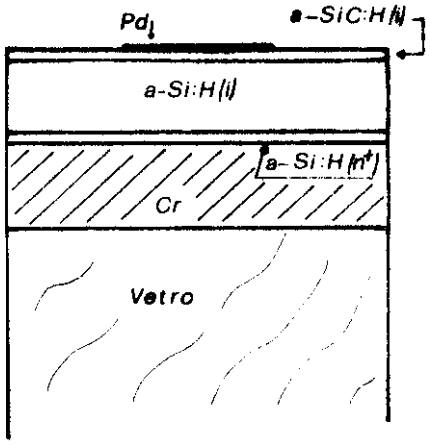

Fig. 8.12) Schematic of the layers of the materials that compose the etherostructure device.

In figure 8.12) the schematic of the layers of the etherojuction device is shown. In practice it differs from the previous one by an additional layer of intrinsic amorphous silicon-carbide of about 200 Å.

A typical *I-V* characteristic of the produced samples is shown in Fig. 8.13) in semilogarithmic scale; here the behavior of the inverse current is proposed too. Note the low inverse saturation current ($I_0 = 1.5 \cdot 10^{-11}$ *A*), with a corresponding current density $J_0 = 2.1 \cdot 10^{-10}$ A/cm^2, the good ideality as well as the good rectification factors at 0.5 Volts.

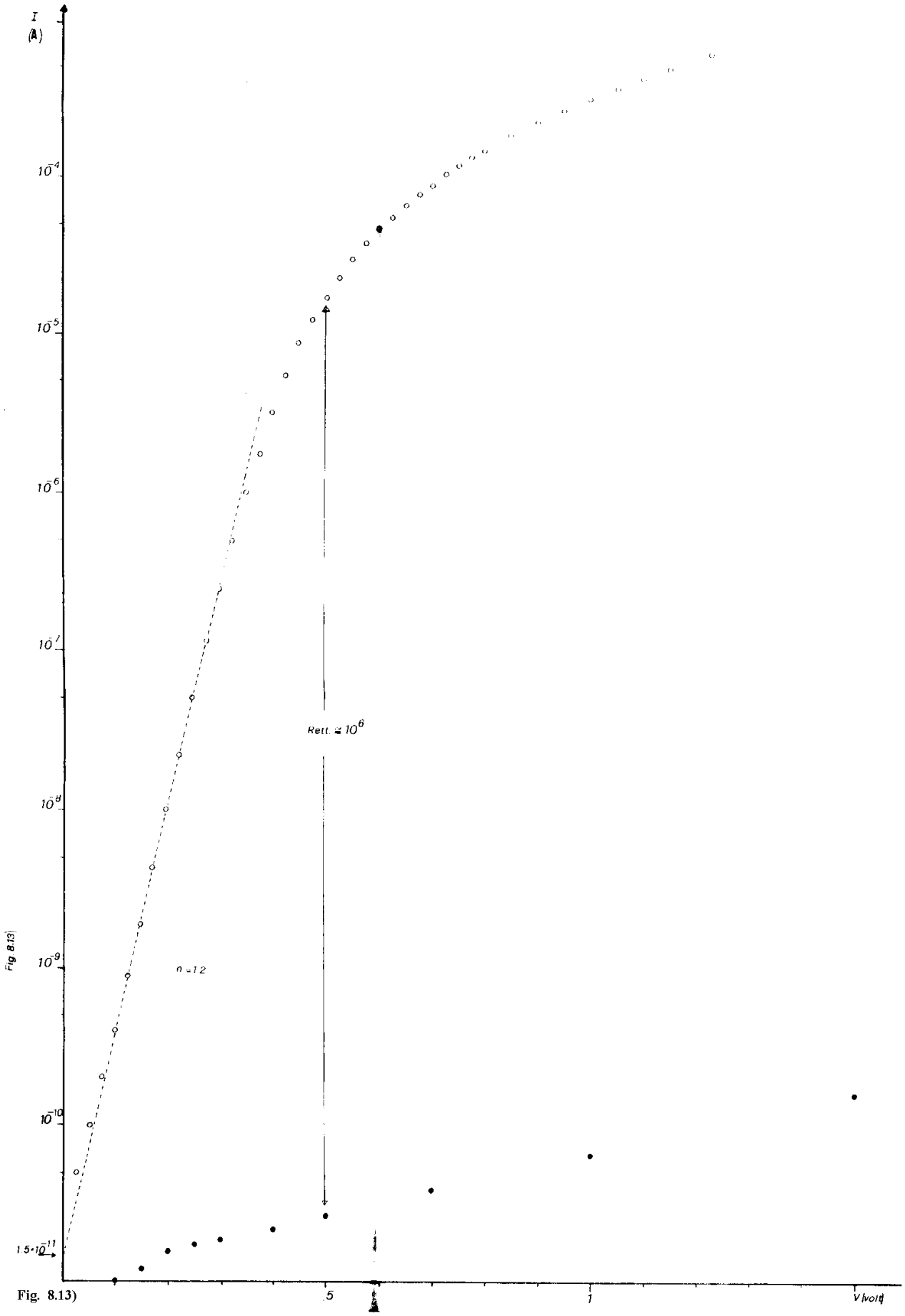
I
(A)
10^{-4}
10^{-5}
10^{-6}
10^{-7}
10^{-8}
10^{-9}
10^{-10}
$1.5 \cdot 10^{-11}$
Rett. ≅ 10^{6}
n ≈ 12
.5
1
V (volt)

Fig. 8.13)

By maintaining the a-Si:H thickness constant, we tried to vary the thickness of the a-SiC:H and the result is shown in Table I.

Table I

Thickness (Å)	n	J_0 (A/cm^2)	R_s (Ω)
150	1.2 (1)	$1.4 \cdot 10^{-10}$ (1)	230 ± 20 (2)
200	1.2 (3)	$2.1 \cdot 10^{-10}$ (3)	470 ± 50
400	1.3 (4)	$5.0 \cdot 10^{-10}$ (4)	830 ± 80 (5)

(1) ref. Fig. 8.14)
(2) ref. Fig. 8.15)
(3) ref. Fig. 8.13)
(4) ref. Fig. 8.16)
(5) ref. Fig. 8.17)

The values expressed in the first two lines of Table I are those typical of many samples, while those of the third line refer to a single test.

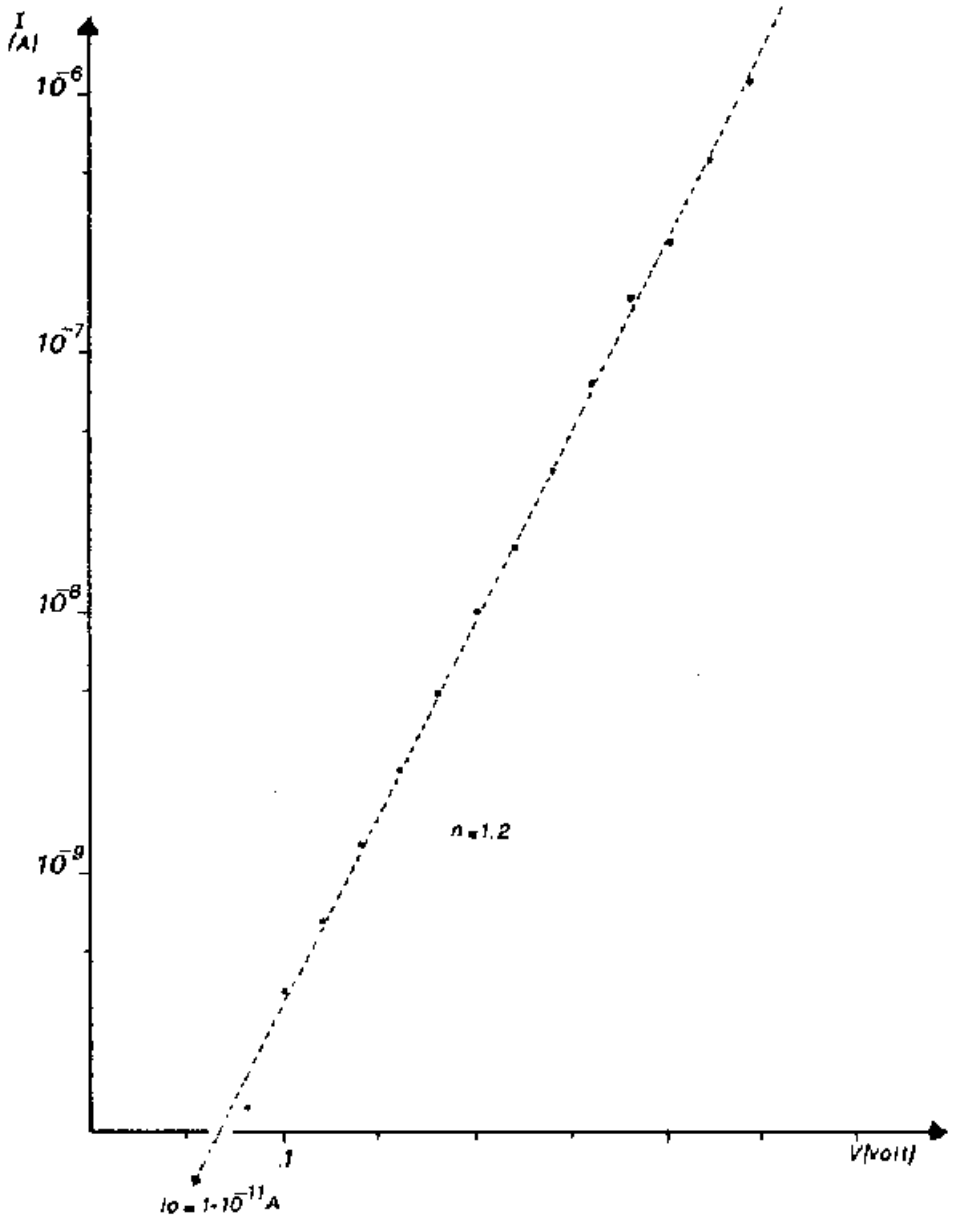

Fig. 8.l4) Linear path of the semilogarithmic characteristic of the sample with 150 Å a-SiC:H.

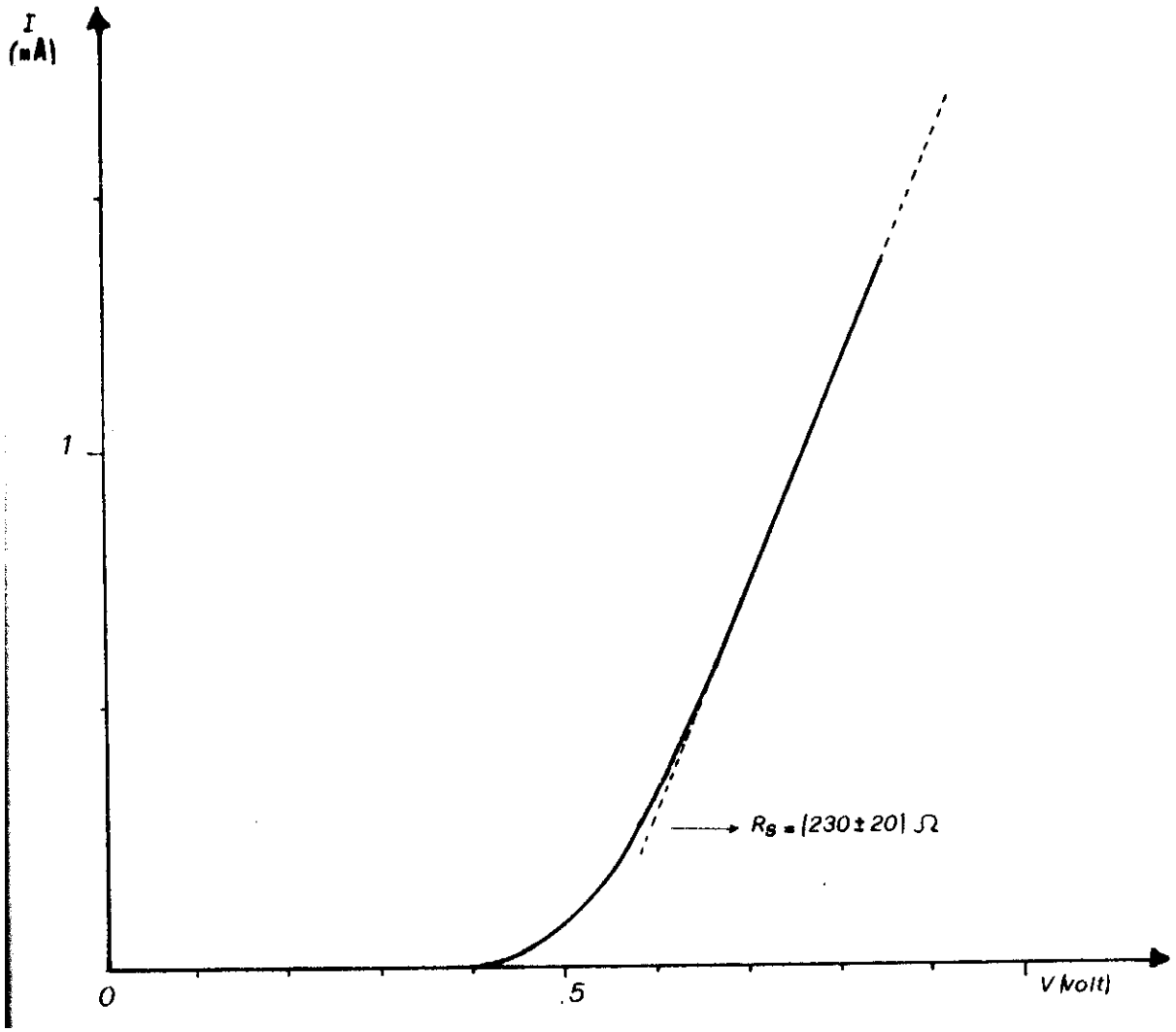

Fig. 8.15) *I–V* characteristic utilized for the series resistance calculation for the sample with 150 Å a-SiC:H.

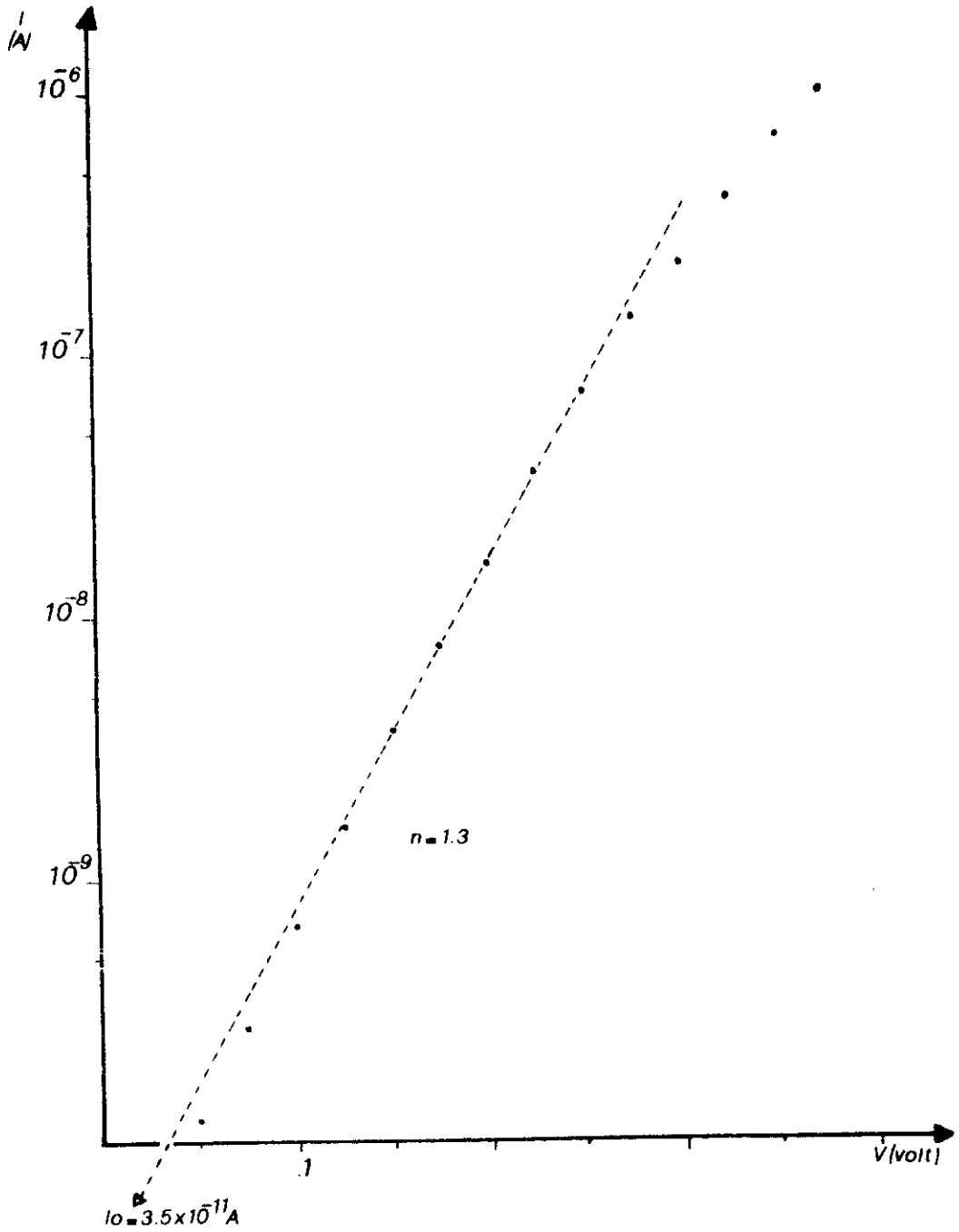

Fig. 8.16) $I(V)$ of the sample with 400 Å a-SiC:H.

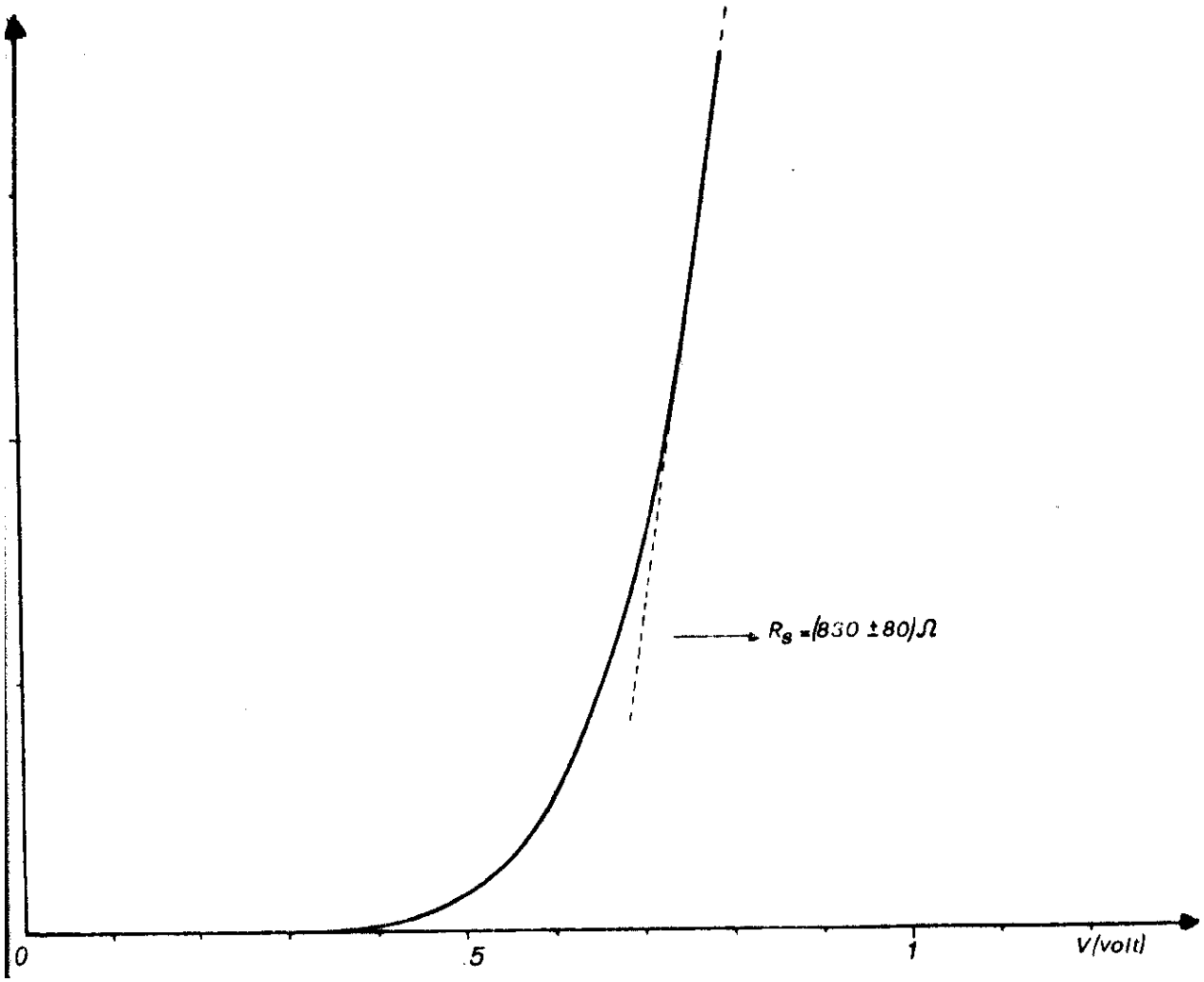

Fig. 8.17) *I*–V characteristic of the sample with 400 Å di a-SiC:H.

The complete behavior down to the “break-down” of one of our etherojunction Schottky barrier diodes is shown in Fig. 8.18).

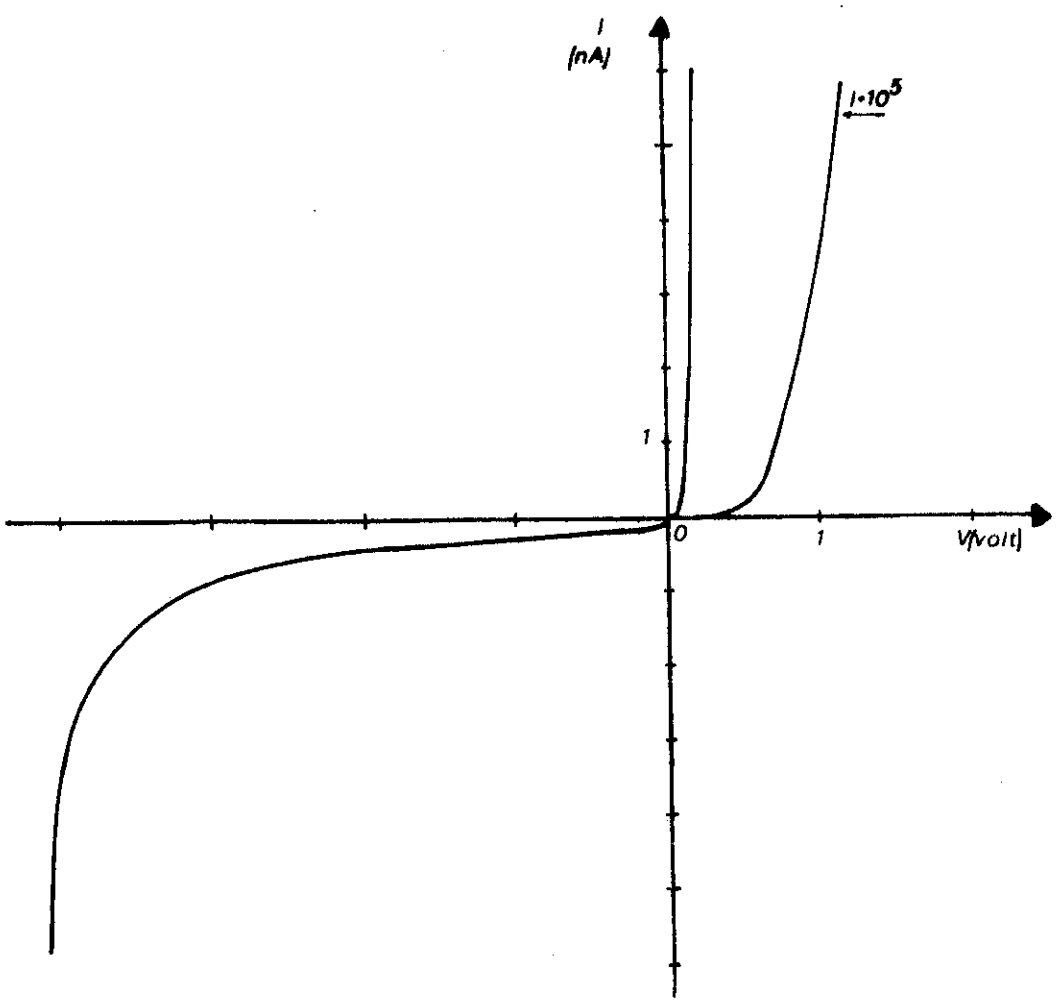

Fig. 8.l8) Complete *I–V* characteristic of a heterojunction Schottky barrier diode of ours. Note the "break-down" at 4.2 V.

The last analysis proposes a comparison between the current-voltage characteristics under solar illumination of the two types of produced devices, that is without and with the heterojunction, shown in Fig. 8.19) and in Fig. 8.20) respectively.

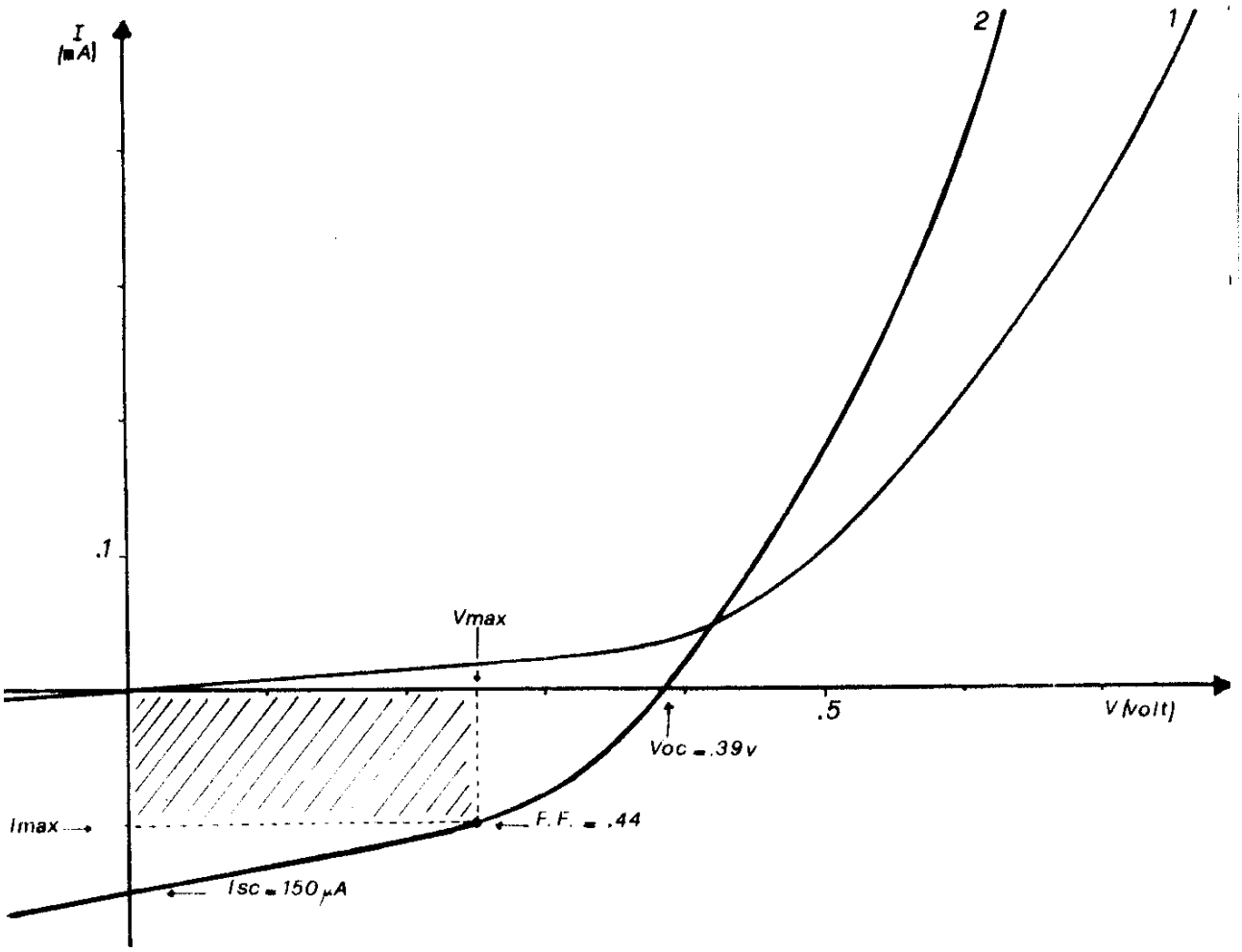

Fig. 8.19) *I-V* characteristic without and with a AM1 solar illumination (100 mW/cm^2) represented by curve 1 and 2 respectively. Note the different slope at high direct polarizations, that is due to the variation of the R_s.

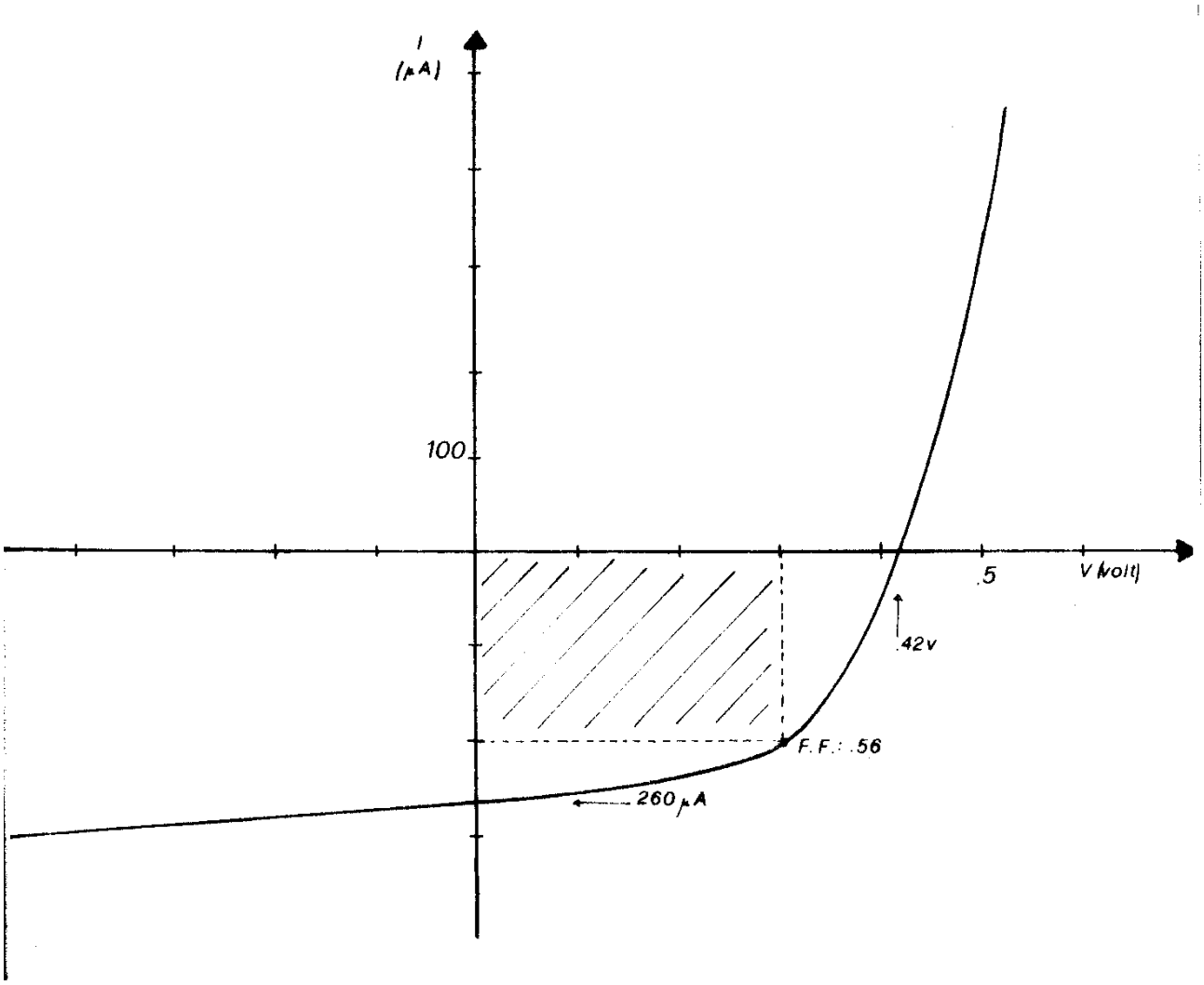

Fig. 8.20) *I-V* characteristic of the etherojunction Schottky barrier diode under AM1 solar illumination. The area of the "maximum power rectangle" (shadowed) results to be about 9 μW/cm^2 on l mW/cm^2 of the incident solar light, to be compared to the 4 μW/cm^2 got from the rectangle of Fig. 8.19).

8.4 Pd/a–Si:H DEVICES SPECTRAL RESPONSE

The measurement apparatus is shown in Fig. 8.21).

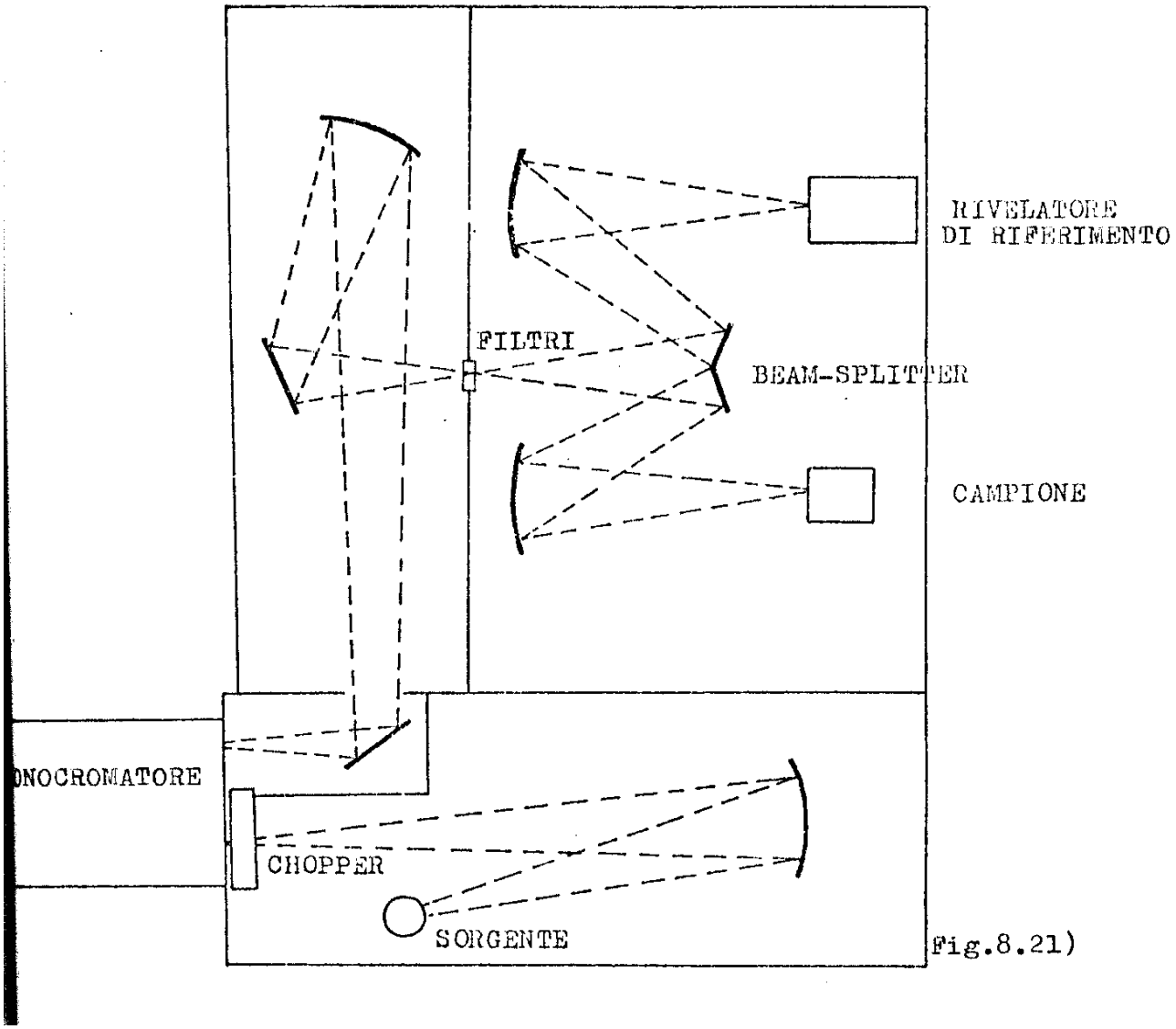

Fig.8.21)

The source (SORGENTE), a tungsten filament lamp, is focused through a spherical mirror on the entry slit of a Jarrel-Ash monochromator (MONOCROMATORE). The monochromatic light coming from the exit slit at first crosses a system of mirrors whose purpose is to move the beam away from the entry optics to allow the setup of the beam-splitter, the sample (CAMPIONE) and the reference detector (RIVELATORE DI RIFERIMENTO).

The beam-splitter is obtained by two plain mirrors tilted of 15° with respect to the direction of the incident light. The two beams are then focused on the sample and on the reference detector. A Hamamatsu RS 45 photocell with a know spectral response has been used as a reference detector, it is sensitive in the range 2500 – 8000 Å. The photocurrent of the two channels was revealed by two Kethley 480 4.5 digits Picoammeters. However to improve the signal to noise ratio the light was modulated with a mechanical "chopper" and the signals revealed through two PAR 124 lock-ins amplifiers. In this case the photocell signal is collected from 1 MΩ load resistance. The value of the load resistance on the sample is selected small in comparison to the shunt resistance of the diode, so that the read voltage is proportional to the short-circuit current of the diode.

An analogic to digital converter (ADC) is put at the analogical exit of the picoammeters or of the lock-in amplifiers of the two above mentioned measurement channels, in order to input the measurement data into a HP 35 desk computer, which elaborates and records them on a tape.

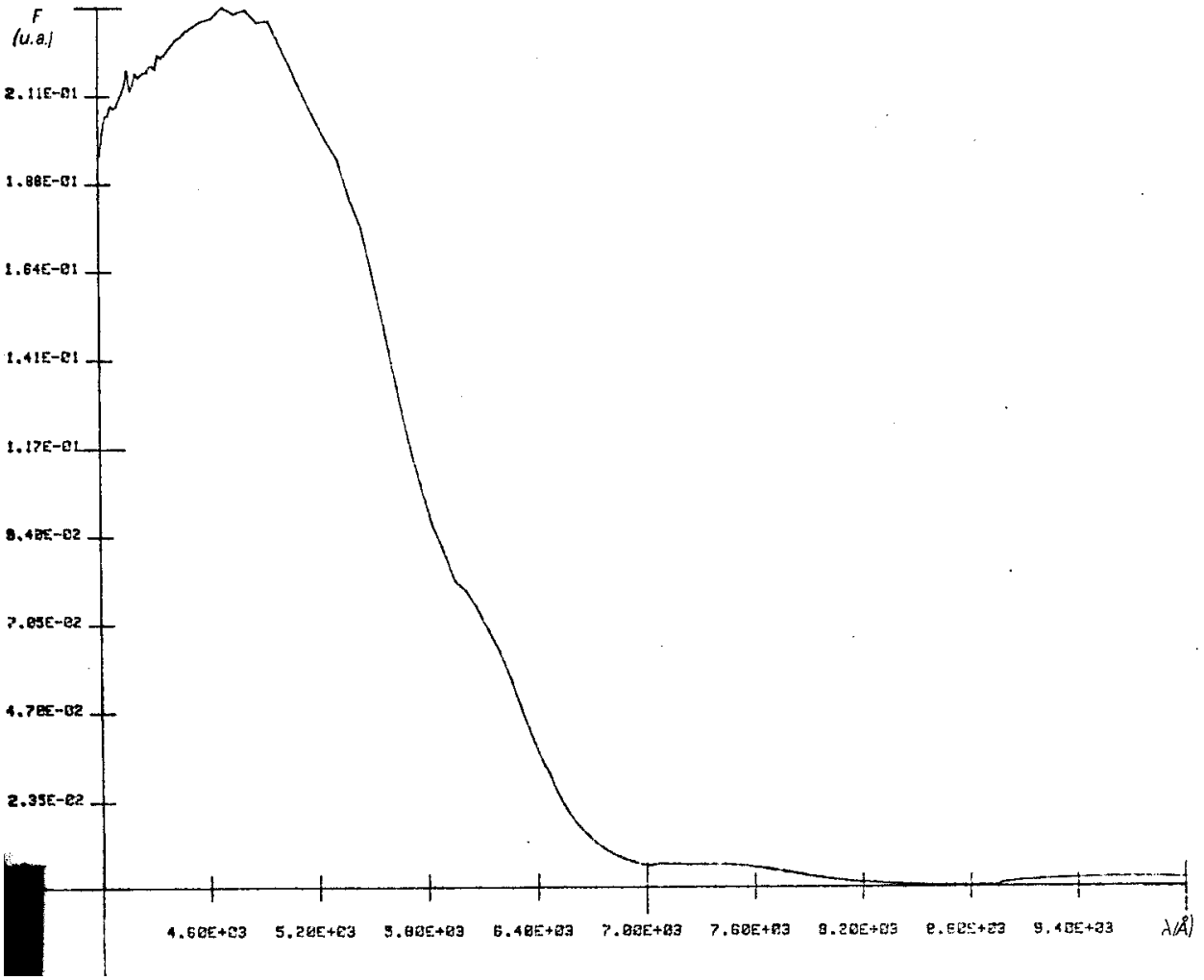

Fig. 8.22) Photoresponse of one of ours Pd/a-Si:H(i) Schottky barrier diode.

In Fig. 8.22) the typical photoresponse of the simple Schottky barrier devices (without a-SiC:H layer) is shown. Note a maximum at 4800 Å.

The small oscillations observed at long wavelengths are the interference fringes generated by the incident light and the light reflected by the chrome back contact.

8.5 Pd/a−SiC:H/a−Si:H DEVICES SPECTRAL RESPONSE

A typical photoresponse of the etherojunction Schottky barrier devices realized during this Thesis work is shown in figure 8.23). Two maxima are noticed: one at 3900 Å and one at 4600 Å. Here the interference fringes ought to the mechanism previously described are present too.

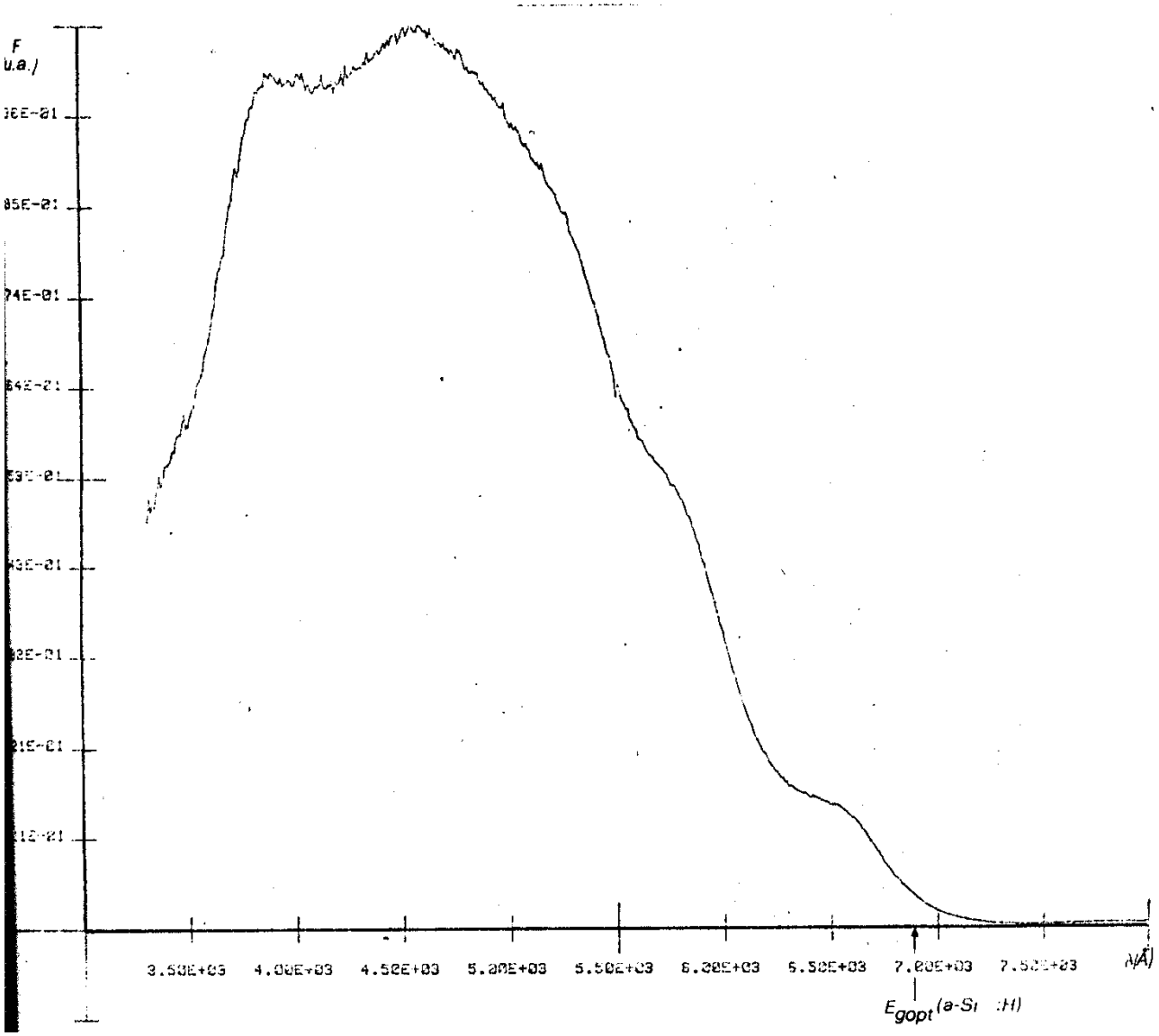

Fig. 8.23) Typical photoresponse of our produced etherojunction Schottky barrier devices.

The inverse polarization (V_{inv}) effect on the spectral response of these diodes is shown in Fig. 8.24) for λ = 4000, 5000 e 6000 Å.

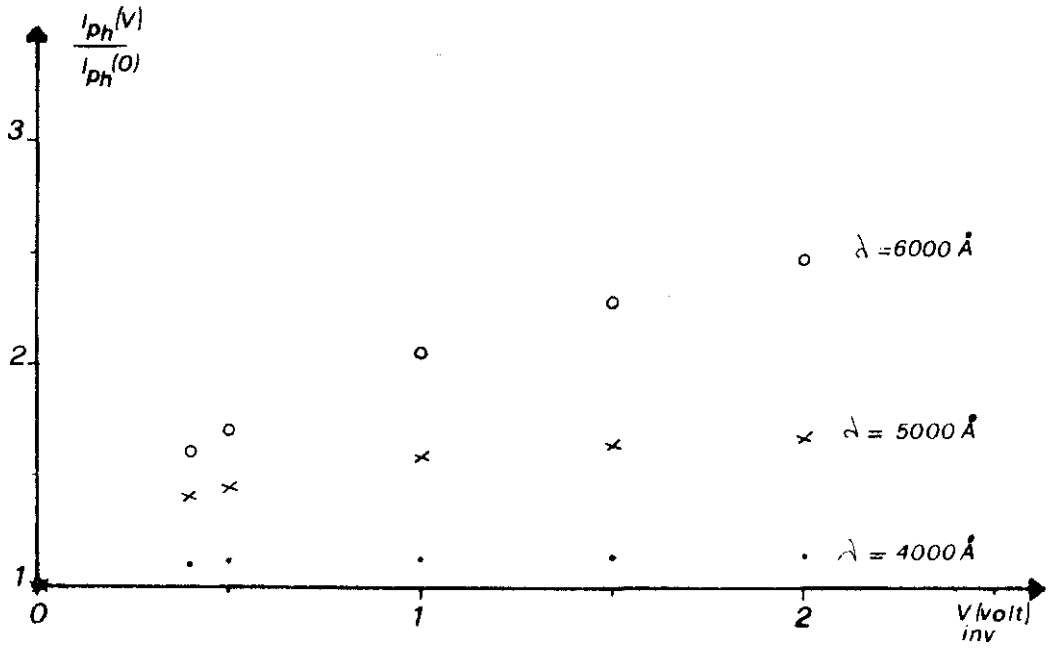

Fig. 8.24) Photocurrent / short-circuit current ratio at different inverse voltages and at three different wavelengths.

The photocurrent has the tendency to saturate when V_{inv} increases, and as quickly as smaller the wavelength is.

The spectral responses for V_{inv} = 0 V, 0.4 V e 1.5 V are shown in Fig. 8.25). The big increase of the sensitivity at longer wavelengths as V_{inv} grows up is of particular interest in sight of possible practical applications.

The collection efficiency "η_{coll}" has been measured with a He-Ne laser by correcting it for the transmission of the palladium (60%): for V_{inv} = 1.5 V, at the principal peak we find η_{coll} (5100Å) = 0.8.

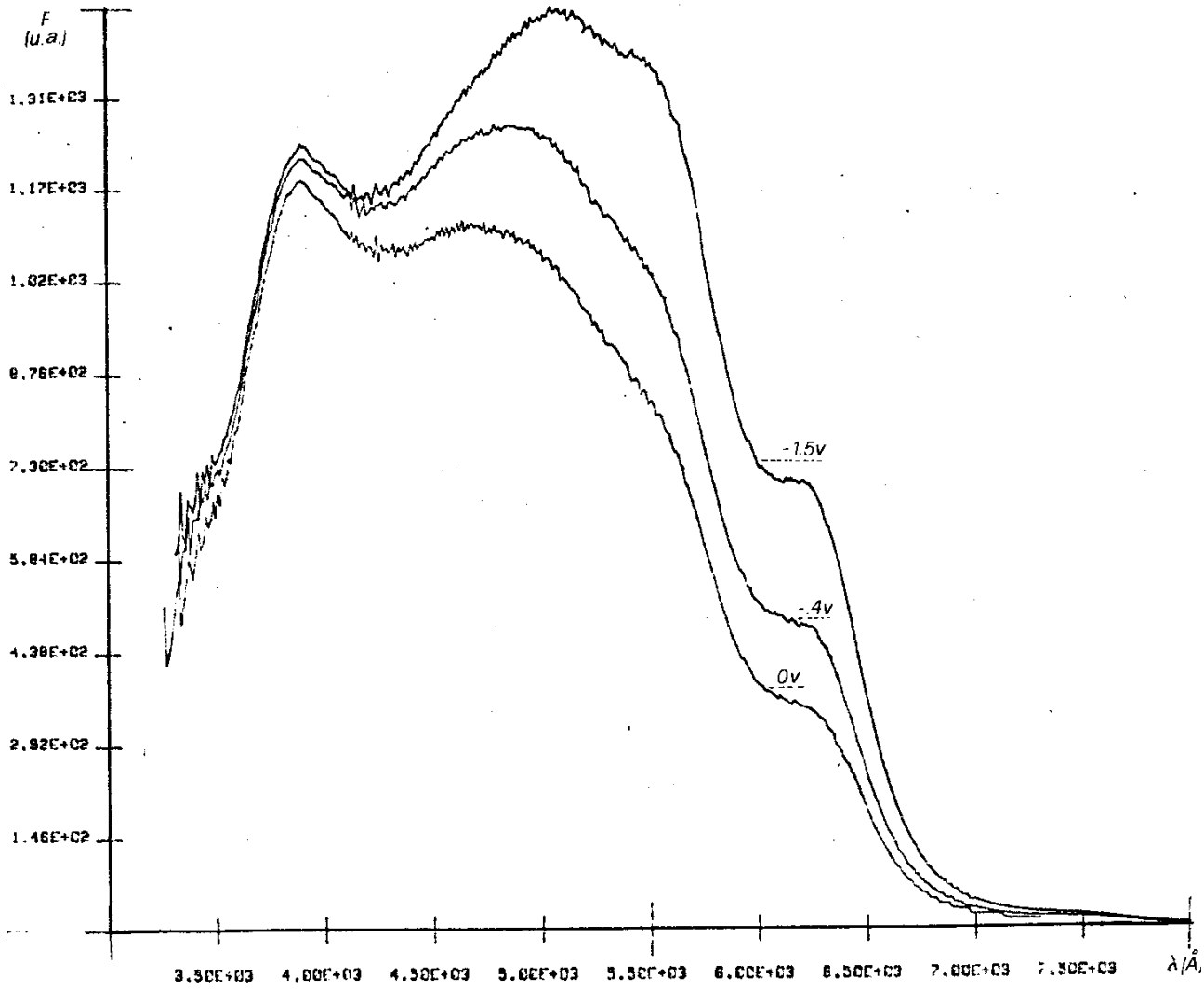

Fig. 8.25) Pd/a-SiC:H/a-Si:H etherojunction diode photoresponse when varying the inverse polarization.

A photoresponse spectrum has been obtained also for a silicon-carbide (400 Å) sample and the result gave a strong decrease of the response at long wavelengths (> 4500 Å) with the disappearance of the second maximum.

BIBLIOGRAPHY

1 A.E. Delaloy - R.W. Griffith, J. Appl. Phys. **52**(10) (1981)

2 E.H. Rhoderick, “Metal Semiconductor Contacts”, Clarendon Press - Oxford (1978)

3 A. Madan - W. Czubayi - J. Yang, Appl. Phys. Lett. **40**(3), 234 (1982)

4 H. Wieder - M. Cardona - C.R. Guarnieri, Phys. Stat. Sol. **92**(b), 99 (1979)

CHAPTER IX

“DISCUSSION AN CONCLUSIONS”

The best results found in the literature for Pd/a-Si:H diodes give inverse saturation density current $J_0 = 10^{-9}$ A/cm^2 and ideality factors $n \cong 1.1, 1.2$[1].

In similar structures we find notable deviations from the exponential behavior at low direct polarizations ($V < 0.2$ V) (see fig.8.4)), the J–V characteristic in this case can be described by:

$$J = J_0 \exp\left(\frac{qV}{nKT}\right) + J_{ecc}(V) \ .$$

The excess current (J_{ecc}), that seems not to depend on the temperature [see Fig.8.6)], can be due to a mechanism of tunnel through the barrier, made possible by the presence of an elevated density of states in the gap. Such effect is absent in our Pd/a-SiC:H/a-Si:H diodes, and, excluding the effects related to the series resistance, they follow the law $J = J_0\left(\exp\left(\frac{qV}{nKT}\right) - 1\right)$.

The obtained J_0 values are an order of magnitude lower than the ones of the Pd/a-Si:H diodes found in the literature and moreover we got a notable reproducibility of the results.

Since the low saturation currents J_0 is a very attractive characteristic in a diode for several applications, i.e. the noise of a photodiode grows with J_0, this result appears interesting and here we will try to explain it in terms of the diffusive theory of the transport in the Schottky barriers (see Chapt. V).

Let us rewrite here the Eq. 5.11) by setting $E_c = -q\psi$:

9.2) $$J = qD_n N_c\left(\exp(qV/KT) - 1\right) \Big/ \int_0^W \exp(E_c(x)/KT)dx \ .$$

We must calculate the term:

9.3) $$H = \int_0^W \exp(E_c(x)/KT)dx$$ for the amorphous material (a-Si:H or a-SiC:H); in the meanwhile we can write:

9.4) $$H = \int_0^W \exp(E_c/KT)\frac{dx}{E_c}dE_c \ .$$

The term $\frac{dx}{dE_c}$ can be drawn from the equations 4.24) and 4.27) of Chapter IV for the examined case. By keeping in mind that:

$X_f = 0$, $N_D = 0$ (undoped material)

$z = -x$

and that:

$1/2\ (\cosh(X_c) - 1) = \sinh^2(X_c/2)$ then:

9.5) $$\frac{dE_c}{dx} = -\sqrt{2}q\left(\frac{g_{\min}}{\varepsilon_0\varepsilon}\right)^{1/2} E_{ch}\left(\cosh(X_c)-1\right)^{1/2} = -\sqrt{2}q\left(g_{\min}/\varepsilon_0\varepsilon\right)^{1/2} E_{ch}\sqrt{2}\sinh(X_c/2)$$

and by putting $X_c = \frac{E_c - E_{cb}}{E_{ch}}$ we get:

9.6) $$H = \frac{1}{2q}\left(\frac{\varepsilon\varepsilon_0}{g_{\min}}\right)^{1/2}\frac{1}{E_{ch}}\int_{E_c(W)}^{E_c(0)}\frac{\exp(E_c/KT)}{\sinh\left(\frac{E_c - E_{cb}}{2E_{ch}}\right)}dE_c$$

9.7) $$H = \frac{1}{2q}\left(\frac{\varepsilon\varepsilon_0}{g_{\min}}\right)^{1/2}\frac{1}{E_{ch}}\exp(E_c(0)/KT)\int_{E_c(W)}^{E_c(0)}\frac{\exp\left(\frac{-E_c(0)+E_c}{KT}\right)}{\sinh\left(\frac{E_c - E_{cb}}{2E_{ch}}\right)}dE \ .$$

Since $2E_{ch} \cong 0.2$ eV $\gg KT$, we can write:

9.8) $$H \cong \frac{1}{2q}\left(\frac{\varepsilon\varepsilon_0}{g_{\min}}\right)^{1/2}\frac{1}{E_{ch}}\exp\left(\frac{E_c(0)}{KT}\right)\frac{KT}{\sinh\left(\frac{E_c(0)-E_{cb}}{2E_{ch}}\right)}\cdot\int_{E_c(W)}^{E_c(0)}\exp\left(-\frac{E_c(0)-E_c}{KT}\right)d\left(\frac{E_c(0)}{KT}\right) \Rightarrow$$

9.9) $$H = \frac{1}{2q}\left(\frac{\varepsilon\varepsilon_0}{g_{\min}}\right)^{1/2}\frac{1}{E_{ch}}\exp\left(\frac{E_c(0)}{KT}\right)\frac{KT}{\sinh\left(\frac{E_c(0)-E_{cb}}{2E_{ch}}\right)} \ .$$

Being $E_c(0) = q\phi_b$, $E_c(0) - E_{cb} = (V_{do} - V)q$, Eq.s 9.9), 9.3) e 9.2), and by remembering that $D_n = \mu_n KT/q$, altogether give:

9.10) $$J = q\mu_n N_c \xi_{\max}\exp(-q\phi_b/KT)\left(\exp(qV/KT)-1\right)$$

where $\xi_{\max} = 2\left(g_{\min}/\varepsilon\varepsilon_0\right)^{1/2} E_{ch}\sinh\left(\frac{q(V_{do}-V)}{2E_{ch}}\right)$ is the field value at the metal-semiconductor interface.

Now for $tgh\left(\frac{qV_{do}}{2E_{ch}}\right) \cong 1$:

9.11) $$J = J_0\exp\left(\frac{-qV}{2E_{ch}}\right)\left(\exp\left(\frac{qV}{KT}\right)-1\right)$$, where

9.12) $$J_0 = 2q\mu_n N_c (g_{\min}/\varepsilon\varepsilon_0)^{1/2} E_{ch} \cosh\left(\frac{qV_{do}}{2E_{ch}}\right) \exp\left(\frac{-q\phi_b}{KT}\right) = J_s \exp\left(\frac{-q\phi_b}{KT}\right) .$$

In direct polarization, for $qV \gg KT$, Eq. 9.11) can be approximated as:

9.13) $$J = J_0 \exp\left(\frac{qV}{nKT}\right) , \text{ with}$$

$$n = 1\Big/\left(1 - \frac{KT}{2E_{ch}}\right) .$$

On the basis of the model of Shur and coworkers for the field of junction (see Chapt. IV) and of the diffusion theory of the transport (see Chapt. V), from this equation it is seen that deviations of the ideality factor n from the unity can happen in the amorphous silicon, even in absence of those mechanisms discussed in Chapter V.

For E_{ch} = 0.1 eV we got the n = 1.14 value similar to what observed experimentally. The equation 9.12) can be used to explain the lowering of J_0 observed in our Pd/a-SiC:H/a-Si:H devices.

In fact, by assuming negligible the discontinuity between the valence bands of the a-SiC:H and of the a-Si:H, as proposed by Hamakawa[2], we get the band scheme shown in Fig. 9.1) for the etherojunction structure of the two materials, and it results that: $\phi_{b2} = \phi_{bl} + \Delta E_g$, where ϕ_{b2} is the barrier from the metal to the semiconductor for the a-SiC:H, ϕ_{bl} the one for the a-Si:H, and ΔE_g is the difference between the two gaps. From the data got in the literature we have ϕ_{bl} = 0.94 eV and therefore ϕ_{b2} = 1.1 eV for ΔE_g = 0.16 eV (see Chapt. VIII).

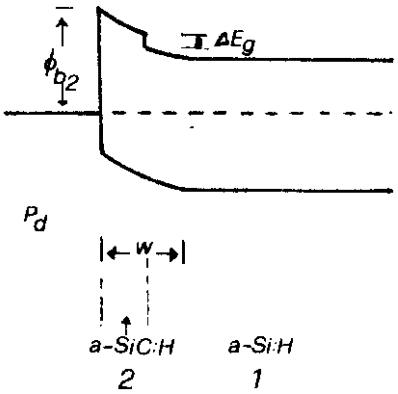

Fig. 9.1) Energy band scheme adopted by us (not in scale).

The ratio between the J_0 in the two cases (with or without the silicon-carbide layer) will be given by:

9.14) $$\frac{J_{02}(a\text{-}SiC{:}H)}{J_{01}(a\text{-}Si{:}H)} = \frac{J_{s2}}{J_{s1}} \exp(-(\phi_{b2} - \phi_{b1})/KT) \ .$$

From our results:

$J_{02} \sim 10^{-10}$A/cm^2 and $J_{01} \sim 10^{-9}$A/cm^2 , therefore we get:

$\frac{J_{s2}}{J_{s1}} \cong 60$; such a difference in J_s in the two materials is probably due to a higher value of g_{min} for the a-SiC:H. On the other hand the higher density of the states in the gap assumed by the present model for this material is consistent with the strong reduction of the photoconductivity[3] observed in the silicon-carbide in comparison to the amorphous silicon.

In substance however it is noticed that the advantage achieved through the higher value of ϕ_b in our Pd/a-SiC:H structure is partly canceled by the increase of the surface field (ξ_{max}).

To get then a further reduction of J_0 is necessary to decrease the density of states in the gap of the amorphous silicon-carbide and so far only a little effort has been devoted to this problem in this and other laboratories.

Again a direct consequence of the presence of the silicon-carbide layer with the aforesaid characteristics is the remarkable sensitivity of the spectral response to the polarization of these devices. In fact in a comparison to the case of the Pd/a-Si:H barrier, the region (W), in which the field is sufficiently elevated to annul the effects of recombination, results very small in absence of polarization.

The application of the inverse voltage extends W and increases the collection efficiency at long wavelengths [see Fig.8.25)]

Up to date of the present investigation however the maximum located to 3900 Å in the photoresponse spectrum is not clear.

Research works currently in progress in Japan (Sanyo) for the realization of solid state image sensors based on the amorphous silicon employ three diodes p-i-n for each element, one with a selective filter for blue, one with a filter for green and one with a filter for red. If the discrimination among the three colors could be obtained with a single diode by varying only the applied voltage, the advantage would be remarkable either from the complexity and the resolution view points.

BIBLIOGRAPHY

1 C.R. Wronski - D.E. Carlson - R.E. Daniel, Appl. Phys. Lett. **29**(9), 602 (1976)

2 Y. Tawada - K. Tsuge - M. Kondo - K. Nishimura - H. Okamoto - Y. Hamakawa, Proc. IV Int. Phot. Sol. Ener. Conf. – Stresa, 698 (1962)

4 Y. Tawada - M. Kondo - H. Okamoto - Y. Hamakawa, Proc. 9th Int. Conf. Am. Liq. Sem. – Grenoble, 1 (1981)

ACNKOWLEGMENTS

Besides the clear and expert supervisor, Dr. Piero Migliorato, the author wishes to thank also all the researchers, the professors, the technicians and the colleagues of the G15 group of the “Guglielmo Marconi” Institute of Physics at the The University of Rome, “La Sapienza”; in particular the Profs. Andrea Frova and Florestano Evangelisti, the researcher Paolo Fiorini, and the technician Renato Moretto; this work of Thesis would never have been possible without their help.

ADDENDUM

After further measurements on the devices realized with the a-SiC:H/a-Si:H etherojunctions, we concluded that the maximum of the photoresponse spectrum located a 3900 Å was an artifact, due to a normalization and calibration defect on the reference photodiode.

In fact the following figure of the photoresponse (Fotorisposta) got in Dr. Marcello Garozzo's laboratory at "AssorEni", Monterotondo (Rome), does not show any peak at low wavelengths (Lunghezza d'onda).